TAMPEREEN TEKNILLINEN YLIOPISTO

TATU KALLIONPÄÄ

MAGNETOSTRICTIVE ENERGY HARVESTING FROM STEEL

Examiners:
Professor Pekka Ruuskanen
Professor Jukka Vanhala
Examiners and subject accepted by the dean of the Faculty of Computing and Electrical Engineering on 2 May 2018

TIIVISTELMÄ

TAMPEREEN TEKNILLINEN YLIOPISTO
Sähkötekniikan tutkinto-ohjelma
Kallionpää, Tatu: Magnetostriktiivinen energianlouhinta teräksestä
Diplomityö, 100 sivua
Toukokouu 2018
Pääaine: Sulautetut järjestelmät
Tarkastajat: Professori Pekka Ruuskanen ja Professori Jukka Vanhala
Avainsanat: Energianlouhinta, magnetostriktio, magnetoelastinen ilmiö, elastinen aalto, impedanssinsovitus, tasasuuntaus

Energian louhiminen tarkoittaa elektronisten laitteiden toimintaan tarvittavan energian hankkimista laitteiden käyttöympäristöstä. Mahdollisia energian lähteitä laitteiden toimintaympäristössä ovat muun muassa valo,lämpötilaerot, sähkömagneettinen säteily ja kineettinen energia. Energianlouhintamenetelmien kehittyminen yhdessä elektronisten laitteiden energiankulutuksen pienenemisen kanssa voi lähitulevaisuudessa mahdollistaa monien laitteiden energiaomavaraisuuden, joka tarkoittaa laitteiden huoltotarpeen pienenemistä, toimintavarmuuden parantumista ja paristojätteen määrän vähenemistä.

Työn kokeellisen osan päätavoitteena oli kehittää uutta magnetoelastiseen ilmiöön perustuva energianlouhintamenetelmä, jolla voidaan louhia energiaa teräsrakenteissa etenevistä elastisista alloista, sekä menetelmän kanssa käytettävää louhintaelektroniikkaa. Magnetoelastinen ilmiö on ferromagneettisissa materiaalisissa havaittava ilmiö, joka aiheuttaa muutoksen materiaalin magnetoitumassa materiaalin muodon muuttuessa. Ilmiötä kutsutaan myös käänteiseksi magnetostriktiiviseksi ilmiöksi. Magnetoituman muutos aiheuttaa muutoksen myös materiaalin lävitse kulkevassa magnettivuossa. Koska muutos magneettivuossa indusoi jännitteen käämiin, jonka lävitse vuo kulkee, magnetoelastista ilmiötä voidaan hyödyntää energian louhimisessa. Uuden energianlouhintamenetelmän periaattena on louhia energiaa iskumaisesti kuormitetusta terästangosta tangon ympärillä olevalla kelalla. Iskumainen kuormitus aiheuttaa terästankoon elastisen allon, joka aikaansaa tankoon vaihtelevia puristus -ja venymämyötymiä. Koska teräs on ferromagneettinen materiaali, puristus -ja venymämyötymät muuttavat tangon magnetisaatiota, ja magnetisaation muutos voi indusoida jännitteen tangon ympärillä olevaan käämiin. Siten osa elastisen aallon kuljettamasta energiasta voidaan muuttaa sähköenergiaksi. Työn puitteissa rakennettiin testauslaitteisto, jolla menetelmää voidaan kokeilla, kokeellinen louhintageneraattori ja elektronisia piirejä, jotka voivat ladata litium-ioniparistoa louhitulla energialla. Menetelmällä saatava keskimääräinen teho riippuu iskumaisen kuormituksen voimakkuudesta ja taajuudesta, mutta elastisen aallon liikkeen aikana saavutetut tehot olivat 1-5 mW. Tämä on riittävä keskimääräinen teho esimerkiksi pienitehoisen langattoman anturin käyttämiseksi.

Työhön kuuluu myös kirjallisuuskatsaus, jonka tavoitteena on antaa lukijalle perustiedot olemassa olevista kineettisen energian louhimismenetelmistä ja magnetostriktiivisten ilmiöiden luonnontieteellisestä perustasta.

ABSTRACT

TAMPERE UNIVERSITY OF TECHNOLOGY
Master's Degree Programme in Electrical engineering
KALLIONPÄÄ, TATU: Magnetostrictive energy harvesting from steel
Master of Science Thesis, 100 pages
May 2018
Major: Embedded systems
Examiners: Professor Pekka Ruuskanen and Professor Jukka Vanhala
Keywords: Energy harvesting, magnetostriction, magnetoelasticity, elastic wave, impedance matching, rectification

Energy harvesting is defined as electronic devices acquiring the energy they need to operate from their environment. Potential energy sources in the environment include light, temperature gradients, electromagnetic radiation and kinetic energy. The development of energy harvesting technologies together with a drop in the energy consumption of electronic devices may in the near future make many devices energy independent, which means a drop in the maintenance need of the devices, greater reliability and a reduction in the amount of battery waste.

The main aim of the experimental part of this thesis was to present and further develop a new kinetic energy harvesting method, which can harvest energy from elastic waves propagating in steel structures, and to develop harvesting electronics that can be used with the new method. This new method is based on the magnetoelastic effect, which is a natural phenomenon that causes the magnetization of a ferromagnetic material to change when the dimensions of the material are changed. This phenomenon is also known as the inverse magnetostrictive effect. A change in the magnetization of a material will also cause a change in the magnetic flux passing through the material. Since a change in the magnetic flux of a coil will induce and electromotive force in the coil, the magnetoelastic effect can be utilized in energy harvesting. The basic idea behind the new method is harvesting energy from an impact loaded steel bar with a coil wound around the bar. Impact loading a steel bar will cause an elastic wave to propagate along the bar, which will cause alternating compressive and tensile stresses in the steel bar. Since steels are ferromagnetic materials, the strains will alter the magnetization of the bar inducing an electromotive force in a coil around the bar. Thus a part of the kinetic energy carried by the elastic is transduced to electrical energy. In the experimental part a test setup, an experimental harvesting generator and electronic harvesting circuits, to be used with the method, were implemented. The mean power that can be achieved with the experimental method depends on the magnitude and frequency of the impact loading, but during testing mean output power of the harvesting generator was between 1-5 mW, when an elastic wave was propagating in the bar. This is a sufficient mean power for a low power wireless sensor.

The thesis also includes a literature survey, which aims to give the reader basic knowledge of existing kinetic energy harvesting methods and magnetostrictive phenomena.

CONTENTS

ABBREVIATIONS AND NOTATIONS

A	gain
A	cross sectional area
d	damping coefficient
d	piezoelectric strain coefficient
d	distance
D	duty cycle
$\mathbf{d_e}$	electrical damping coefficient
$\mathbf{d_m}$	mechanical damping coefficient
$\mathbf{d'_{33}}$	magnetoelastic coupling coefficient
$\mathbf{d_{33}}$	magnetostrictive coupling coefficient
E	Young's modulus
e.m.f	electromotive force
F	force
H	magnetic field strength
K	transistor transconductance factor
k	spring constant
k	coupling coefficient
L	electrical inductance
l	length
m	inertial mass
P	power
B	magnetic flux density
$\mathbf{P_d}$	damping power
$\mathbf{P_e}$	electrical damping power
Q	Q factor of an RLC circuit
Q	electric charge
R	electrical resistance
$\mathbf{R_s}$	series resistance
S	effective surface area of a coil
$\mathbf{S^H}$	elastic compliance
T	cycle time
$\mathbf{T_c}$	curie temperature

U	Energy or work
V	voltage
W	width
$\mathbf{Y_0}$	amplitude of vibration
ε	absolute permittivity
ε	strain
ζ	damping factor
ζ_e	electrical damping factor
ζ_m	mechanical damping factor
η	efficiency
σ	mechanical stress
σ	stress
φ	magnetic flux
ω	angular frequency
ω_n	natural frequency of a resonator

1 INTRODUCTION

Energy harvesting is defined as electronic devices powering themselves partially or entirely with ambient energy obtained from their operational environment. Currently batteries are the most typical way of powering wireless electronic devices, but the constantly falling energy consumption of electronic circuits has made powering wireless devices with small amounts of energy harvested from the environment increasingly feasible. Powering wireless devices with harvested energy can help make commnon wireless devices more compact and maintenance free, since the need for bulky batteries, that need to be periodically replaced, may be entirely removed. Energy harvesting also plays a large part in making many new technologies, such as wireless networks, wearable or implantable devices and internet of things devices, more practical, as in many cases powering these devices with wiring or batteries is impractical. Unsurprisingly many academic articles, addressing the subject, have been published in recent years. [1][2]

The potential energy sources commonly presented by academic sources are light or other electromagnetic radiation, thermal gradients and kinetic energy.[3] This master's thesis focuses on kinetic energy harvesting, which means using any movement in the environment to generate electrical energy.[4] Creating electrical energy from kinetic energy obviously requires the use of some mechanism, that transduces kinetic energy into electrical energy. Transduction mechanisms, that are most commonly addressed by academic publications, are piezoelectricity, electromagnetic induction and electrostatic force.[4][5] Recently some articles, proposing the use of magnetostriction or triboelectricity for transducing kinetic energy to electrical energy, have been published.[6][7][8]

The aim of this master's thesis is to give a brief overlook into kinetic energy harvesting, presenting and testing a new magnetostriction based energy harvesting method and developing harvesting electronics to be used with the new method.

The overlook into kinetic energy harvesting is given as a literature survey. The literature survey consists of chapters 2-5. Chapter 2 takes a brief look into kinetic energy harvesting methods in general and more specifically into energy harvesting from ambient vibrations. Chapter 3 briefly explains how the most commonly used transduction mechanisms function. Chapter 4 takes a brief look into magnetostrictive phenomena and

presents a few energy harvesting applications suggested in academic publications. Chapter 5 gives an overlook of electronic circuits used for conditioning and storing harvested electrical energy.

Chapter 6 presents an entirely new magnetostriction based energy harvesting method. The new method, like all magnetostrictive energy harvesting methods, is based on the inverse magnetostrictive effect or the magnetoelastic effect, which causes the density of the magnetic flux passing through a ferromagnetic material to change when the material is deformed[6]. The change in the magnetic flux can induce a voltage in a coil and thus generate electrical energy. Unlike previously presented magnetostrictive energy harvesting methods, the new method directly harvests energy from elastic waves propagating in structural steel by using the steel itself as the magnetostrictive material.

Chapter 7 presents a test setup for testing the new method. The chapter also presents an experiment for testing how much power the method can deliver to a simple resistive load. The coupling coefficient of the method is also estimated.

Chapter 8 presents experimental harvesting electronics developed for use with the new harvesting method. Three different alternative rectifiers and two alternative voltage conditioning circuits were developed.

Chapter 9 presents test results obtained with the developed experimental harvesting electronics. The rectifying circuits were tested independently using a function generator as an input voltage source. The voltage conditioning circuits were tested with the test setup presented in chapter 7 to determine how much energy could be harvested and stored in a rechargeable battery.

Chapter 10 summarizes all the preceding chapters and presents conclusions. The chapter also presents ideas for future work.

2 KINETIC ENERGY HARVESTING

Mechanical energy can be found almost anywhere in the form of vibrations, compressive or tensile stresses, linear motion and rotational motion which makes kinetic harvesting this energy an appealing way of powering wireless sensors and other energy autonomous devices. The source of mechanical energy can for instance be human movement or vibrating machinery.[4]

Obviously electronic devices can not be directly powered by kinetic energy. Thus some way of transducing the kinetic energy into electrical is needed and various mechanisms can be utilized for this purpose. Kaźmierski and Beeby [4] present piezoelectric, electromagnetic and electrostatic transducers as commonly used types of transducers. Recently, using the inverse magnetostrictive effect, or magnetoelastic effect, for transducing kinetic energy has received some attention and academic papers, such as [6] and [7], proposing it's use have been published.

The kinetic energy harvesting method most often seen in academic publications seems to be a resonant spring mass system intended for harvesting energy from ambient vibrations. The basic idea behind this method is having a spring suspended mass that begins oscillating when the system is subjected to ambient vibration. The oscillation of the mass is damped electrically by some transduction mechanism and thus electrical energy is produced. In most application environments the amplitudes and accelerations of the ambient vibrations are very small and the resonant spring mass system is the only practical way of extracting meaningful amounts of energy. However a spring mass system will only vibrate strongly at it's characteristic frequency. If there are no ambient vibrations matching the characteristic frequency, the spring mass system will not resonate and the output power of the generator will fall drastically. In other words, the bandwidth of resonating vibration generators is limited. This energy harvesting method is explained in greater detail in subchapter 2.1. [4][5]

As previously stated, kinetic energy exist in the environment in many different forms. Many methods for harvesting these forms of energy have also been proposed in academic publications, but as many of these are unique and very application specific meaningfully summarizing or classifying all these is not possible.

2.1 Linear vibration energy harvesting

One of the few ways of harvesting energy from small vibrations in the environment is a resonating spring mass system generator. In many academic sources, such as [4], [5] , [9], [10], [11] this seems to be treated as the default solution for vibration energy harvesting.

Such a system can be modeled as a simple single degree of freedom damped spring mass resonator. An illustration of such a model can be seen in Fig. 2.1 The model consists of an inertial mass *m,* a spring with a spring constant *k* and a damping coefficient *d* made up of both electric damping d_e and mechanical damping d_m which represents friction, air resistance etc. The inertial mass *m* represents whatever oscillating mass the generator has. The spring with spring constant *k* represents whatever factors that resist the displacement of the mass from it's equilibrium position. The damping coefficient d_e represents damping due to the transduction of kinetic energy to electrical energy and d_m represents damping due to other factors such as friction and air resistance. Thus the basic idea behind this kind of generator is that vibrations in the environment cause a relative displacement of the inertial mass, which means kinetic energy from the environment is transferred to the spring-mass system. The kinetic energy is then transduced to electrical energy through the electrical damping.[12]

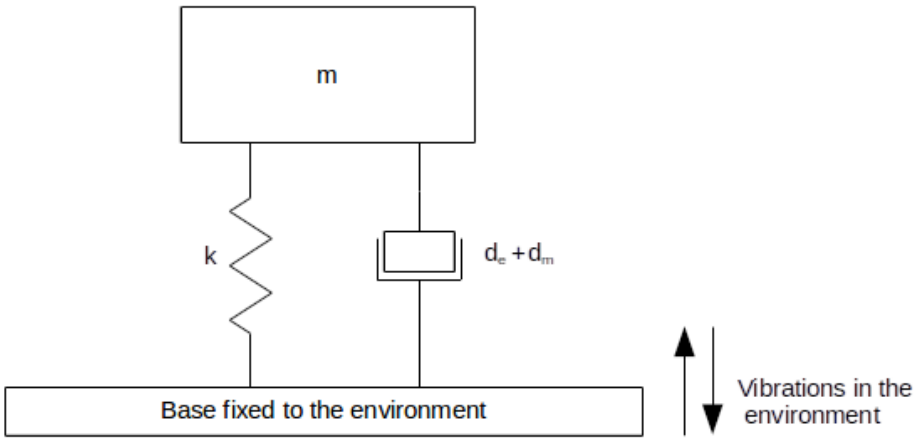

Figure 2.1 *Linear vibration energy harvesting model.*

It should be noted the this model is not tied to any specific transduction mechanism or detailed implementation. The only requirement for the applicability of this model is that the generator being modeled is linear; i.e. that the spring force is linearly relative to the displacement of the mass and the damping is linearly relative to the speed of the change of the displacement.[9]

The sum of forces and accelerations acting on the inertial mass can be described by

$$mz''(t)+(d_m+d_e)z'(t)+kz(t)=-my''(t)\ .[9] \tag{2.1}$$

In the above equation *z(t)* represents the displacement of the inertial mass from it's resting position or the spring deflection. *y(t)* represents the displacement of the entire generator caused by the vibrations in the environment.[9]

If the vibration in the environment is sinusoidal the mean power dissipated in the total damping of the generator is

$$P_d=\frac{m\zeta_T Y_0^2(\omega/\omega_n)^3\omega^3}{(1-\omega/\omega_n)+(\zeta_t(\omega/\omega_n))^2}\ .[9] \tag{2.2}$$

In the above equation Y_o is the amplitude of the vibration, ω is the angular frequency of the vibration, ω_n is the natural frequency of the system and ζ_T is the total damping factor of the system. The total damping factor ζ_{Tt} is made up of the electrical damping ζ_e factor and ζ_m. Thus $\zeta_{T=}\ \zeta_{m+}\ \zeta_e = (d_{e+}d_m)/2m\omega_n$. The natural frequency of the resonator is determined by

$$\omega_n=\sqrt{\frac{k}{m}}\ .[9] \tag{2.3}$$

The power dissipated in the electrical damping, i.e. the electrical power produced, is determined by

$$P_e=\frac{m\zeta_e Y_0^2(\omega/\omega_n)^3\omega^3}{(1-(\omega/\omega_n)^2)^2+(2\zeta_t(\omega/\omega_n))^2}\ .[9] \tag{2.4}$$

From the equation above it can be seen that the produced electrical power is proportional to the cube of the frequency. This means that much more power will be generated in applications where the frequency of ambient vibration is high. It can also be seen that

the natural frequency affects the produced power. The maximum electrical power, for a given vibration frequency, is achieved when the natural frequency is tuned to exactly match the ambient vibration. The maximum electrical power is thus

$$P_e = \frac{m\zeta_e Y_0^2 \omega_n^3}{4\zeta^2} .[9] \tag{2.5}$$

Williams et al. [12] note that the selectivity of the generator depends on the total damping factor. If the damping factor is small, the power achieved when the ambient vibration matches the natural frequency of the generator is large. However a small damping factor also results in the electrical power falling steeply when the ambient vibrations don't match the natural frequency. Conversely a large total damping factor results in a smaller power at the natural frequency, but also a greater useful bandwidth. Fig. 2.2 shows the effect of different damping factors on dissipated power, as a function of frequency.

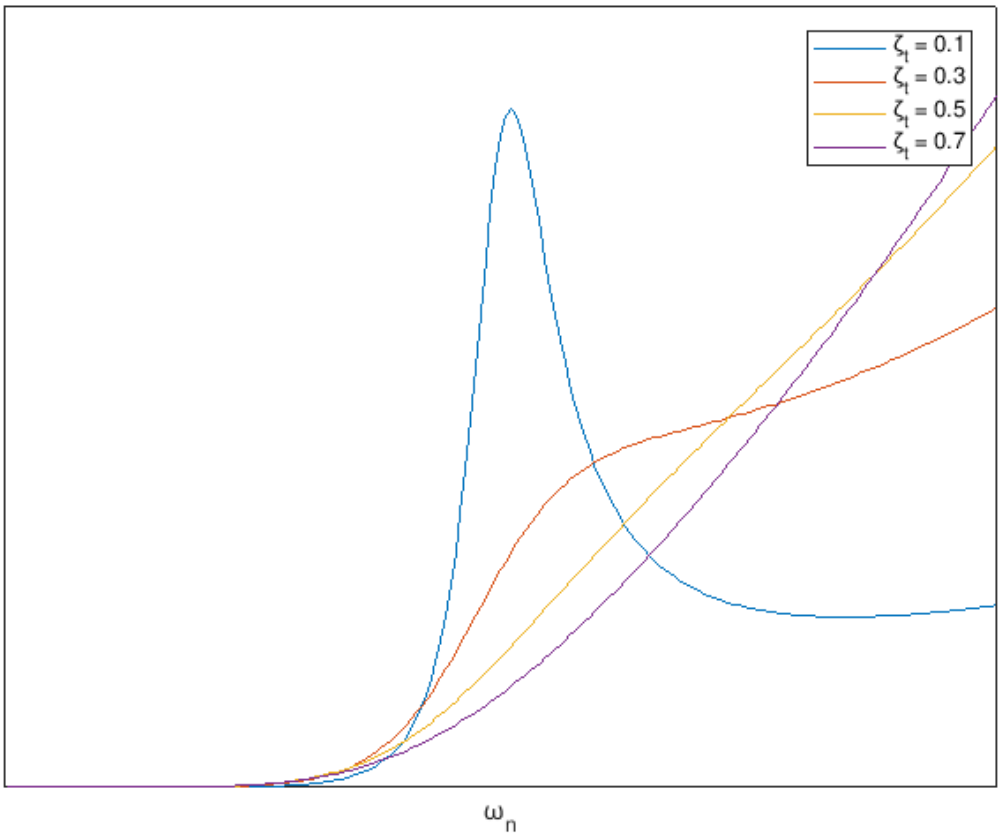

Figure 2.2 *Dissipated power with different damping coefficients as a function of frequency.*

The above figure shows, that if the ambient vibrations are focused around a certain point, power generation can be increased by tuning the resonator to this point and having a low damping coefficient. On the other hand, if the ambient vibration is spread over a broad spectrum, a higher damping would be beneficial for harvesting energy from a broader frequency spectrum.

3 TRANSDUCTION MECHANISMS

This chapter presents the transduction mechanisms, besides the inverse magnetostrictive phenomenon, that are most often utilized for transducing kinetic energy to electrical energy. The chapter focuses on the causes of the phenomena and their relevant properties for energy harvesting. Detailed descriptions of energy harvesting schemes utilizing these mechanisms will not be discussed here.

When transduction is accomplished by deforming or straining a material that can directly transduce kinetic energy into electrical or magnetic energy, an important property of the material is it's coupling coefficient. The high coupling coefficient of magnetostrictive transducers is a factor that is often stressed in academic publications, such as [4][5] and [6], addressing the subject. According to Bright [13] coupling coefficient k of a transducer is defined as the quotient of the transduced energy and the input energy of the transducer. The transduced energy is made up of the output energy of the transducer and energy stored in the transducer.[13] Thus the coupling coefficient can be defined as

$$k = \frac{U_{output} + U_{stored}}{U_{input}}, \tag{3.1}$$

where U_{output} is the output energy of the transducer, U_{stored} is energy stored in the transducer and U_{input} is the input energy of the transducer. It should be noted that this can be applied to any system where energy is transduced from one form into an another. In the context of kinetic energy harvesting the relevant case is the case where mechanical energy, that is used to deform a transducing material, is the input energy.[14] In this case the coupling coefficient is

$$k = \frac{U_{output} + U_{stored}}{U_{mechanical}}, \tag{3.2}$$

where $U_{\text{mechanical}}$ is the mechanical work done to deform the transducing material.

3.1 Piezoelectricity

Piezoelectricity is defined as the tendency of some dielectric crystals to polarize electrically when an external mechanical stress causes a strain in the material. Electric polarization in a dielectric material will cause an electric field in the material, which results in an electric potential being developed between the surfaces of a piece of piezoelectric material if the surfaces are electrically isolated from each other. If the surfaces are electrically connected to each other a charge will flow from one surface to the other one. This phenomenon also works conversely; applying an external voltage to a piece of piezoelectric material will create an electric polarization inside the material and thus cause a mechanical strain in it.[15]

Explaining the cause of piezoelectricity in detail is beyond the scope of this master's thesis, but a brief explanation with an example will be given here. The direct piezoelectric effect is caused by a deformation of a centrally asymmetric crystal. Many different kinds of crystal structures exhibit piezoelectricity but an absolute requirement for piezoelectricity is central asymmetry. Gränicher [15] presents zincblende (ZnS) as an example of a simple piezoelectric crystal. Fig 3.1 shows the crystal structure of zincblende presented by Gränicher [15]. It should be noted that the structure shown in Fig. 3.1 is only a part of zincblendes complete unit cell, but since the unit cell is made up of similar tetrahedrons, examining this part is sufficient for explaining zincblendes piezoelectricity. The sulfur ions of zincblende, located in the corners of the tetrahedron, are negatively charged. The zinc ion in the center of the tetrahedron is positively charged. Stressing the pictured structure in the xy-plane will cause edge AB to elongate or contract depending on the direction of the stress. When edge AB is elongated or contracted the reverse happens to edge CD. This will cause the zinc ion in the middle to be displaced along the z-axis, either up or down, which will result in an electric dipole moment being developed in the structure. Since the tetrahedral structure shown here repeats in zincblende and the tetrahedrons all have the same orientation, the dipole moments add up and a net polarization is developed, when zincblende is subjected to mechanical stress.[15]

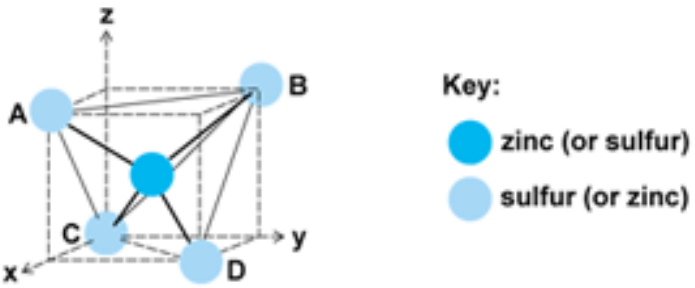

Figure 3.1 *Partial crystal structure of zincblende. [15]*

Since mechanical strain in a piece of piezoelectric material will create an electric potential across the piece, piezoelectricity can obviously be used to transduce kinetic energy in to electrical energy. The basis of all piezoelectric energy harvesting schemes is to use kinetic energy from the environment to cause a strain in a piece of piezoelectric material and then use the energy of the electric potential to power electronic devices.[11]

According to Roundy [16] a piece of piezoelectric material undergoing strain can be electrically modeled as a series connection of a voltage source, a capacitor and a resistor. Fig. 3.2 shows a depiction of such a model connected to a resistive load.

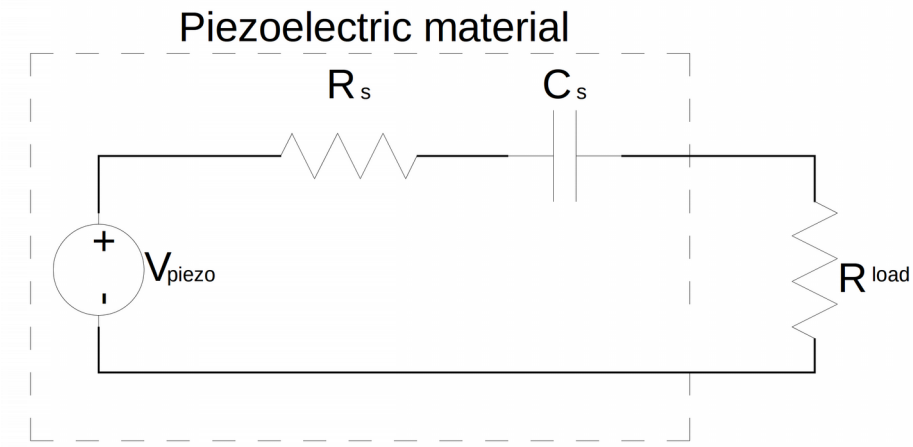

Figure 3.2 *Piezoelectric generator connected to a resistive load.*

According to Roundy [16] the open loop voltage V_{piezo} is determined by

$$V_{piezo} = \frac{-dt}{\varepsilon}\sigma \text{ [16]}, \tag{3.3}$$

where d is the piezoelectric strain coefficient of the material, t is the thickness of the material, ε is the permittivity of the material and σ is the mechanical stress applied to the material.

If the piezoelectric material undergoes periodic variations in the applied stress, V_{piezo} becomes an alternating voltage and current will flow to the load resistor. This means energy is dissipated in the load resistor and thus mechanical energy is transduced to electrical energy.

According to Kaźmierski et al. [4] piezoelectric transducers are characterized by relatively high output voltages, low output currents and high output impedances. Piezoelectric transducers have the benefits of a simple mechanical structure and good compatibility with MEMS processes. On the other hand piezoelectric materials are relatively fragile.

3.2 Electromagnetic

According to Faraday's law of induction a changing magnetic flux through the surface of a conducting circuit will induce an electromotive force, oi the circuit. The induced electromotive force is proportional to the time derivative, or the rate of change, of the magnetic flux. Thus the induced electromotive force is

$$e.m.f = -\frac{d\varphi}{dt}, \tag{3.4}$$

where φ is the magnetic flux. The magnetic flux is a product of the effective surface area of the circuit and the average magnetic flux density passing through the surface. Assuming that the effective surface area remains constant, the induction of an electromotive force is caused by a change in the magnetic flux density. Thus the electromotive force induced in the circuit will be

$$e.m.f = -S\frac{dB}{dt}, \tag{3.5}$$

where S is the effective surface area of the circuit and B is the average magnetic flux density passing through the surface. If the conducting circuit is a coil made up of several turns, the electromotive force equals the sum of the electromotive forces induced in the turns of the coil. If all the turns have the same effective surface area and the magnetic flux density is uniform across the coil, the induced electromotive force is

$$e.m.f = -nS\frac{dB}{dt}, \tag{3.6}$$

where n is the number of turns in the coil.

This natural phenomenon can be utilized in kinetic energy harvesting, typically by producing a magnetic field with strong permanent magnets and using kinetic energy from the environment to move a coil relative to the magnetic field. Most academic publications, such as [4],[5] and [11], seem to address using electromagnetic induction for harvesting energy from ambient vibration, but theoretically it could be used to scavenge energy from any kind of cyclic motion.

When electromagnetic induction is used for harvesting energy from ambient vibrations, using a spring mass resonator system , either the permanent magnet or the coil can be fixed to the frame of the generator while the other is fixed to the inertial mass. When ambient vibrations cause the inertial mass of the generator to move relative to the frame, the permanent magnet and the coil are moved in relation to each other as well, and an electromotive force is induced in the coil.[4]

When the permanent magnet and the coil are moved relative to each other, the magnetic flux density passing through the coil changes as function of relative displacement(z) [5]. As the induced electromotive force is proportional to the time derivative of the magnetic flux density and the magnetic flux density is proportional to the relative displacement the induced electromotive force is

$$e.m.f = -nS\frac{dB}{dz}\frac{dz}{dt}. \tag{3.7}$$

If the coil of the energy harvester is connected to a resistive load, current will flow through the load and the coil. This means that power is transferred to the load. The current flowing through the coil will also create a magnetic field, that opposes the magnetic field which induced the current. This opposing field will cause a force which opposes the relative movement of the coil and the permanent magnet. In other words the relative movement is electrically dampened and kinetic energy is transformed to electrical energy.[5]

Fig. 3.3 shows an electrical representation of an electromagnetic generator connected to a resistive load. R_s represents the resistance of the coil wire, L_s represents leakage inductance of the coil and R_l represents the load resistance. In the depicted circuit, the sum of the voltages is

$$e.m.f - I(R_s + R_l) - L_s \frac{dI}{dt} = 0 \,. \tag{3.8}$$

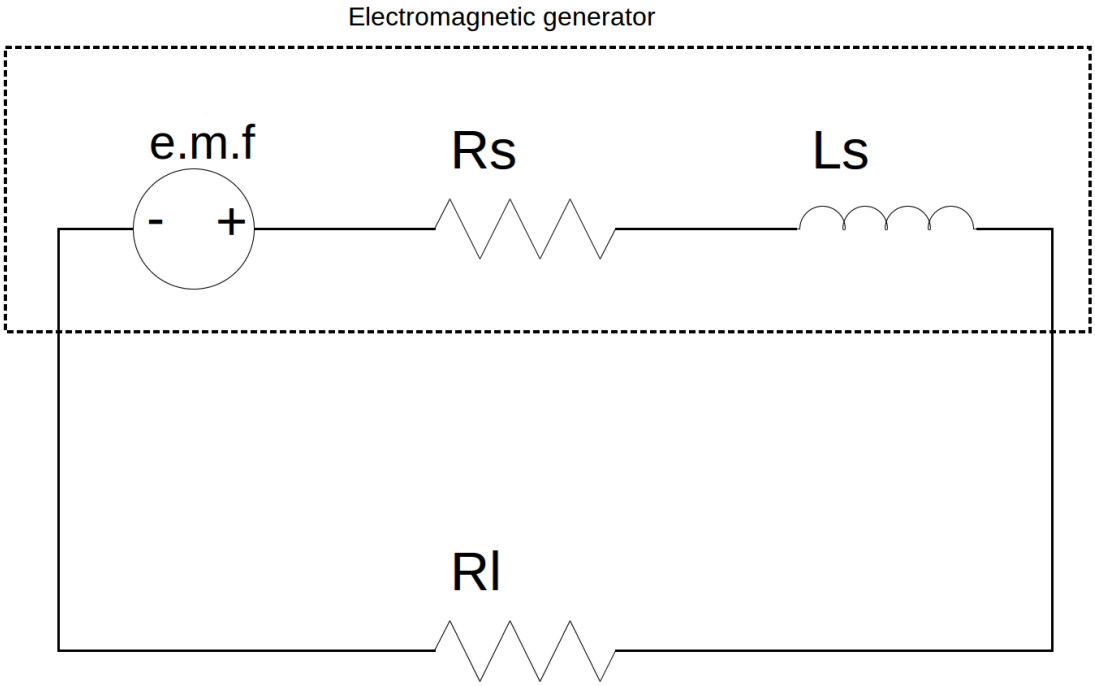

Figure 3.3 *Electromagnetic generator connected to a resistive load.*

According to Kaźmierski et al. [4] and Priya et al. [5] L_s is in most cases insignificant and coil impedance is dominated by it's resistance. For the sake of simplicity we will assume here that $L_s=0$. Now the above equation becomes

$$e.m.f - I(R_s + R_l) = 0 \,. \tag{3.9}$$

Electrical power extracted through the electrical damping is thus

$$P_e = \frac{e.m.f^2}{(R_s + R_l)}. \tag{3.10}$$

Since the power is extracted through the electric damping force, the extracted power must also fulfill the condition

$$P_e = F_{damping}\frac{dz}{dt} = \frac{e.m.f^2}{R_s + R_l}. \tag{3.11}$$

From the above we can see that the damping force must be

$$F_{damping} = \frac{e.m.f^2}{(R_s + R_l)\,dz/dt}. \tag{3.12}$$

If the definition of electromotive force from equation 3.4 is placed to the above equation, the damping force become

$$F_{damping} = \frac{\left(-nS\frac{dB}{dz}\frac{dz}{dt}\right)^2}{(R_s + R_l)\,dz/dt} = \frac{\left(-nS\frac{dB}{dz}\right)^2}{R_s + R_l}\frac{dz}{dt}. \tag{3.13}$$

From the above we can see that the electric damping coefficient d_e must be

$$d_e = \frac{\left(-nS\frac{dB}{dz}\right)^2}{R_s + R_l}. \tag{3.14}$$

Thus it has been shown that the electrical damping coefficient in the case of an electromagnetic harvester is determined by loading, the number of turns in the coil, effective surface area of the coil, coil resistance and magnetic flux density gradient. Aside from the load impedance, these factors are determined by the strength of the permanent magnet/magnets and their arrangement and the design of the coil.[5]

Kaźmierski et al. [4] compare electromagnetic transducers to other alternatives and note that electromagnetic transducers have the benefit of high output currents and do not re-

quire mechanical constraints or an external voltage source. On the other hand Kaźmierski et al. [4] state that electromagnetic transducers produce low output voltages, are difficult to integrate in to MEMS fabrication processes and perform poorly in a micro scale.

3.3 Electrostatic transducers

Electrostatic transducers are essentially based on a capacitor, whose capacitance is varied.[4][5] The energy stored in a capacitor can be expressed as

$$U = \frac{1}{2}\frac{Q^2}{C}, \tag{3.15}$$

where Q is the charge stored in the capacitor and C is the capacitance of the capacitor. Alternatively the energy could be expressed with

$$U = \frac{1}{2}CV^2 . \tag{3.16}$$

The capacitance of the capacitor can be expressed with

$$C = \frac{\varepsilon A}{d} \tag{3.17}$$

where ε is the absolute permittivity of the dielectric between the capacitor plates, A is the overlapping area of the plates and d is the distance between the plates. If the overlapping area of the plates or their distance was to be changed while the voltage across the capacitor or the charge stored in it was kept constant, energy stored in the capacitor would change. In other words the mechanical work, that was done to move the capacitor plates in relation to each other, would be transduced to electrical energy.

Electrostatic transducers can be divided into three main types on depending on how they move the capacitor electrodes to vary the capacitance. These types are in-plane overlapping, in-plane gap closing and out-of-plane gap closing. The in-plane type transducers have comb-like electrodes whose fingers overlap each other. The capacitance between the electrodes can be varied by either changing the amount overlap between the electrode fingers or by changing the gap between the fingers. The in-plane overlapping type changes the amount of overlap and the in-plane gap closing type changes the gap. The

out-of-plane gap closing type varies the capacitance by changing the gap between two large electrodes. Fig. 3.4 shows a depiction of each type of transducer.[4]

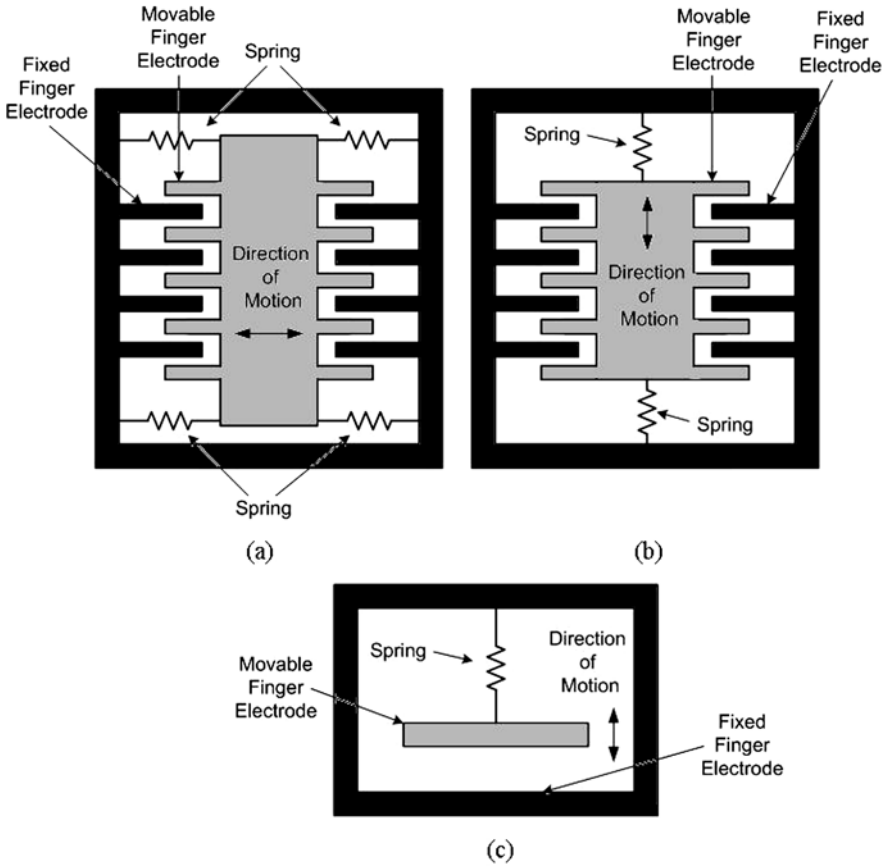

Figure 3.4 *Electrostatic transducer types (a) in-plane overlap; (b) in-plane gap closing; and (c) out-of- plane gap closing. [4]*

As previously stated either the voltage across the transducer capacitor or the charge stored in it has to stay constant, while the capacitance varies. This means that electrostatic tranducers can be operated in two distinct modes: the voltage constrained mode or the charge constrained mode. [4]

In the voltage constrained mode the voltage across the capacitor is indeed held constant and, as the capacitor electrodes are moved so that the capacitance is reduced, charge flows from the capacitor to the electric load. The electric energy gained from the movement of the electrodes is in this case

$$U_{voltage\ constrained} = \frac{1}{2}(C_{max} - C_{min})V^2 \text{ .[17]} \tag{3.18}$$

In the charge constrained mode the charge stored in the capacitor is kept constant (i.e. the capacitor is open-circuited) when the electrodes are moved. Thus the voltage across the capacitor changes to satisfy the condition

$$V = \frac{Q}{C} \text{ [17].} \tag{3.19}$$

When the electrode movement has reached its limit, the capacitor is connected to the electric load and the energy stored in the capacitor is transferred to the load. The energy obtained in this case is:

$$U_{charge\ constrained} = \frac{1}{2}(C_{max} - C_{min})V_{max}V_{start} \text{ [17].} \tag{3.20}$$

Kaźmierski et al. [4] state that electrostatic transducers are characterized by relatively high output voltages, low output currents and high output impedances. Electrostatic transducers are easily integrated into MEMS processes, but need mechanical constraints for their movement. Electrostatic transducer also have the major drawback of needing an external voltage source for electrifying the transducer. Alternatively the transducer plates may be made of precharged electret.[4]

4 MAGNETOSRICTIVE PHENOMENA IN FERROMAGNETIC MATERIALS

4.1 Basics of magnetostriction

The dimensions of ferromagnetic materials change when their magnetization changes. This means that changing the external field being applied to the material will change its dimensions, or in other word cause a strain in it. This effect is called magnetostriction. The strains that can be caused by an external magnetic field are typically very small. Even in strongly magnetic materials saturation magnetostriction, or the strain between zero magnetization and saturation magnetization, is typically in the range of 10^{-5}. Increasing the strength of the external magnetic field being applied to the material beyond what is required for magnetic saturation, will cause a further strain in the material, but this effect is extremely weak. Thus saturation magnetostriction could practically be considered the largest strain that can be caused by an external magnetic field.[18]

The change of dimensions in a magnetic material due to a change in its magnetic state is also known as the Joule effect and it is only one of several different magnetostrictive effects. Magnetostriction also works inversely i.e. a change in the dimensions of a magnetic material causes a change in it's magnetic state. This is known as the magnetoelastic effect or alternatively the Villari effect or the magnetomechanical effect. This change in the magnetic state means that energy is being transduced from the elastic state to the magnetic state. The change in the magnetic state can induce an electromotive force in to a coil according to Faraday's law of induction. Thus the magnetoelastic effect could be utilized in energy harvesting.[6]

There are several other magnetostrictive effects as well. These effects can among other things change the volume, or elasticity of a material.[6] Since these effects do not pertain to energy harvesting, they will not be further discussed here.

4.2 Cause of magnetostriction

Magnetostriction is mainly caused by spin-orbit coupling. Spin-orbit coupling is an interaction between the spin of an electron and its orbit. Due to spin-orbit coupling, when a magnetic field reorients the spin of an electron, the orbit of that electron also changes. [18]

The effect of spin orbit coupling is depicted in Fig. 4.1. The figure shows a row of atoms in a crystal at different temperatures and external magnetic fields. The dots in the figure are atomic nuclei, the arrows represent the magnetic moment of atoms and the ovals represent the electron clouds of atoms.[18]

The uppermost row shows atoms at temperatures above their curie temperature T_c. Since all substances are paramagnetic above their curie temperature, there will be no spontaneous magnetization and thus no spontaneous magnetostriction. The middle row shows atoms in temperatures below T_c and in a zero external magnetic field. Below the curie temperature spontaneous magnetization occurs in ferromagnetic materials. If there is any magnetic anisotropy in the material, the spins orient according to it, and due to spin-orbit coupling, the electron cloud is also oriented according to the anisotropy. The reorientation of electron clouds will force atomic nuclei farther apart from each other in the direction of anisotropy, leading to a strain. This is called spontaneous magnetostriction. If a ferromagnetic material is exposed to a strong external magnetic field, as in the lowest row of Fig. 4.1, the external magnetic will reorient electron spins and electron clouds through spin-orbit coupling. The reorientation of electron clouds will have an effect on the distances between atomic nuclei and thus cause a strain in the material. [18]

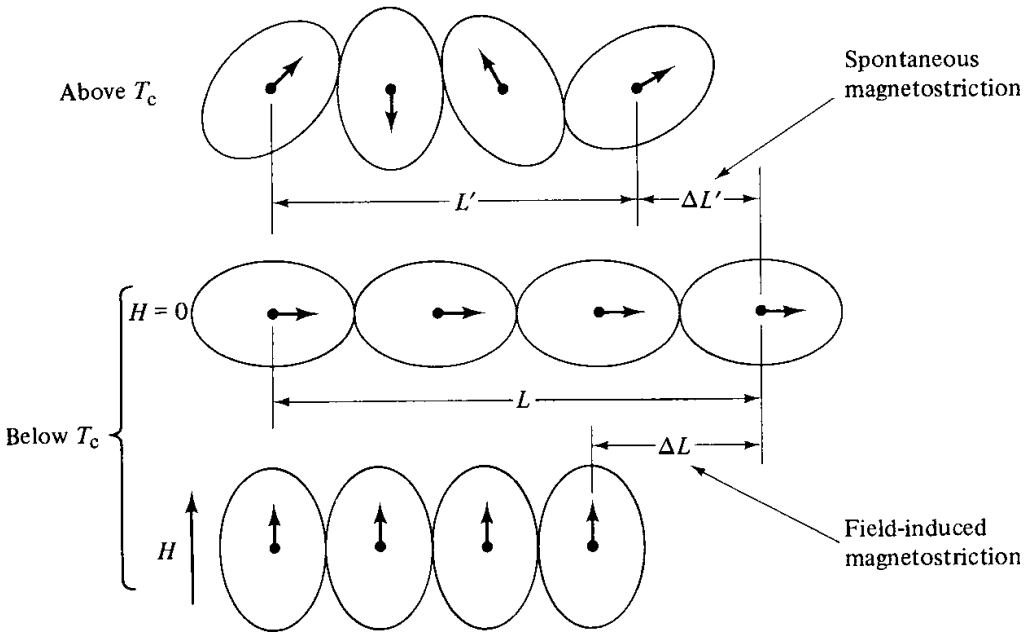

Figure 4.1 *Mechanism of magnetostriction.[18]*

It should be noted that the strains depicted above are vastly exaggerated. As previously stated strains caused by magnetostriction are typically in the order of 10^{-5}.

The smallness of strains, that magnetostriction causes in most materials, is easy to understand if the cause of magnetostrictrion is kept in mind. In most ferromagnetic materials spin-orbit coupling is very weak and thus an external magnetic field will not reorient electron orbits to any significant degree. Conversely the minority of materials, that have relatively large saturation magnetostriction, have strong spin-orbit coupling. A factor, that also contributes to the magnitude of magnetostriction, is the shape of an atoms electron cloud; a strongly nonspherical electron cloud increases the strength of magnetostriction. [18]

4.3 Inverse magnetostrictive effect

As previously stated the strains that can be caused by magnetostriction are small. Even the saturation magnetostriction of dysprosium, which Cullity [18] mentions as an example of a material with a large saturation magnetostriction, is only about $4.5*10^{-3}$.[18] This however does not mean that the phenomenon is inconsequential. Because of magnetostriction, mechanical stress can strongly affect the magnetic properties of ferromagnetic materials. For energy harvesting applications the most significant effect is the change in permeability, since a change in permeability affects magnetic flux density in

the material, which can induce an electromotive force in a coil. Because mechanical stress can change the permeability of a material significantly, the inverse magnetostrictive effect can create a strong coupling between the mechanical and magnetic domains. In energy harvesting applications electromechanical coupling coefficients as large as 0.9 have been achieved with special magnetostrictive materials.[18][6]

Fig. 4.2 shows the effect of mechanical stress on the magnetization of iron. The figure shows the magnetization curves for iron, when it is not mechanically stressed, when it is subjected to a tensile stress and when it is subjected to a compressive stress. From the figure it can be seen that, at external field strengths of less than about 20 Oe, compressive stress increases the magnetic flux density of the material while tensile stress reduces it. The effect of compressive stress is not significant, but tensile stress can decrease flux density in the material by about 40% at best. Interestingly the effect reverses when the external magnetic field strength is increased above about 20 Oe. This is due to the direction of iron's magnetostriction. At low fields the magnetostriction of iron is positive while at strong fields it is negative. [18]

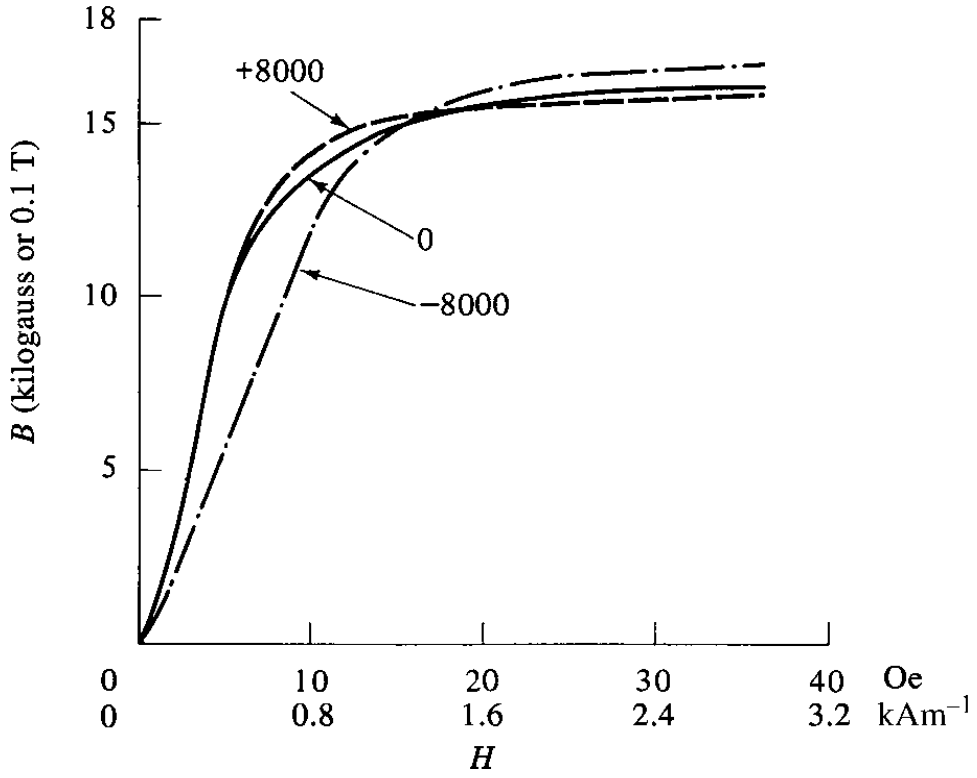

Figure 4.2 *The effect of stress on the magnetization of iron.[18]*

A few other interesting things can be seen from Fig. 4.2. If the magnetic field strength in the material is zero, mechanical stress does not affect the magnetic flux density in the material. This applies to all ferromagnetic materials. If a material is to be used for transducing mechanical energy to magnetic energy, it needs to be magnetized to some degree either by an external magnetic field or residual magnetism. The figure also shows that the change in magnetic flux density varies depending on the magnetic field strength. To maximize the coupling between mechanical and magnetic domains, the material should ideally be magnetized to the point, where the change in magnetic flux density caused by mechanical stress is the greatest.

4.4 Effects of mechanical stress on magnetic domain structures

Since a change in the magnetization of a material is not possible without a change in the magnetic domain structure, stress ,that changes the magnetization of a material, obviously has to have an effect on the domain structure of magnetic materials. Domain structures thus play an integral part in magnetostrictive phenomena. [18]

Fig. 4.3 shows a partial domain structure of a material with positive magnetostriction under different levels of tensile stress and external magnetic field. In (a) the material is in a zero external field and no stress is being applied to it. In (b) a small tensile stress is being applied to the material, which causes domains with magnetization at right angles to the stress axis to decrease in volume, because these domains have a high magnetoelastic energy. As the stress is increased, as in (c), these domains are eliminated completely. From this state a small applied field can saturate the material, because transitioning to saturation only requires a relatively easy 180° wall motion. The saturated state is depicted in (d). Even though stress alone can cause changes in the domain structure of a demagnetized material, this should not be understood as a change in the net magnetization of the material. The domains are still arranged in way that results in a zero net magnetization. However mechanical stress can make it easier for an external stress to rotate magnetic domains and thus magnetize the material. [18]

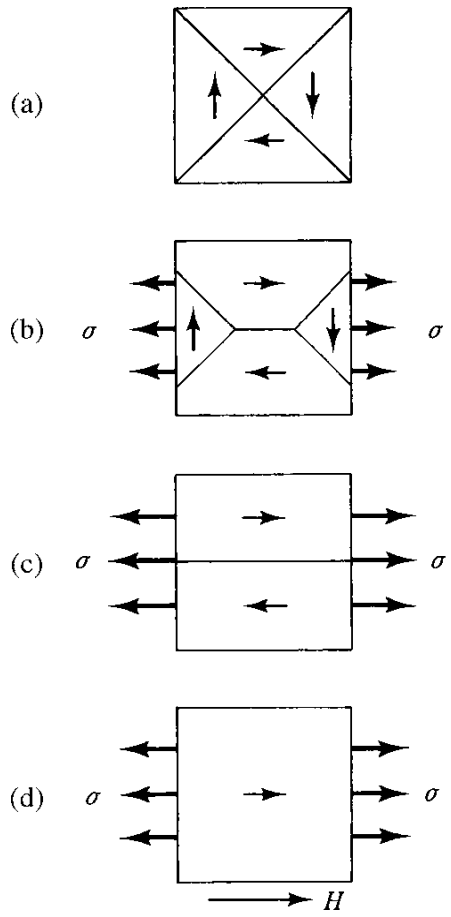

Figure 4.3 *Magnetic domains in a material with positive magnetostriction under tensile stress.[18]*

Likewise compressive stress affects the domain structure of magnetic materials. A picture of material with positive magnetostriction under different compressive stresses can be seen in Fig. 4.4.

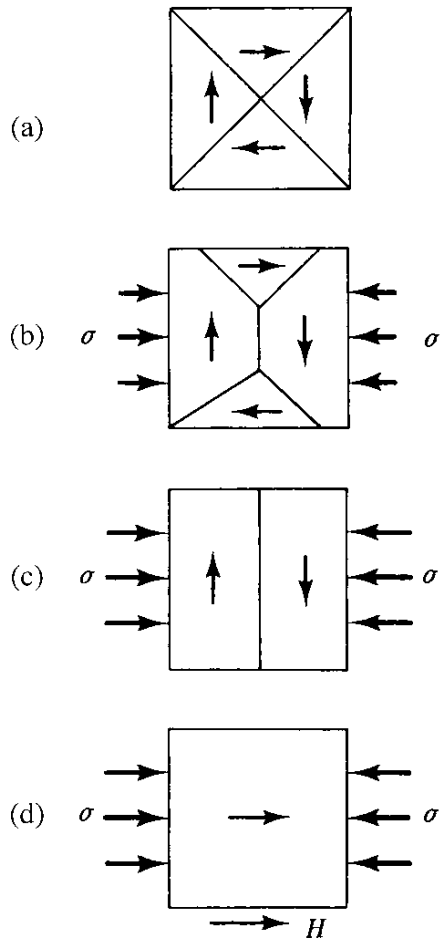

Figure 4.4 *Magnetic domains in a material with positive magnetostriction under compressive stress. [18]*

In Fig. 4.4a the material is in a zero external field and no stress is being applied to it . In Fig. 4.4b a small compressive stress is applied to the material, which causes domains with magnetization at right angles to the stress axis to increase in volume. In Fig. 4.4c increased stress has completely eliminated magnetic domains with magnetization parallel to the stress axis. From this state the material can be saturated by an external magnetic field, but in this case the field has to be stronger, because the field now has to supply enough energy to rotate the magnetization of each domain by 90°. [18]

4.5 Magnetostrictive materials

All ferromagnetic materials exhibit a measurable degree of magnetostriction, but in most materials the effect is too weak to be utilized practical applications.[6] For this reason various materials with strong magnetostrictive properties have been developed. Some of the most commonly used materials will be briefly presented here.

4.5.1 Giant magnetostrictive materials

Rare earth materials tend to exhibit much stronger magnetostrictive properties than most other materials, due to their strong spin-orbit coupling and strongly elliptic electron clouds. For instance terbium and dysprosium have the largest known magnetostriction, though only at very low temperatures close to absolute zero.[18]

Rare earth metals can be alloyed with iron to create materials that have very strong magnetostrictive properties even at room temperatures. Among these are terbium–iron ($TbFe_2$) and Terfenol-D which is an alloy of iron, dysprosium and terbium. These materials are often called giant magnetostrictive materials due to the relatively large magnetostrive strains these materials exhibit. The saturation magnetostriction of these materials can be as large as 2000 microstrains.[6]

Another giant magnetostrictive material which has been proposed for use in energy harvesting is galfenol. Unlike many other strongly magnetostrictive materials galfenol does not contain any rare earth metals but is an alloy of iron and gallium. Galfenol exhibits saturation magnetostriction of around 350 microstrains.[19]

Giant magnetostrictive materials have mostly been applied in actuators, sonar transducers, hydrophones and ultrasonic devices. They can also be used in dynamic sensors such as accelerometers, force sensors, position sensors, and non-contact torque sensors. [6]

4.5.2 Metallic glass

Metallic glasses are magnetic amorphous metal alloys of iron, nickel, and cobalt together with one or more of the following elements: silicon, boron, and phosphorus. Metallic glass differs from most magnetic materials in that, due to its amorphous structure, it has no magneto-crystalline anisotropy. This means that its magnetization is rotated easily and it has low hysteresis.[6]

Some metallic glass alloys can achieve extremely high coupling coefficients of over 0.9, when they have been magnetically annealed. The high coupling coefficient makes metallic glass useful for sensor applications in which external stress or an external magnetic field converts into inductance changes of a metallic glass cored inductor. Despite the high coupling coefficient, metallic glass has not been widely employed in energy harvesting. [6]

4.6 Applications in kinetic energy harvesting

At the time of writing, literature on the use of magnetostriction in energy harvesting seems to be sparse, but a few articles proposing kinetic energy harvesting schemes utilizing the inverse magnetostrictive effect for energy transduction have been published. So far all the detailed published schemes seem to be based on a cantilever beam that has strongly magnetostrictive material laminated on it's surfaces. The basic idea behind this structure is that ambient vibrations or other movement in the environment causes the cantilever beam to flex, which means the magnetostrictive material laminated on the surfaces is strained. This strain causes a change in the magnetic flux passing through the material, and the change in the magnetic flux induces an electromotive force in a pickup coil wound around the cantilever beam. Wang [6], Saber et al. [7], Jafari et al. [20] and Yang et al. [21] propose schemes based on such a cantilever beam generator.

Wang [6] proposes a magnetostrictive kinetic energy harvesting generator, consisting of a copper cantilever beam that has Metglas 2605SC laminated on it's surfaces. According to Wang [6] the metallic glass laminate does not require any external magnetization, since it can be magnetically annealed before use, and the resulting residual magnetism offers sufficient magnetization. Fig. 4.5. shows a picture of the generator. The proposed generator is intended for harvesting energy from ambient vibrations. If the base of the generator was affixed to a vibrating environment, the ambient vibrations would cause the cantilever to vibrate.

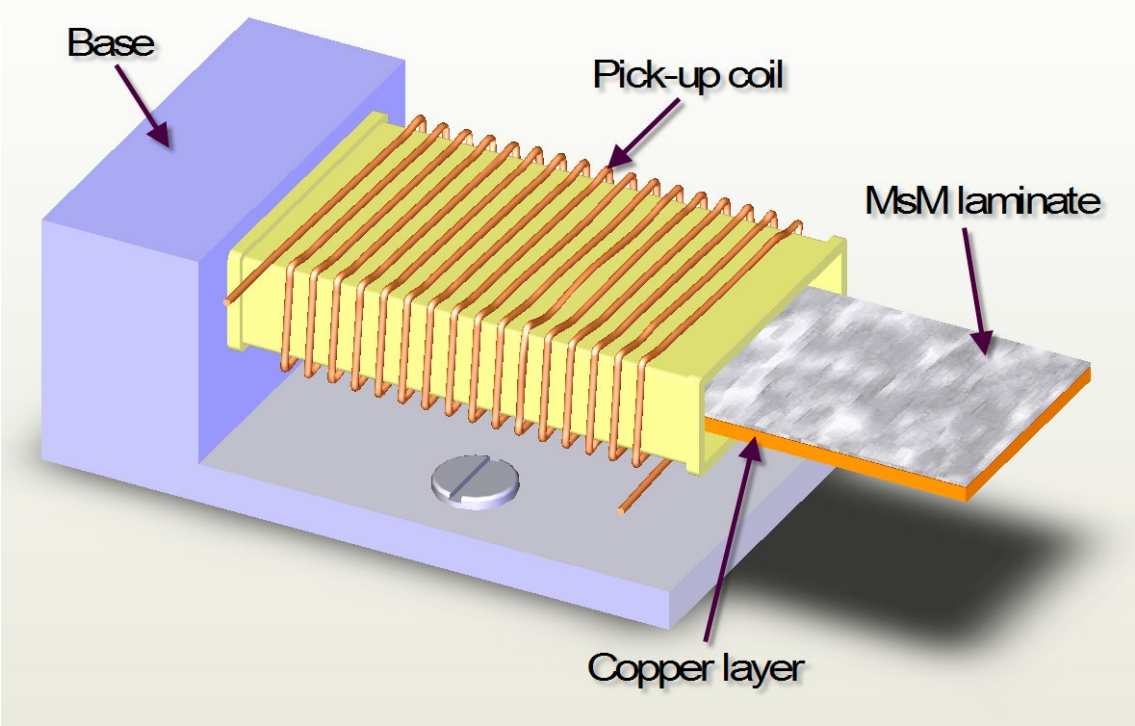

Figure 4.5 *Proposed magnetostrictive energy harvesting generator.[6]*

Wang [6] also proposes a harvesting circuit to be used with the harvesting generator. A schematic of the circuit can be seen in Fig. 4.6. On the left a voltage quadrupler rectifies and boosts the voltage obtained from the harvesting generator. The obtained energy is stored in a 3 farad ultracapacitor. Finally the voltage from the ultracapacitor is boosted and regulated, by a smart voltage regulator, to a level suitable for the device being provided with energy. Wang [6] reports that the energy harvesting generator connected to the energy harvesting circuit can charge the ultracapacitor with an average power of 576 µW, when the generator is excited with a frequency of 1100 Hz and peak acceleration of 8.06m/s². According to the paper this power results in a power density of 606 µW/cm², for the generator.

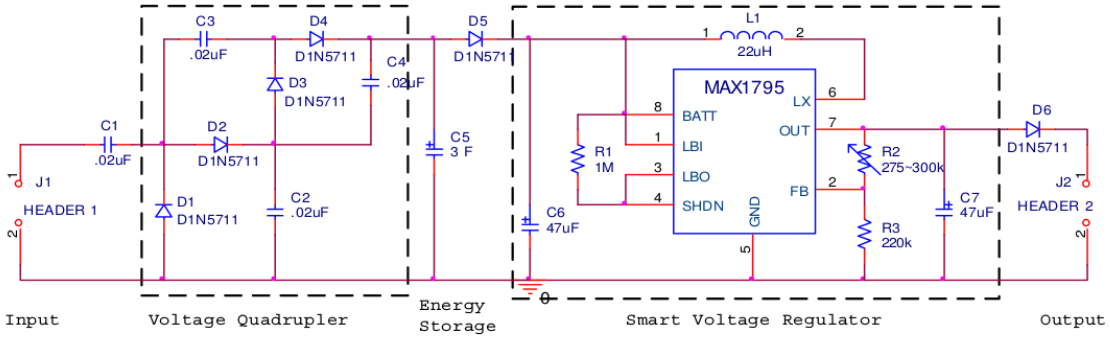

Figure 4.6 *Energy harvesting circuit.[6]*

Saber et al. [7] and Jafari et al. [20] present ambient vibration generators, very similar to the one presented by Wang [6], but only describe them as models and present simulated results. Both of the presented models are based on cantilever beams laminated with Metglas 2605SC. The harvesting generator model presented by Saber et al. [7] can be seen in Fig. 4.7 and the harvesting generator presented by Jafari et al. [20] is shown in Fig. 4.8

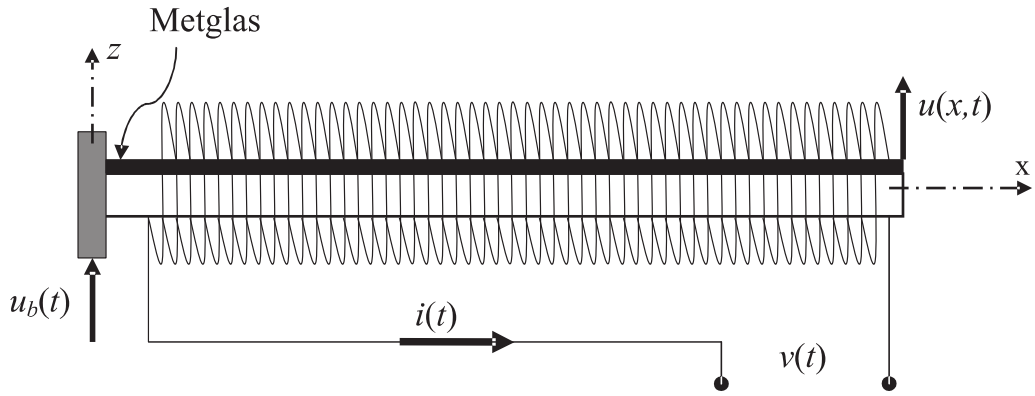

Figure 4.7 *Cantilever beam with Metglas 2605SC laminate and a surrounding pickup coil.[7]*

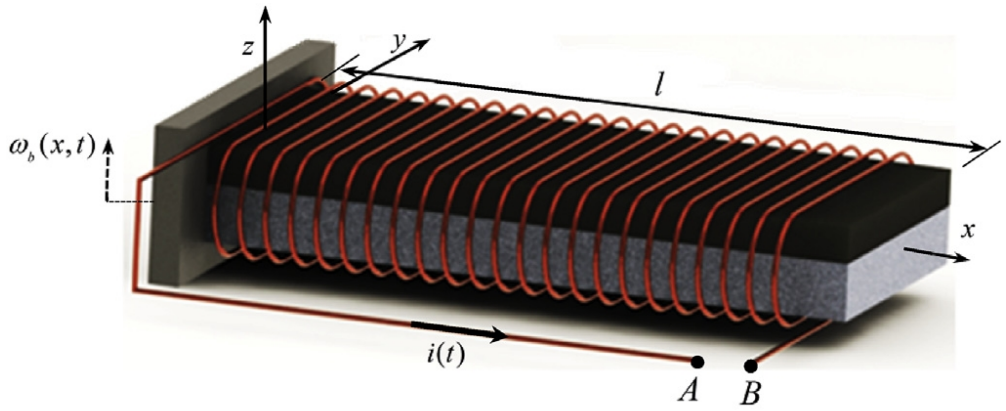

Figure 4.8 *Cantilever beam with Metglas laminate and a pickup coil.[20]*

Yang et al. [21] propose a slightly different kind of a cantilever based magnetostrictive kinetic energy harvesting generator. A picture of this generator can be seen in Fig. 4.9. A few differences are immediately apparent. The cantilever transducer is not intended for directly harvesting energy from ambient vibrations, but instead a sawtooth mechanism is used to up-convert slow linear movement in the environment, in this case finger tapping, to high frequency vibrations. As the tapping pad on the right is pushed down, the cantilever is flexed and mechanical energy is stored in it. When the tapping pad is pushed past each tooth in the sawtooth mechanism, the cantilever is released to vibrate at it's natural frequency. The vibration causes alternating strains in the galfelnol laminate on top of the cantilever, which induces a voltage in the coil surrounding the cantilever. The mechanical energy stored in the flexed cantilever is thus transduced to electrical energy. As the sawtooth mechanism has three teeth, fully depressing the tapping pad produces electrical energy in three bursts. It should also be noted that here the magnetostrictive material is magnetized with a permanent magnet instead of residual magnetism.[21]

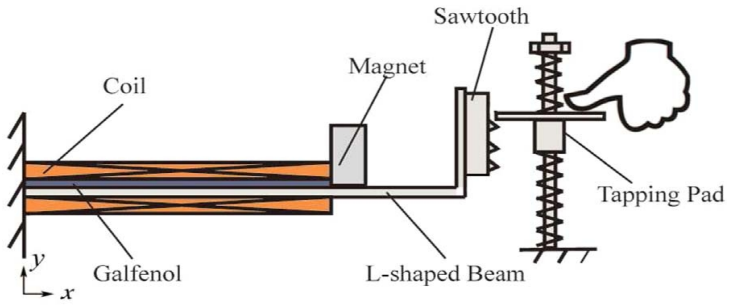

Figure 4.9 *Magnetostrictive up-converting cantilever generator.[21]*

Yang et al. [21] state that the generator, connected to a 10 ohm resistive load, produces a mean output power of 5.3mW, when it is excited by fully depressing the tapping pad at a frequency of 10 Hz.

5 ENERGY HARVESTING ELECTRONICS

In many energy harvesting applications electrical energy from the transducer is not suitable for directly powering electronic circuits or energy storage. The voltage from the transducer often needs to be rectified as in the case of vibrational energy harvesting or RF-energy harvesting. Also the voltage level from the transducer is often not suitable for energy storage or powering circuits; in piezoelectric harvesting the voltage can be tens or even hundreds of volts while in thermoelectric energy harvesting it can be mere tens of millivolts. Thus the voltage often needs to be stepped up or down and regulated.

According to maximum power transfer theorem, obtaining maximum external power from a voltage source requires that the load impedance equals the complex conjugate of the source impedance. It should be noted that this impedance matching does not result in maximum energy transfer efficiency; making the load impedance greater than the source impedance results in greater efficiency since a greater proportion of the source power is transferred to the load. Since in most energy harvesting applications the energy is essentially free, maximizing the power transferred to the energy harvesting circuit, instead of energy efficiency, makes sense.

Since, in many energy harvesting applications the energy source is not constant, some kind of energy storage is needed if the device being powered is to be used when the energy source doesn't provide sufficient energy. Rechargeable batteries and supercapacitors are commonly used as energy storage devices.[6]

In some cases energy harvesting systems also include circuitry to monitor and manage the harvested energy. Such circuitry can among other things report the amount of energy in the storage device to the device being powered, shut down the device being powered, or bypass the energy storage device when the harvested energy is sufficient to power the device.[6]

5.1 Rectification in energy harvesting circuits

As previously stated, energy harvesting sources which produce an alternating current require rectification to power electric circuits. Preferably the rectifier should transform the alternating current to direct current with the highest possible energy efficiency.

The following subchapters present different rectification topologies seen in energy harvesting publications.

5.1.1 Diode bridge rectifier

A standard diode bridge made of small signal or rectification diodes could be used for rectification in energy harvesting applications. A standard diode bridge rectifier is shown in Fig. 5.1.

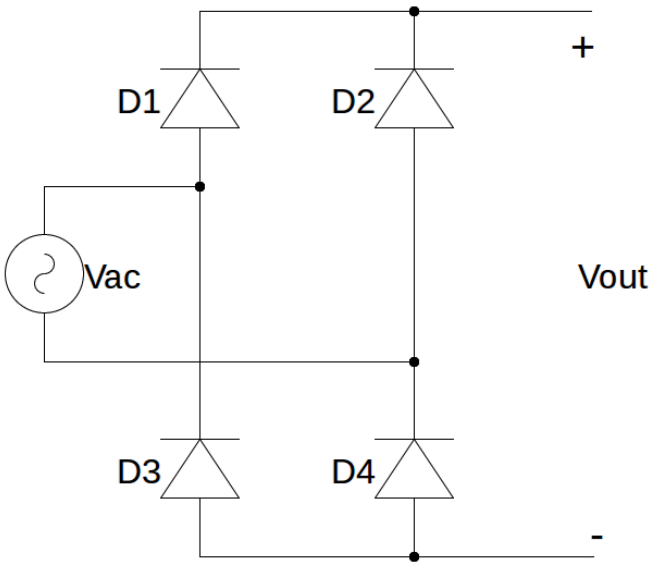

Figure 5.1 *A diode bridge rectifier.*

A diode bridge functions as follows. When input voltage V_{ac} is greater than output voltage V_{out} diodes D1 and D4 are forward biased and conduct. Thus current will flow from the input to the output. If the polarity of V_{ac} is reversed, diodes D2 and D3 are forward biased and conduct. If the absolute value of V_{ac} is smaller no diodes are forward biased, and no current will flow from the input to the output. [22]

A large limitation of the diode bridge is the forward voltage drop of the diodes. The forward voltage drop is determined by the diodes exponential *I-V* relation, but in most cases it can be assumed that the voltage drop across the diode is a constant V_d when the

diode is forward biased.[22] Therefore when a diode bridge is conducting the voltage drop across it will be twice the voltage drop across an individual diode. Therefore the power loss in the diode bridge is

$$P_{loss} = 2 V_d I \text{ .[22]} \tag{5.1}$$

Since power transferred to the load is

$$P_{load} = V_{load} I \text{ ,} \tag{5.2}$$

the energy efficiency of the diode bridge is

$$\eta = \frac{P_{load}}{P_{load} + P_{loss}} \tag{5.3}$$

$$\eta = \frac{V_{load} I}{V_{load} I + 2 V_d I} \tag{5.4}$$

$$\eta = \frac{V_{load}}{V_{load} + 2 V_d} \text{ .} \tag{5.5}$$

Obviously the efficiency of the diode bridge will be poor unless the voltage applied to the harvesting circuit is much greater than the diode forward voltage. Also, if the voltage in the diode bridge's input is lower than $2V_d$, no significant current will pass through the rectifier.

Since the forward voltage drop over typical silicon diodes is around 0.7 V, the efficiency of a silicon diode bridge can be poor in energy harvesting applications where the source voltage is low. Voltage drop in the diode bridge can be reduced by replacing regular silicon diodes with schottky diodes, although this will generally increase the component cost of the rectifier.[22]

5.1.2 MOSFET bridge rectifier

The diodes of a rectifier bridge can be replaced with diode connected MOSFET-transistors. Diode connected MOSFETs are typically either p-channel or n-channel enhancement mode MOSFETS that have their drains tied to their gates. A bridge rectifier made of two diode connected p-channel MOSFETs and two n-channel MOSFETs can be seen in Fig. 5.2. This type of rectifier is often seen in integrated circuits, since it can be easily manufactured with standard CMOS-technology. [22][23][24]

The main limitation of MOSFET bridge rectifiers is, that the MOSFETs in it will be operating in their saturation region which means that they will never be fully turned on or off. This means that there will be a voltage drop greater than the threshold voltage of the transistor across the diode connected MOSFET. This voltage drop will of course lead to power being dissipated in the transistor and thus power loss.[22] [23][25]

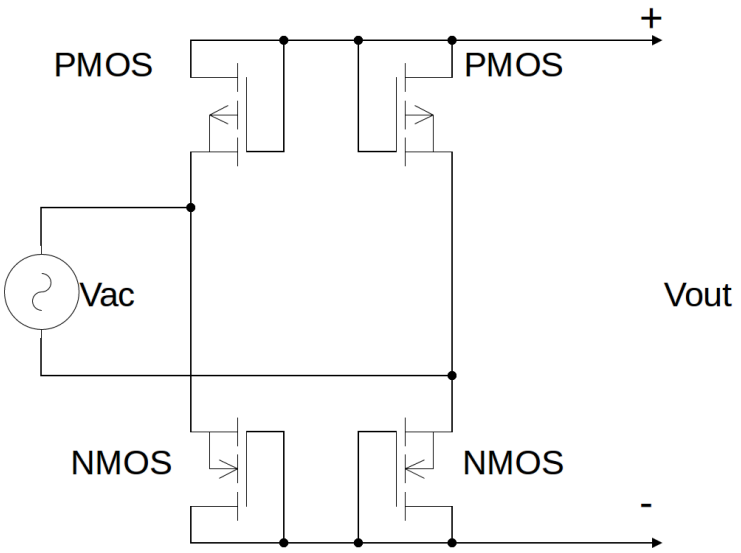

Figure 5.2 *A MOSFET bridge rectifier.*

According to Szarka et al. [22], voltage drop across a conducting diode connected MOSFET equals

$$V_{SD} = \sqrt{\frac{2I}{K(W/L)}} + V_T \text{,} \tag{5.6}$$

where I is the current passing through the transistor, K is the transistors transconductance factor, W is the width of the transistor's channel , L is the length of the cahnnel

and V_T is the transistor's threshold voltage. Power dissipated across a diode connected MOSFET must then equal

$$P_{MOS} = V_{SD} * I = \left(\sqrt{\frac{2I}{K(W/L)}} + V_T\right) * I \,. \tag{5.7}$$

Total power loss in the rectifier is of course the sum of power loss in one p-channel MOSFET and power loss in one n-channel MOSFET , since the current will be passing through one of each. Now the energy efficiency of a MOSFET bridge rectifier equals

$$\eta = \frac{P_{load}}{P_{load} + P_{loss}} \tag{5.8}$$

$$\eta = \frac{P_{load}}{P_{load} + P_{NMOS} + P_{PMOS}} \,, \tag{5.9}$$

where P_{NMOS} is power dissipated in an n-channel MOSFET and Pp_{MOS} is power dissipated in an p-channel MOSFET.

Since the voltage drop across a conducting diode connected MOSFET will be greater than the transistor's threshold voltage, a MOSFET bridge rectifier is not necessarily a large improvement over a diode bridge in terms of energy efficiency.[22][23] Szarka et al. [23] present results of a simulation in which a MOSFET bridge rectifier realized with TSMC 0.18 μm technology was simulated in LTSPICE IV. When the input of the simulated rectifier was a 10 Hz sine wave with a 2 V amplitude and the load of the rectifier was a 3 kilo-ohm resistor, the simulation yielded an energy efficiency of about 0.50.[23] In comparison, simulating a diode bridge realized with 1N4148 diodes in LTSPICE XVII yields an energy efficiency of about 0.41, with the same input and load.

5.1.3 Gate Cross-Coupled Rectifiers

As previously explained, when a conducting MOSFET is not fully turned on, voltage drop across it will be fairly large. If the voltage drop across a MOSFET based rectifier is to be significantly reduced, the transistors need to be fully turned on. One approach for turning rectifying transistors on and off, or commutating them, is the so called gate

cross-coupled topology. This essentially means, that the gates of rectifying MOSFETs are connected to one terminal of the rectifiers input while the other terminal is connected to the drains of the MOSFETs. This way the alternating input voltage will commutate the the rectifying MOSFETs.[23]

One rectifier topology based on cross-coupled MOSFETs is the negative voltage converter, which is also called the fully cross-coupled rectifier in some sources.[26] A negative voltage converter is a rectifier made of two n-channel enhancement mode MOSFETs and two p-channel enhancement mode MOSFETs. A negative voltage converter can be seen in Fig. 5.3. The rectifying circuit functions as follows, assuming all the transistors have the same threshold voltage. When V_{ac} is positive and greater than the threshold voltage, PMOS1 and NMOS2 are turned on and conduct. When V_{ac} is negative and it's absolute value is greater than the threshold voltage, PMOS2 and NMOS1 are turned on and conduct. When $|V_{ac}|$ is smaller than than the threshold voltage, no diodes are turned on and no current flows from the input to the output. Since all the MOSFETs in the rectifier are fully turned on when the rectifier conducts, the voltage drop over the rectifier can be very low and thus the power loss in it can also be very small. Negative voltage converters however have the major drawback of having practically no reverse isolation. Since MOSFETs are bidirectional devices, this means that when the input voltage is greater than the threshold voltage of the MOSFETs but smaller than the output voltage, there is nothing blocking the flow of current from the output to the input and thus reverse leakage losses can be very large. If an application requires a smoothing capacitor in the output of the rectifier this rectifier type may be rendered unusable or at least relatively inefficient. A negative voltage converter of course also requires that the input voltage exceeds the threshold voltage of the transistors so it might not be suited for very low input voltages, despite its very low forward voltage drop. [22][23]

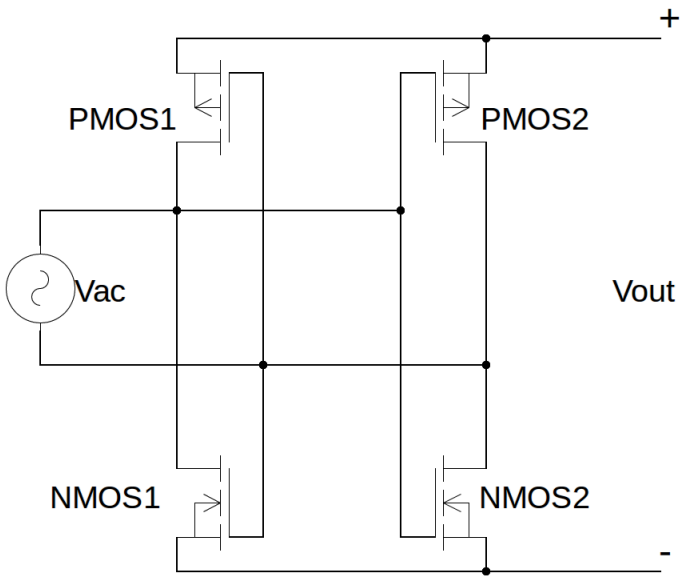

Figure 5.3 *A negative voltage converter.*

Another rectifier topology, that combines features from the MOSFET bridge rectifier and negative voltage converter is called the gate cross-coupled rectifier. A cross coupled rectifier consists of two diode connected MOSFETs and two cross-coupled MOSFETs. A gate cross-coupled rectifier is depicted in Fig. 5.4. The n-channel MOSFETs NMOS1 and NMOS2 function exactly the same way as the n-channel MOSFETs in the negative voltage converter; they are turned on and conduct when input voltage is greater than their threshold voltage. The p-channel MOSFETs on the other hand function as diode connected MOSFETs. Gate cross-coupled rectifiers thus exhibit forward voltage drops that are somewhere between that of a negative voltage converter and a MOSFET bridge rectifier. A gate cross-coupled rectifier however avoids the issue of reverse leakage currents experienced with negative voltage converters entirely, due to the diode connected transistors. [22][23]

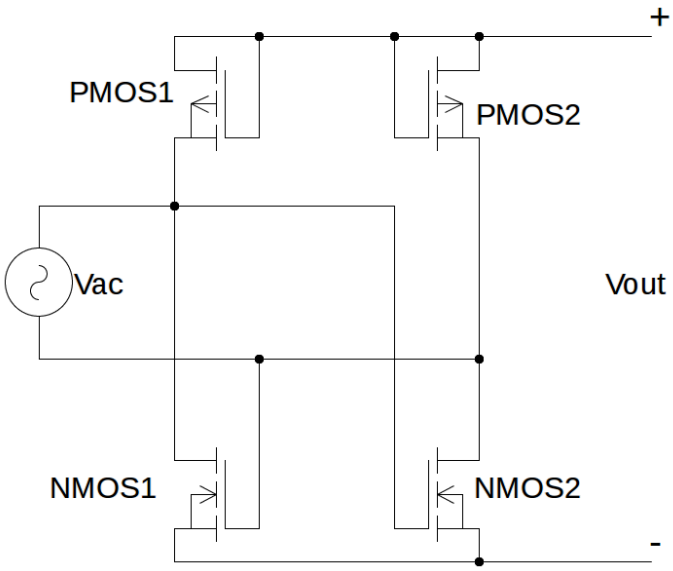

Figure 5.4 *A gate cross-coupled rectifier.*

An alternative way of solving the issue of reverse leakage currents seen in a negative voltage converter, while still retaining low forward voltage drops, is replacing two of the cross-coupled MOSFETs with Schottky diodes. Fig. 5.5 shows a picture of the topology.

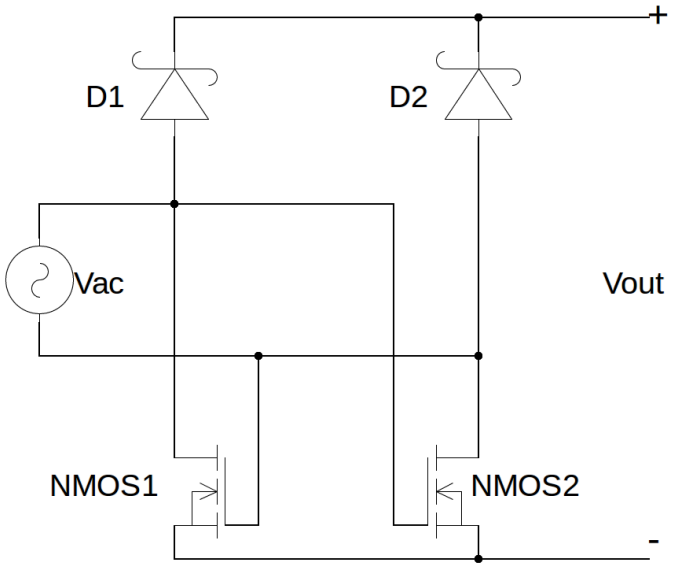

Figure 5.5 *A rectifier with two schottky diodes and two cross-coupled MOSFETs.*

Rectification circuits based on the topology seen in Fig. 5.5 have been proposed in academic articles such as [27]. Integrated rectifier circuits based on the topology are also commercially available; ON Semiconductors NMLU1210[28] is an example of such an integrated circuit.

5.1.4 Active rectification

Both forward conduction losses and reverse leakage losses can be reduced with active rectification. The switching elements used in an active rectifier are typically MOSFETs driven by some kind of a comparator circuit, that monitors the source-drain voltage of the MOSFET and turns the MOSFET on or off by adjusting it's gate voltage. [23]

Many active rectifier topologies presented in academic papers seem to be a variation of the negative voltage converter, that has some of it's passively commutated MOSFETs replaced with actively controlled ones. Guo et al. [29] for instance present a rectifier topology consisting of two cross-coupled p-channel MOSFETs and two comparator driven n-channel MOSFETs. A picture presented in [29] showing this topology can be seen in Fig. 5.6. In this topology the p-channel MOSFETs function exactly like they would in a negative voltage converter. The n-channel MOSFETs function somewhat differently; whenever the source-to-drain voltage of the MOSFET is negative, the associated comparator pulls the MOSFET's gate up and thus turns it on. When the source-to-drain voltage is positive, the MOSFET's gate is pulled down and the MOSFET is turned off. Thus the actively driven MOSFETs allow current to flow from the ground to the input terminal, with low conduction losses, and prevent reverse leakage currents.

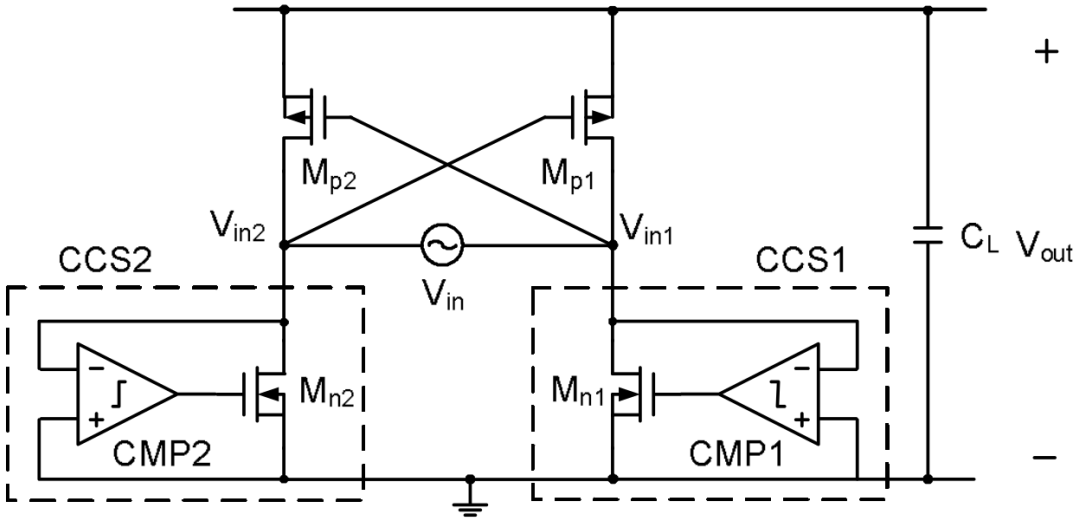

Figure 5.6 *An active rectifier with actively controlled and gate-cross coupled MOSFETs.[29]*

An active rectifier can also be a negative converter followed by an active diode which prevents reverse leakage currents. Peters et. al [30] [31][32] present rectifier circuits based on this topology. Fig. 5.7 shows a depiction of this topology. The negative voltage

converter part functions exactly the same way as in the entirely passive case. The active diode part however prevents reverse leakage currents while allowing forward currents with a very low forward voltage drop. When the drain-voltage source of PMOS3 in Fig. 5.7 is positive, comparator CMP pulls the p-channel MOSFET's gate down and turns the MOSFET on. When the drain-source voltage is negative, the comparator pulls the MOSFET's gate up, thus turning the MOSFET off.

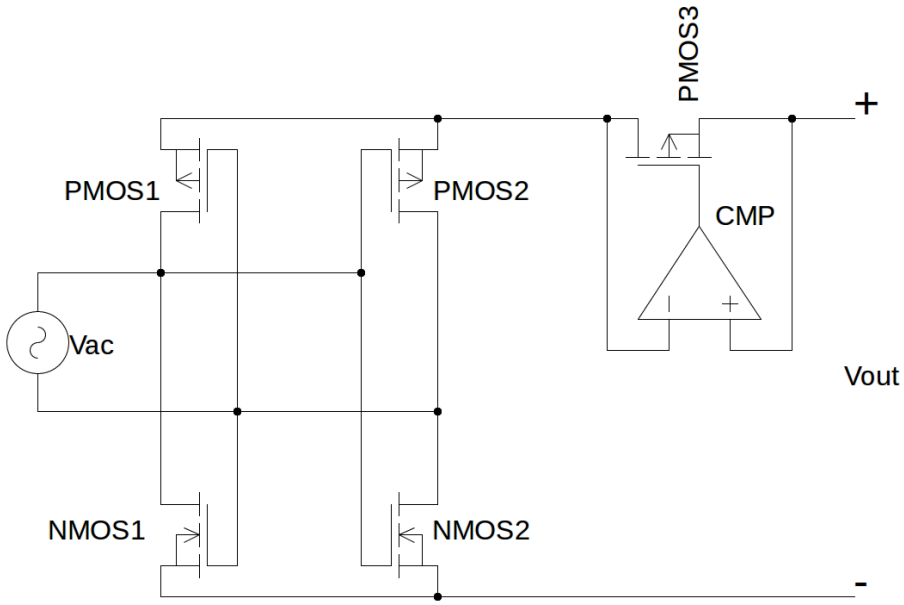

Figure 5.7 *A negative voltage converter followed by an active diode.*

While active rectifiers can achieve both low forward voltage drops and small reverse leakage currents, they of course have the drawback, that the active driving circuitry consumes a part of the harvested energy. The control circuitry of active rectifiers may also require a regulated voltage supply, which can cause issues with self starting i.e. when the energy harvesting device needs to start without any previously stored energy. Since the power consumed by the control circuitry tends to be a constant and not increase with the amount of harvested energy, the efficiency of active rectifiers tends to go up with harvester power levels.[23]

5.2 Voltage conditioning and impedance matching

As previously stated, the voltage provided by the harvesting transducer is often not suitable for powering electronic devices or energy storage. Thus the voltage may need to be stepped up or down and regulated to a desired level. Both Szarka et al. [23] and Briand et al. [33] seem to treat boost-mode and buck-mode switched mode regulators as the standard option for voltage regulation, but note that linear regulators may be used as

well. The need for regulated supply voltages is obviously not limited to devices powered with harvested energy. The requirements for the supply voltage are dictated by the device being powered regardless of the energy source. Since voltage regulation isn't a subject specifically pertaining to energy harvesting, it will not be discussed in detail here.

Voltage conditioning circuits however have an another purpose in energy harvesting: presenting a suitable input impedance to the energy harvesting generator.[33] As has been shown previously, electric loading has an effect on how kinetic energy harvesters function. For instance linear vibration energy harvesters are actually only linear when the electric damping is linear and produce the greatest output power, when the electric damping is equal to mechanical damping.[4] The input impedance of the harvesting circuit also affects how much of the transduced energy is actually transferred to the load and how much is dissipated in the internal resistance of the generator.

Many of the topologies proposed for impedance matching and harvester utilization optimization are specific to certain transduction mechanisms and generator designs. For example synchronous electric charge extraction methods, which are based on extracting energy from the internal capacitance of a piezoelectric transducer at maximum mechanical displacement, can only be used with piezoelectric generators.[34] Presenting all possible detailed harvesting circuits would not be practical here, so instead the most common principles of impedance matching seen in academic publications will be presented here along with some examples.

5.2.1 Resistive input impedance emulation

In some kinetic energy harvesting applications, such as a linear electromagnetic vibration harvester, a nearly ideal load for electric power production is a resistor of a certain value. In a practical application a resistor obviously isn't a very useful load though. A more useful load would be a voltage conditioning circuit, that appears to be a resistor to the harvesting generator.

One approach to making a voltage conditioning circuits input appear roughly resistive is a switched mode voltage converter operated in discontinuous current mode. Briand et al. [33] present a boost mode converter that emulates a resistive input impedance. This boost converter together with it's current and voltage waveforms is shown in Fig. 5.8 Since the inductor current of a converter operated in discontinuous current mode falls to zero during every switching cycle, the magnitude of the following current spike is determined by the input voltage. This means that the average input current is roughly in

phase with the input voltage, as can be seen in Fig. 5.8 (b). The apparent input resistance of this voltage converter is determined by

$$R = \frac{2L}{DT}, \tag{5.10}$$

where L is the inductance the inductor, D is the duty cycle at which the converter is operated and T is the converters operation cycle time.[33]

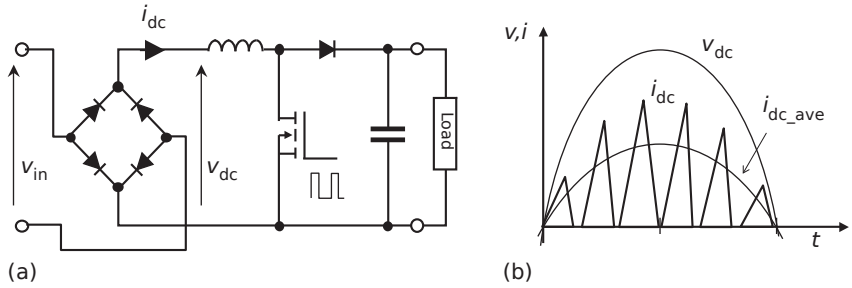

Figure 5.8 *A resistor emulator and it's voltage/current waveforms.[33]*

The above example shows a boost mode converter emulating a resistive load, but similar methods have also been presented for use with buck[35], buck-boost[36] and flyback converters[37].

An another way of making a switched mode voltage converter emulate a resistive load, is measuring the input current and input voltage and adjusting the converter's duty cycle to force the voltage and current into phase with each other. In other words, a feedback control loop is used to control the duty cycle of the converter so that the converters input appears resistive. Fig. 5.9. shows a boost converter employing this impedance matching method.[33]

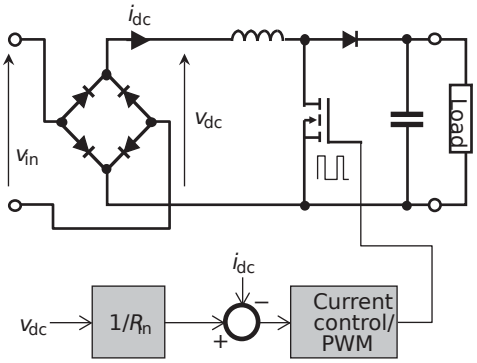

Figure 5.9 *A resistor emulator controlled by a feedback loop.[33]*

The feedback method has the benefit, that the converter can be operated in continuous current mode or discontinuous current mode. Operating the converter in continuous current mode may be beneficial due to smaller conduction losses. The circuitry used for measuring the converter's input current and controlling the duty cycle will however obviously consume some energy and may require a conditioned voltage supply.[33][23]

Discontinuous current mode voltage converters operated at a constant duty cycle seem to be practical even at very low power levels. Paing et al. [38] present such a converter, for RF energy harvesting, that achieves energy efficiencies of 85%–92.8% at harvested power levels of 8µW-420µW.

5.2.2 Complex impedance matching

According to maximum power transfer theorem, the greatest real power is transferred from a voltage source to a load, when the load is the complex conjugate of the source's output impedance. Thus in many energy harvesting applications maximum harvester utilization can be achieved, when the voltage conditioning circuit's input impedance is the complex conjugate of the generator's output impedance.[23] If an energy harvesting generator has an output impedance with fixed real and reactive components, complex conjugate matching could quite easily be achieved with a resistance emulating voltage converter and reactive passive components. However, if the frequency at which the generator is operated changes, the reactive component of the generator's output impedance also to changes.[33] This means that perfect complex conjugate matching cannot be achieved with passive components, if the energy harvester is operated at varying frequencies. Cammarano et al. [39] also note the fact that realistic energy harvesting generators have a reactive output impedance and state that this reduces the output power of resonant spring-mass generators along with narrowing their useful bandwidth. Cammarano et al. [39] report experimental results showing, that matching a load to a resonant energy harvesting generator, with capacitors and inductors, can improve real power output and widen the harvester's -3dB power bandwidth. This would suggest that even an imperfect complex matching can offer benefits.

To achieve a complex conjugate matching at varying frequencies, a power conditioning circuit capable of adjusting the reactive part of it's input impedance is needed. Briand et al [33] present a boost-rectifier capable of emulating a desired complex impedance. This boost-rectifier is pictured in Fig. 5.10. According to Briand et al. [33], since a reactive load implies energy flow from the source to the load and vice versa, a load capable of sinking and supplying energy, or operating in four quadrants, in any desired manner

should be able to emulate any reactive impedance. As the presented circuit could indeed sink or supply energy according to how the MOSFETs are driven, it should indeed be able to emulate an arbitrary reactive load, if it is suitably controlled. Briand et al. [33] however do not elaborate what kind of a control loop could be used to drive the MOSETs.

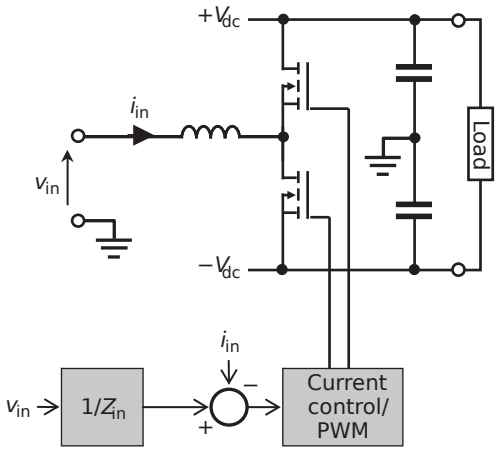

Figure 5.10 *Complex impedance emulator controlled by a feedback loop.[33]*

An adaptive reactive load could also be realized by actively connecting and disconnecting capacitors or inductors in to the load. Davis et al. [40] for instance proposes using multiple shunt capacitors, that can be connected parallel to the load to achieve a desired reactive load. Fig. 5.11. shows the circuit presented by Davis et al. [40].

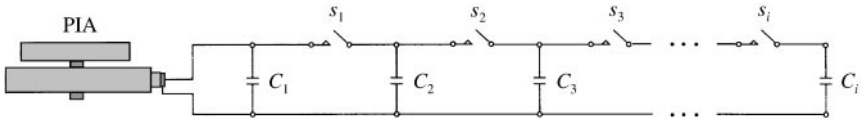

Figure 5.11 *Ladder circuit for adjusting a capacitive load .[40]*

The desired capacitance can be achieved by closing a suitable number of switches to connect capacitors parallel to the load.[40]

5.2.3 Maximum power point tracking

Voltage conditioning circuits employing maximum power point tracking, alternatively known as maximum power transfer tracking, continuously measure their output power and use a feedback control loop to adjust their operating point and find the point at which maximum power transfer from the harvesting generator is achieved. [33]

Maximum power point tracking schemes are widely employed with photovoltaic cells. [41] Photovoltaic cells appear to be a good candidate for power point tracking for a few reasons. Photovoltaic cells produce a DC-voltage, which means that simply adjusting the real part of the loading is sufficient to achieve maximum power transfer. Thus complex impedance matching is not needed. Also, as photovoltaic cells produce a constant power output as long as the amount of light they receive is constant, the control algorithm can be very simple; it is sufficient to find the operating point where the instantaneous output power is maximized. Kinetic energy harvesting methods unfortunately do not share these characteristics. As kinetic energy harvesters produce an alternating voltage, complex impedance matching may be necessary to achieve maximum power transfer. The output power of kinetic energy harvesting generators also varies along with their output voltage and thus simply tracking instantaneous power is not sufficient for finding the maximum power transfer point. Rather the output power needs to be tracked for at least one half cycle to obtain a meaningful measurement.

As Briand et al. [33] and Szarka et al. [42] note, kinetic energy harvesting systems, especially high Q-factor spring-mass resonators, can take some time to settle into a steady state. According to Szarka et al. [42] a digital feedback based MMPT-algorithm can not make changes to the electrical loading of a vibration kinetic energy harvester until it is very close to it's steady state, or the system will become unstable. Should there be frequent changes in the mechanical input of a kinetic energy harvester, an MPPT-algorithm will be unable to find the maximum power transfer point of the system, because it will change before the tracking algorithm can find it. This means that using feedback based MPPT schemes in applications, where the mechanical input changes frequently and quickly, will not likely be feasible.

Voltage conditioning circuits employing maximum power point tracking can be as simple as a switched mode voltage converter, whose duty ratio is controlled by a maximum power point tracking algorithm. Szarka et al. [42] present an example of this kind of a scheme. In the presented scheme a boost converter boosts the voltage from a linear electromagnetic vibration harvesting generator. The duty cycle of the boost converter is controlled with a simple perturb and observe algorithm, which adjusts the duty cycle incrementally up and down and always continues incremental adjustment to the direction that causes the measured output power from the generator to increase.

Maximum power point tracking schemes can also employ complex impedance emulating voltage converters, like the one depicted in Fig. 5.10, and use a maximum power

point tracking algorithm to find the optimal complex impedance load. Saggini et al. [43] present such a scheme for piezoelectric energy harvesters. In the presented scheme a piezoelectric generator is loaded with complex impedance emulating converter, which emulates a parallel connection of a resistor and an inductor. The values to be emulated are found with a down hill simplex algorithm, which is a numerical method used for finding the maximum or minimum of a function with an arbitrary number of variables. [44]

6 ENERGY HARVESTING FROM ELASTIC WAVES IN STEEL

6.1 New proposed energy harvesting method

Most academic articles, that address the use of magnetostriction in energy harvesting propose, that some special material with strong magnetostrictive properties is used for transducing kinetic energy into electrical energy. However since steel is a ferromagnetic material, it should possible to harvest kinetic energy directly from strained steel.

The aim of this master's thesis is to study kinetic energy harvesting from a loaded cylindrical steel bar. The steel bar in question is stressed by impacts from an another steel object. In other words the end of the rod is struck by an another steel object intermittently. The other end of the steel rod is supported by a hard rigid base.

The detailed behavior of steel under impact stress is a complicated subject and outside the scope of this thesis, and thus will not be discussed in length here. However a short simplified description is in order. When the end of the steel rod is struck, the impact sends an elastic wave along the rod. The elastic wave consist of alternating tensile and compressive strains. When the elastic wave reaches the end of the rod, part of the wave is transferred to the base and part is reflected back. When the reflected wave reaches the impacted end of the bar, the wave is once again reflected back. [45]

Since striking the metal bar in question causes alternating tensile and compressive strains to propagate along the bar, the magnetoelastic effect should cause alternating changes in the magnetization of the bar. These alternating changes in magnetization could then induce an alternating voltage in a pickup coil, thus transducing kinetic energy carried by the elastic wave to electrical energy. As previously mentioned, ferromagnetic materials do not exhibit the magnetoelastic effect, if magnetic field strength in them is zero. Also the magnetic field strength affects the strength of the magnetoelastic effect. The harvesting generator in this scheme should thus include, in addition to the pickup coil, something that magnetizes the steel bar to a point where the magnetoelastic effect is sufficiently strong.

Details of the harvesting generator will not be described here. Here it is sufficient to say that the generator consists of a coil wound around the steel bar, permanent magnets that magnetize the bar and a plastic body that holds the coil and magnets in place. Fig. 6.1 illustrates the concept of this energy harvesting scheme. In the figure a striking hammer impacts the end of a steel bar around which a pickup coil is wound. Below the steel bar is a supporting base.

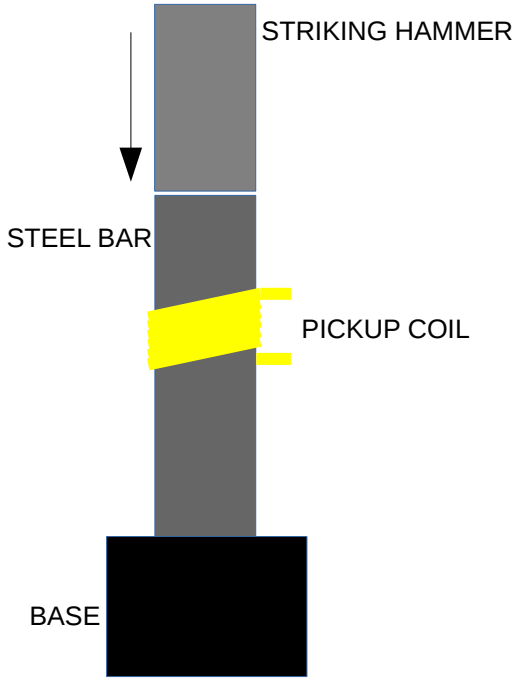

Figure 6.1 *Magnetostrictive energy harvesting from an impact loaded steel bar.*

This proposed method has several potential benefits over harvesting energy from ambient vibrations. First of all this method does not require the addition of any moving parts, that could wear out or break down under stress. This method also does not require the use of any exotic and expensive materials for energy transduction; only strong permanent magnets may be needed for magnetizing the steel bar. Perhaps most importantly the bandwidth limitation problems, associated with energy harvesting from ambient vibrations, may be entirely avoided. As previously explained, in the case of a spring mass resonator kinetic energy from the environment is transferred to the resonator most efficiently, when the ambient vibrations match the resonator's resonant frequency. When the ambient vibrations do not match the resonant frequency of the harvester, the output of the harvester tends to fall rapidly. In the case of this new proposed method, kinetic energy should be transduced to electric energy regardless of the frequency of the elastic wave.

6.2 Modeling of the transduction mechanism

Lets take a slightly closer look at how kinetic energy is transduced to electric energy in this scheme. According to Dapino et al. [46] the effects of magnetostriction and the magnetoelastic effect can be described with two linear equations.

$$\varepsilon = s^H \sigma + d_{33} H \tag{6.1}$$

$$B = d'_{33} \sigma + \mu^\sigma H \tag{6.2}$$

In the above equations ε is strain, s^H is elastic compliance at a certain H field, d_{33} is magnetostrictive coupling coefficient, d'_{33} is magnetoelastic coupling coefficient, σ is mechanical stress, μ^σ is the permeability of the material, H is magnetic field strength in the material and B is magnetic flux density in the material. From equation 6.2 we can determine, assuming that $\mu^\sigma H$ remains constant, the change in the magnetic flux density caused by an applied stress. This change equals

$$\Delta B = d'_{33} * \Delta \sigma \ . \tag{6.3}$$

$$\Delta B = d'_{33} * \Delta \sigma \ . \tag{6.4}$$

And the rate of change or time derivative equals

$$\frac{d}{dt} B = d'_{33} \frac{d}{dt} \sigma \ . \tag{6.5}$$

If we assume that stress and magnetic field strength are uniform in the material, the rate of change in the magnetic flux φ of the pickup coil would equal

$$\frac{d}{dt} \varphi = A d'_{33} \frac{d}{dt} \sigma \ , \tag{6.6}$$

where A is the cross sectional area of the bar. Thus, according to Faraday's induction law, the electromotive force induced in the pickup coil, of n turns equals

$$e.m.f = n\frac{d}{dt}\varphi = nAd'_{33}\frac{d}{dt}\sigma \ . \tag{6.7}$$

Now lets take a look at the electrical side of the pickup coil. The pickup coil could be modeled as a series connection of the induced electromotive force, pickup coil resistance and leakage inductance. If the pickup coil is connected to a load, say a resistor, the induced electromotive force would drive a current through the circuit. For the sake of simplicity we will assume that impedance caused by the leakage inductance is insignificant compared to the impedance of the load and coil resistance. Now the current through the coil equals

$$I = \frac{e.m.f}{R_{coil}+R_{load}} = \frac{nAd'_{33}\frac{d}{dt}\sigma}{R_{coil}+R_{load}} \ . \tag{6.8}$$

Power dissipated in the coil and load resistance equals

$$P = \frac{(e.m.f)^2}{R_{coil}+R_{load}} = \frac{\left(nAd'_{33}\frac{d}{dt}\sigma\right)^2}{R_{coil}+R_{load}} \ . \tag{6.9}$$

Since mechanical stress σ is defined as

$$\sigma = F/A \ , \tag{6.10}$$

where F is force and A is cross sectional area, electrical power can also be expressed as

$$P_{electrical} = \frac{n^2A^2d'^2_{33}\left(\frac{d}{dt}\frac{F}{A}\right)^2}{R_{coil}+R_{load}} = \frac{n^2d'^2_{33}\left(\frac{d}{dt}F\right)^2}{R_{coil}+R_{load}} \ . \tag{6.11}$$

Force F is the mechanical force being applied to the material surrounded by the pickup coil. Since magnetostriction is quite weak in steel, the force can mostly be explained by the mechanical strain of the material. Thus the force can be fairly accurately deter-

mined, if the strain and Young's modulus of the material are known. Because Young's modulus is defined as

$$E = \frac{\sigma}{\varepsilon} = \frac{(F/A)}{\varepsilon}, \tag{6.12}$$

the force equals

$$F = EA\varepsilon . \tag{6.13}$$

Now the electrical power can be expressed as

$$P_{electric} = \frac{n^2 d_{33}'^2 (\frac{d}{dt} EA\varepsilon)^2}{R_{coil} + R_{load}} = \frac{E^2 A^2 n^2 d_{33}'^2 (\frac{d}{dt}\varepsilon)^2}{R_{coil} + R_{load}} . \tag{6.14}$$

To get to the coupling coefficient of this method, an expression is needed for the mechanical power used to cause a strain in the material surrounded by the pickup coil. As mechanical power is simply a product of force and velocity, the mechanical power in this case is the product of the applied force and the rate at which the length of the material changes. Mechanical power can thus be expressed as

$$P_{mechanical} = F \frac{d}{dt} l . \tag{6.15}$$

If equation 6.12 is inserted to the above mechanical power becomes

$$P_{mechanical} = EA\varepsilon \frac{d}{dt} l . \tag{6.16}$$

Since length under strain is

$$l = l_o + \varepsilon l_o , \tag{6.17}$$

where l_0 is the original length, mechanical power becomes

$$P_{mechanical} = EA\varepsilon \frac{d}{dt}(l_0 + \varepsilon l_0) = EA\varepsilon l_0 \frac{d}{dt}\varepsilon \ . \tag{6.18}$$

Now we have an expression for the coupling coefficient in equation 6.18.

$$k = \sqrt{(\frac{P_{electric}}{P_{mechanical}})} = \sqrt{(\frac{EAn^2 d'^2_{33}(\frac{d}{dt}\varepsilon)}{(R_{coil} + R_{load})\varepsilon l_0})} \ . \tag{6.19}$$

The above is only intended to give a rough idea of how kinetic energy is transduced to electrical energy; it is not intended to be an accurate usable model, as it contains many coarse simplifications. First of all, according to Dapino et al. [46] the linearized equations, describing the magnetostrictive properties of a material, are only applicable when the material is at roughly constant magnetic field and strains in it are small. In this case the magnetostrictive behavior of the material is nearly linear, and the linear equations are reasonably accurate. However, when the material in question experiences significant strains and magnetic field strength in it varies, it's magnetostrictive behavior is nonlinear and affected by hysteresis. In other words, the magnetostrictive and magnetoelastic coupling coefficients are not only nonconstants, but vary nonlinearly depending on stress and magnetic field strength and are also affected by the past magnetic state of the material. The presented model also assumes that the magnetic field of the pickup coil is confined to the material surrounded by the coil. In reality, a part of the magnetic field of course passes through the material above and below the pickup coil, and it's effect should also be accounted for by an accurate model. Even in the material surrounded by the pickup coil, contrary to the assumptions behind this model, magnetic field strength and strains might not be uniform. The magnetic field applied by the permanent magnets will also likely be stronger near the surface of the bar and weaker near it's center.

The main drawback of the proposed method is the difficulty of accurately modeling it. To the author's knowledge no rigorous, accurate models that could be applied to this scenario have been published at the time of writing. This means that developing the harvesting generator and associated harvesting electronics, to be used with this method, will mostly be a matter of trial and error.

7 TESTING THE ENERGY HARVESTING METHOD

A test setup was constructed for testing the energy harvesting method presented in the previous chapter. The setup was used to test how much power the method can deliver to a resistive load. The coupling coefficient of the method was also evaluated. The test setup and test results acquired with it are presented in this chapter.

7.1 Experimental test setup

The new proposed energy harvesting method was tested with a test setup made up of the following parts:

- A carbon steel bar functioning as the magnetostrictive material and the medium of the elastic wave. This round bar has an external diameter of 32 mm and a hole running through the bar has a diameter of 10 mm. The length of this bar is 1000 mm. From here on transducer bar will be used as the term for this bar.
- A harvesting generator fixed to the transducer bar. This generator holds the permanent magnets needed for magnetizing the steel bar and a pickup coil. The ends of the pickup coil are attached to a BNC connector for easy connectivity with a coaxial cable.
- Another steel bar used for striking the transducer bar. This steel bar is made of the same material as the first one and has the same cross section. The length of this bar is 495 mm and it's weight is about 5.6 kg. This bar is used for striking by lifting it up manually and letting it fall on the transducer bar.
- Rigging for holding the transducer bar in place and guiding the striking bar, so that the striking bar impacts the transducer bar in a consistent manner.
- A solid steel base for the transducer bar.
- A Kyowa KFG-5-120-C1-11L1M2R strain gauge attached to the transducer bar.

Figure 7.1 *Test setup for the new energy harvesting method.*

A photograph of the test setup can be seen in Fig. 7.1. The proposed energy harvesting method can be tested on this setup by manually lifting the striking bar and letting it fall on the transducing bar. The striking bar impacting the transducer bar will cause an elastic wave to propagate downwards in the transducer bar. As the elastic wave passes the harvesting generator, the generator converts a part of the kinetic energy in the wave to electrical energy through the magnetoelastic effect.

Since the ends of the pickup coil in the generator are connected to a BNC connector, energy harvesting electronics, test loads and measuring instruments can easily be connected to the generator with a coaxial cable. The strain signal from the strain gauge is amplified with a TE Connectivity 142A strain gage amplifier, so that the correlation between the strain and harvested energy can be studied.

7.2 Testing the energy harvesting method with a resistive load

Since no accurate model exist for the new energy harvesting method, solving the optimal loading analytically or numerically is not possible. Testing the method with varying resistive loads could however give some idea of the energy levels that could be achieved with this method. In other words, if a certain amount of energy is dissipated in a resistor connected to the harvesting generator, when the trandsucer bar is struck, it is shown that at least this amount of energy could be potentially harvested with this method. For this reason the test generator was tested with various resistive loads.

For the tests, a printed circuit board holding a 2 kilo-ohm trimmer potentiometer and two SMA connectors was manufactured, so that the trimmer potentiometer could be used as an adjustable resistive load. The test generator was connected, with a coaxial cable, to one of the SMA connectors and the other SMA connector was connected to an oscilloscope channel, so the oscilloscope would see the voltage across the trimmer potentiometer. Fig. 7.2 shows an electric schematic depicting the electric circuit for the test setup.

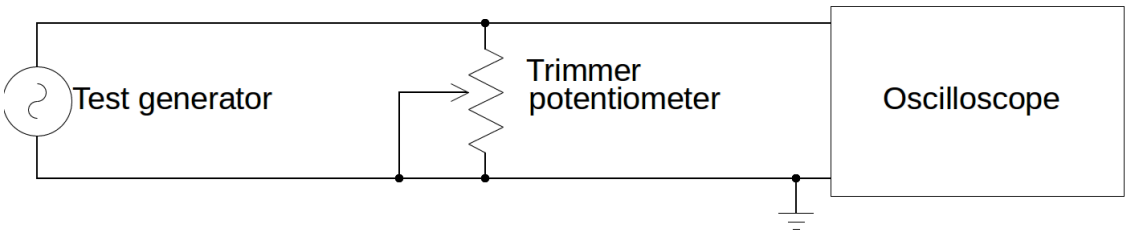

Figure 7.2 *Test setup for testing with a resistive load.*

The test was conducted as follows. The striking bar was lifted by 370 mm, the maximum amount permitted by the test setup, and allowed to fall on the transducer bar. The resulting voltage waveform was stored on the oscilloscope. The time scale of the oscilloscope was set so that a 100 ms long period was stored in the oscilloscope. 100 ms was chosen as the time period to be stored, because this gave sufficient time for the elastic wave propagating in the transducer bar to fully subside. From the stored waveform the following things were calculated:

- Peak power dissipated in the trimmer potentiometer.
- Mean power dissipated in the trimmer potentiometer.
- Energy dissipated in the trimmer potentiometer during the 100 ms time period.

The measurement was repeated with resistance values between 50 and 500 ohms with an increment of 50 ohms. The test results for each resistance value are presented in table 7.1.

Table 7.1 *Test results with a resistive load.*

Load resistance	Peak power(mW)	Mean power(mW)	Energy(µJ)	Peak voltage across the load(V)
50 ohm	134	1.58	158	2.62
100 ohm	118	2.18	218	3.43
150 ohm	247	2.7	270	6.09
200 ohm	340	3.4	340	6.09
250 ohm	306	4.19	419	8.75
300 ohm	274	4.12	412	9.06
350 ohm	320	3.9	390	10.6
400 ohm	308	3.49	349	11
450 ohm	355	3.06	306	12.6
500 ohm	252	2.44	244	11.2

The greatest amount of energy was dissipated in the trim potentiometer with a load resistance of 250 ohms. Interestingly peak power does not seem to correlate with mean power. This may be due to inconsistency in the elastic wave, i.e. the waveform of the elastic wave caused by the impact varies between measurements. Alternatively this may be due to the nonlinearity of the magnetoelastic effect.

To give some idea of the voltage waveform produced by the test generator, the voltage waveform across a 250 ohm resistive load is shown in Fig. 7.3. Fig. 7.4 shows the corresponding accumulation of energy dissipated in the resistive load.

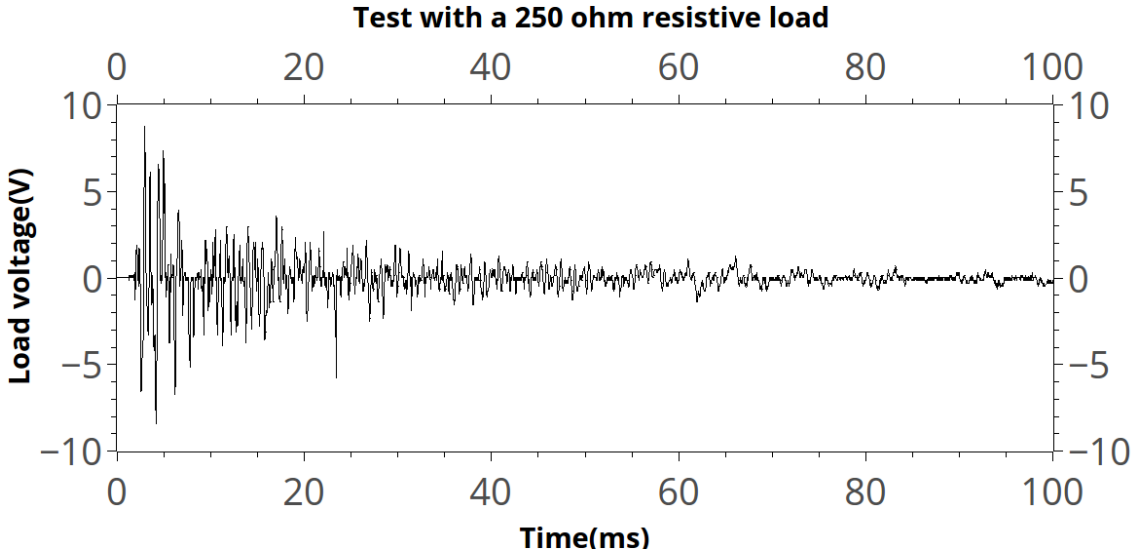

Figure 7.3 *Voltage waveform across a 250 ohm resistive load.*

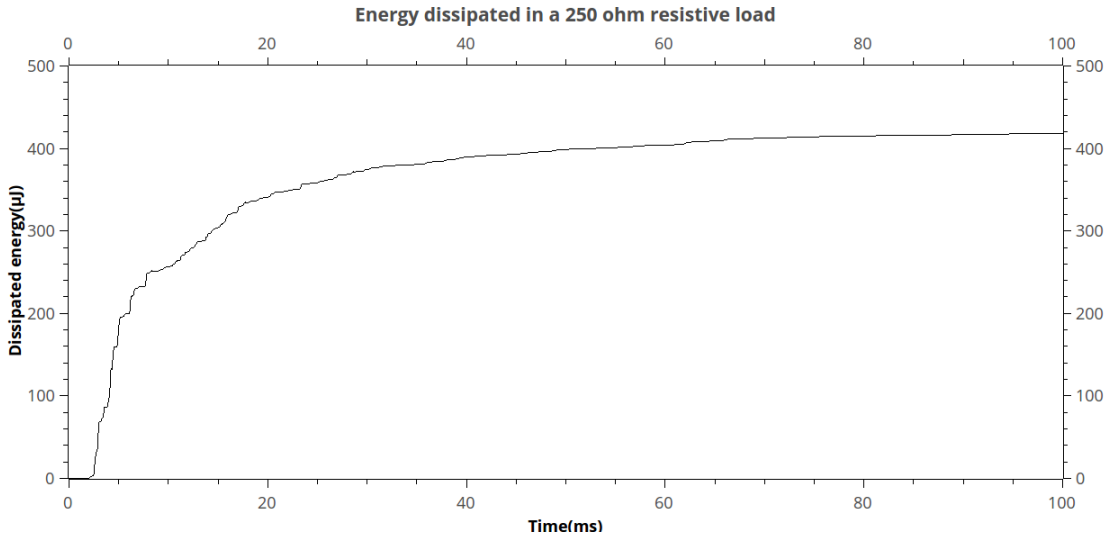

Figure 7.4 *Energy dissipated in the load.*

As can be seen from Fig. 7.4, 90 percent of the energy is dissipated within about 30 milliseconds from the beginning of the waveform. This result is quite meaningful for how the mean power output of the energy harvesting method grows as the frequency of strikes to the transducer bar increases; as long as most of the available energy is extracted before the next strike hits the transducer bar,mean power output should increase linearly with the frequency of strikes.

As Fig. 7.4 shows, the peak voltages at the beginning of the waveform are nearly 9 volts, but the voltage quickly drops after the beginning. This may mean that energy harvesting electronics capable of fully utilizing this method have to be capable of both dropping and boosting the voltage obtained from the test generator.

Dementyev et al. [47] demonstrate it is possible to run a wireless sensor, that transmits an 8-byte package every 5 seconds at 0 dBm transmission power, with a mean power consumption of 0.66 mW. If the test setup was to be impacted only two times per second, with the 250 ohm load, it would produce a mean output power of about 0.8 mW. Of course dissipating power in a resistor is not the same as harvesting usable electrical energy, but this test does indicate, this energy harvesting method could produce sufficient power for an energy efficient wireless sensor.

7.3 Estimating the coupling coefficient of the energy harvesting method

To estimate the coupling coefficient of the proposed energy harvesting method, the strain caused by the elastic wave was measured during the test with a 250 ohm resistive load. Fig. 7.5 shows the waveform of the measured strain.

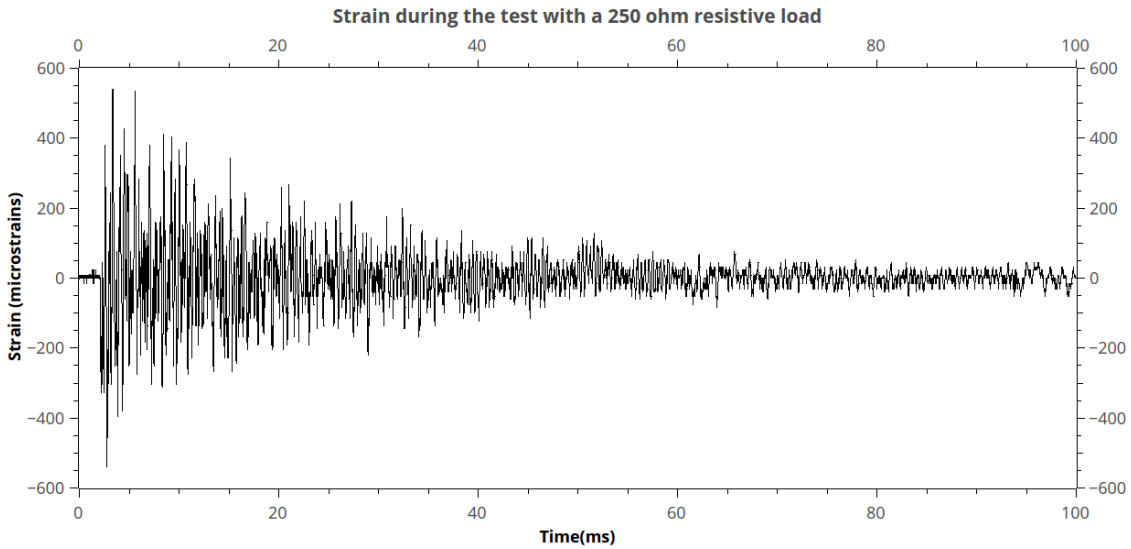

Figure 7.5 *Strain in the transducer bar during a test with a resistive load.*

Since coupling coefficient is defined as the ratio between energy transduced to the electric/magnetic domain and the mechanical work done to the transducing material, both the electrical and mechanical energy need to be determined.

Here, the transduced energy will be estimated to be the energy dissipated in the load and pickup coil resistances. The actual transduced energy is likely somewhat larger, since a part of the magnetic energy produced by the magnetoelastic effect will be consumed in eddy currents. Instantaneous power dissipated in the coil and load resistances can be determined if instantaneous current and the resistances are known. As current through a resistor equals

$$I(t)=\frac{V(t)}{R}, \tag{7.1}$$

where *U(t)* is voltage across the resistor and *R* is the resistance of the resistor, instantaneous current in this can be determined from the voltage waveform by dividing the instantaneous voltage with 250. Power dissipated in the load and coil resistances equals

$$P(t) = I^2(t) * (R_{load} + R_{coil}) , \tag{7.2}$$

$$P(t) = \left(\frac{V_{load}(t)}{R_{load}}\right)^2 * (R_{load} + R_{coil}) . \tag{7.3}$$

In the above $V_{load}(t)$ is voltage across the load resistor, R_{load} is the load resistance and R_{coil} is the coil resistance. Because the coil resistance of the test generator is 35 ohms the above can be expressed as

$$P(t) = \left(\frac{V_{load}(t)}{250}\right)^2 * (250 + 35) . \tag{7.4}$$

Overall dissipated energy can be determined by numerically integrating the calculated instantaneous power. For the test with 250 ohm load the dissipated electrical energy equals 477 µJ.

Mechanical work done to the transducing material can be determined from the strain waveform, since mechanical work done to the material is stored in the material as elastic potential energy, which can be determined if strain is known. According to Hooke's law elastic potential energy of an object equals

$$U_e = \frac{EA\Delta l^2}{2 l_o} , \tag{7.5}$$

where *E* is the Young's modulus of the material, *A* is the cross sectional area of the object, Δl is change in the length of the object and l_0 is the original length of the object. Because strain is defined as

$$\varepsilon = \frac{\Delta l}{l_0} , \tag{7.6}$$

Δl can be determined from

$$\Delta l = l_0 \varepsilon \,. \tag{7.7}$$

Now elastic potential energy can be expressed as

$$U_e = \frac{EA(l_o \varepsilon)^2}{2 l_o} = \frac{EA l_o \varepsilon^2}{2} \,. \tag{7.8}$$

In this case, the transducing material will be considered to be the section of the transducing bar surrounded by the pickup coil. The pickup coil is 5 millimeters tall, so here l_0 is 5 mm. The cross sectional area of the transducer bar is, as described in subchapter 6.3, 725.5 mm². Young's modulus will be assumed to be 210 GPa, which is a typical value for steel. Now elastic potential energy can be calculated for each point in the strain waveform seen in Fig. 7.5. Fig. 7.6 shows the corresponding elastic potential energy in the transducing material. It should be noted that Fig. 7.6 shows the absolute value of elastic potential energy, i.e. the figure does not differentiate between tensile and compressive energy.

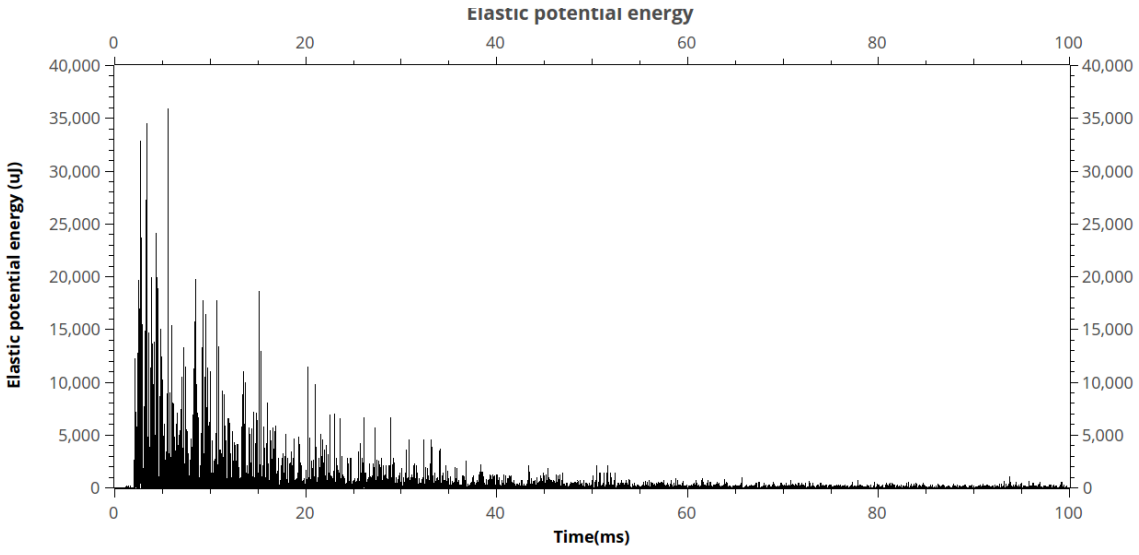

Figure 7.6 *Elastic potential energy in the transducing material.*

As previously mentioned, what needs to be solved is the amount of work done to the transducing material. Mechanical work done to the transducing material can be solved by simply summing each addition of elastic potential energy to the material. Any de-

creases in the elastic potential energy should be disregarded, since a decrease in the elastic potential energy implies the material doing mechanical work to the environment. The sum can be determined numerically from a chronological list of elastic potential energy values by calculating the change in the absolute elastic potential energy during every time-step and adding the change to the sum if the change is positive. If the change is negative or zero, nothing is added to the sum. For clarification this algorithm is shown as C style pseudocode in algorithm 7.1.

```
float elastic_potential_energies[];
float mechanical_work=0;

for (i=0,i<elastic_potential_energies.size,i++){
  if (abs(elastic_potential_energies[i+1])>abs(elastic_potential_energies[i])){
 mechanical_work=+abs(elastic_potential_energies[i+1])>abs(elastic_potential_energies[i)
}}

return mechanical_work;
```

Algorithm 7.1. *Algorithm for finding mechanical work done to the transducing material*

The above algorithm yields 3.88 J as the mechanical work done to the transducing material during the test with a 250 ohm resistive load. Since the dissipated electrical energy was 477 μJ, the overall coupling coefficient during the test was roughly 0.00012 or 0.012%.

It should be understood that the method used for estimating the coupling coefficient here would not be suitable for a case where the coupling coefficient is significant. This is because the work needed to cause a certain strain in the material would be larger than predicted by Hooke's law, as a significant part of the mechanical work would be transduced to electrical or magnetic energy. However in a case such as this, where the energy transduced to electrical energy is relatively negligible, this method is sufficient for roughly estimating the coupling coefficient.

8 DEVELOPED EXPERIMENTAL ELECTRONICS

Dissipating energy in a resistor is not definitive proof that the new method can be used to power electronic devices. However recharging a battery in a controlled manner with the method, would be definitive proof, as energy stored in a battery can easily be used to power electronics. For this reason rectifier circuits and voltage conditioning circuits, capable of recharging a 3 V Li-Ion were developed and tested with the method. The developed circuits are presented in this chapter.

8.1 Rectification

Since the developed magnetostrictive generator produces output voltages of less than 10 V, when loaded, large voltage drops in rectification could lead to a large part of the transduced electrical energy being dissipated in the rectifier. For this reason three alternative rectifier bridge circuits, with a focus on low threshold voltages and low forward voltage drops, were developed. This subchapter describes the developed bridge rectifiers.

8.1.1 Negative voltage converter

This rectifier topology was presented in subchapter 5.1.3. It consists of two p-channel and two n-channel MOSFETs, that have their gates cross-coupled. A negative voltage converter was chosen to be one of the topologies to be tested due to it's simplicity and potential for low forward conduction losses.

To maximize the forward conduction angle of the rectifier and minimize it's forward voltage drop, a low gate-to-source threshold voltage and a low drain-to-source on-resistance were prioritized in the selection of the MOSFETs to be used. The option best fitting this criteria was judged to be DMC2038LVT, which is a complementary pair of enhancement mode MOSFETs. In other word DMC2038LVT consist of one n-channel and one p-channel MOSFET in a single package. Thus a negative voltage converter can be realized with two DMC2038LVTs. According to the datasheet[48] of DMC2038LVT, the gate-to-source thresholds of both transistors are between 0.4 and 1.0 volts. The on-

resistance is at most 56 milliohms for the n-channel MOSFET and 168 milliohms for the p-channel MOSFET. An electric schematic of the negative voltage converter can be seen in Fig. 8.1. A photograph of the assembled negative voltage converter can be seen in Fig. 8.2.

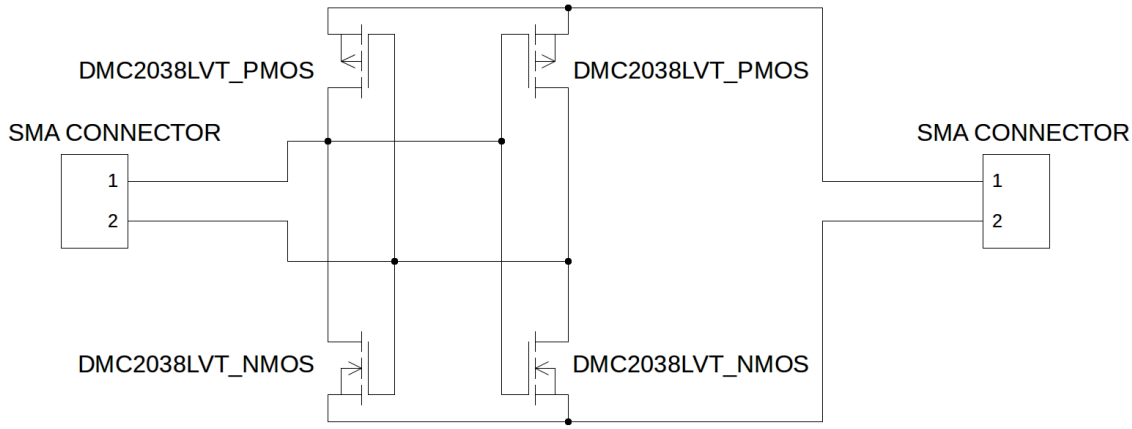

Figure 8.1 *An electrical schematic of the experimental negative voltage converter.*

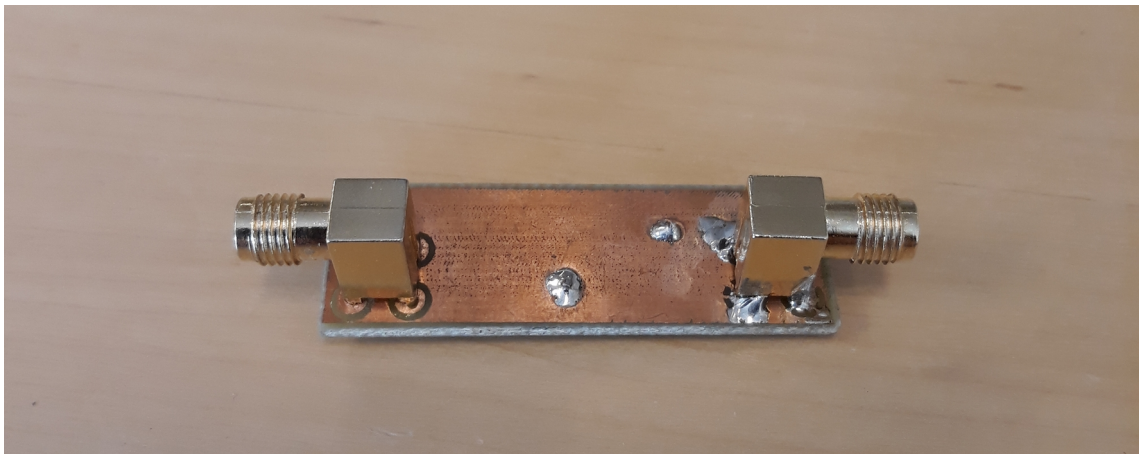

Figure 8.2 *A photograph of the experimental negative voltage converter.*

The negative voltage converter was assembled on standard FR-4 printed circuit board, and for easy connectivity the input and output of the converter were connected to angled SMA coaxial connectors.

8.1.2 Gate cross-coupled rectifier with Schottky diodes

As a negative voltage converter has no reverse isolation whatsoever, when the MOSFETs in it are turned on, reverse current losses may be large, if the load has a significant reactive component. Since many practical loads, such as a switched mode voltage con-

verter, have a filtering capacitor in their input, a negative voltage converter may not be very efficient or even practical with realistic loads. For this reason, a rectifier bridge combining proper reverse isolation with low forward voltage drop was also developed. This rectifier combines gate-cross-coupled n-channel MOSFETs and schottky diodes. The basic topology of this rectifier was presented in subchapter 5.1.3. Fig. 8.3 shows an electrical schematic of the developed rectifier. The rectifier was also assembled on an FR-4 printed circuit board similarly to the negative voltage converter presented in subchapter 8.1.1.

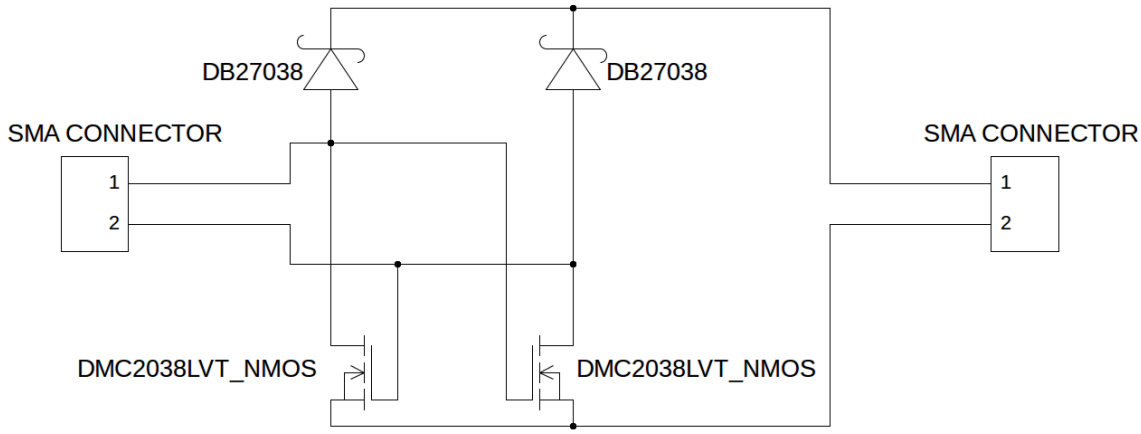

Figure 8.3 *an electrical schematic of the experimental gate cross-coupled rectifier with Schottky diodes.*

To minimize forward conduction losses, the Schottky diodes were selected for low forward voltage drop. The Schottky diode that was selected is Panasonic's DB27038. According to it's datasheet[49] a DB27038 schottcky diode has a forward voltage drop below 0.4 V at forward currents below 100 mA. DMC2038LVT n-channel MOSFETs were used as the gate-cross coupled MOSFETs. The forward voltage drop of this rectifier should be the sum of the Schottky diodes forward voltage drop and whatever voltage drop is caused by the passing current across the on-resistance of the n-channel MOSFET.

8.1.3 Negative voltage converter and active diode

The only way to fully combine low forward conduction losses and good reverse isolation seems to be active rectification. In an attempt to achieve this, a relatively simple active rectifier bridge was developed. This rectifier bridge consists of a negative voltage converter followed by an active diode. An electrical schematic of the developed active rectifier is shown in Fig. 8.4. The active rectifier was assembled on an FR-4 printed circuit board similarly to the negative voltage converter presented in subchapter 8.1.1.

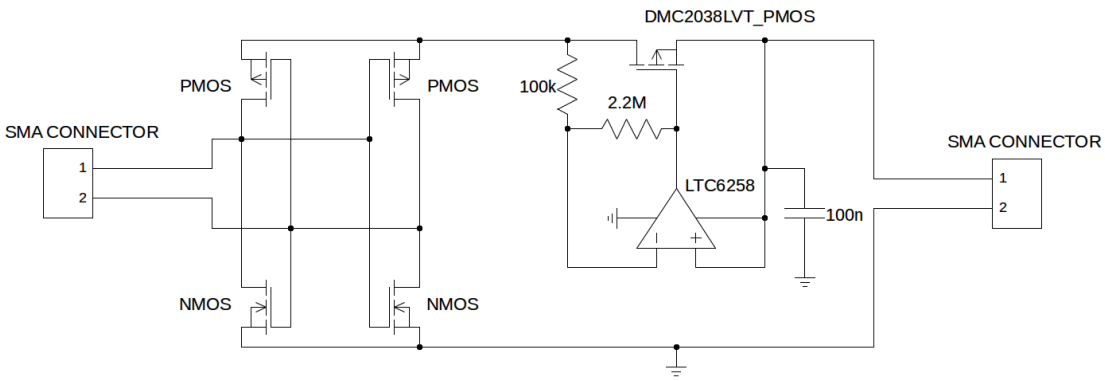

Figure 8.4 *Experimental active rectifier.*

The negative voltage converter part is identical to the negative converter presented in subchapter 8.1.1 and provides rectification with low forward conduction losses. The purpose of the active diode is only to stop reverse leakage currents while causing as low a forward voltage drop as possible.

The active diode is realized with a p-channel enhancement mode MOSFET that is driven by an operational amplifier. The DMC2038LVT MOSFET was used in the active diode as well, since it's low gate-to-source threshold voltage means that it can be fully turned on even at low voltage levels. Turning the MOSFET on fully is crucial for reducing forward conduction losses.

The operation of the active diode is most easily understood by separately thinking about forward conduction and reverse isolation operation cases. Fig. 8.5 shows a picture of the active diode in forward conduction mode.

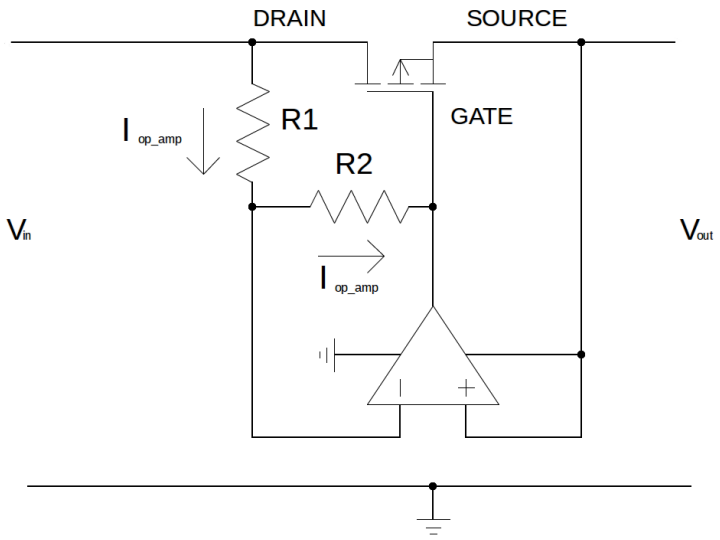

Figure 8.5 *Active diode in forward conduction mode.*

When the active diode is in the forward conduction mode, a positive voltage drop is developed between the MOSFET's drain and source. Assuming the open loop voltage gain of the operational amplifier is practically infinite, the operational amplifier will sink enough current into it's output to bring the inputs to the same voltage. This current is denoted with I_{op_amp} in Fig. 8.5. Since the inputs of the operational amplifier are at the same voltage and the positive input is shorted to the source of the MOSFET it follows that

$$V_{-} = V_{source}\,, \tag{8.1}$$

where V_{-} is the voltage at the negative input of the operational amplifier and V_{source} is the voltage at the source of the MOSFET. The voltage at the drain of the MOSFET is

$$V_{drain} = V_{source} + V_{drop}\,, \tag{8.2}$$

where V_{drop} is the forward voltage drop across the MOSFET. Assuming the inputs of the operational amplifier have practically infinite input impedance, the same I_{op_amp} will pass through both of the resistors in the active diode. The magnitude of this current equals

$$I_{op\_amp} = \frac{V_{drain} - V_{-}}{R_1} = \frac{V_{source} + V_{drop} - V_{-}}{R_1} \tag{8.3}$$

$$I_{op\_amp} = \frac{V_{-} + V_{drop} - V_{-}}{R_1} = \frac{V_{drop}}{R_1}\,, \tag{8.4}$$

where R_1 is the resistance of resistor R1 in Fig. 8.5. The voltage at the gate of the MOSFET equals

$$V_{gate} = V_{-} - I_{op\_amp} * R_2\,, \tag{8.5}$$

where R_2 is the resistance of resistor R2 in Fig. 8.5. Since

$$V_{-} = V_{source} \tag{8.6}$$

and

$$I_{op\_amp} = \frac{V_{drop}}{R_1}\,, \tag{8.7}$$

the voltage at the gate of the MOSFET can also be expressed as

$$V_{gate} = V_{source} - \frac{V_{drop}}{R_1} * R_2 = V_{source} - V_{drop} * \frac{R_2}{R_1}\,. \tag{8.8}$$

Thus the gate-to-source voltage of the MOSFET equals

$$V_{gate} - V_{source} = \frac{-V_{drop}}{R_1} * R_2 = -V_{drop} * \frac{R_2}{R_1}\,. \tag{8.9}$$

Or

$$V_{gate} - V_{source} = -V_{drop} * \frac{2.2\,M}{100\,k} = -22\,V_{drop}\,. \tag{8.10}$$

Assuming the maximum gate-to-source threshold voltage of a DMC2038LVT p-channel MOSFET is always above -1 V, a voltage drop of roughly 45 mV across the active diode should be sufficient to turn the MOSFET fully on. At small currents the forward voltage drop should be in this range. If the forward current is large enough to cause a significant voltage drop across the on-resistance of the MOSFET, the forward voltage drop can be larger.

Fig. 8.6. shows the active diode operating in reverse isolation mode. When the active diode is in reverse isolation mode, the drain-to-source will be negative. This means the positive input of the operational amplifier will be in a higher voltage than the negative input, which will cause the operational amplifier to drive it's output to the supply voltage. Since the output current I_{op_amp} will cause some voltage drop in R2 and the supply voltage and positive input are shorted together, the negative input will remain at a lower voltage than the positive input. Thus the output and the MOSFETs gate will always be at the supply voltage of the operational amplifier when the active diode is operating in reverse isolation mode. As the gate and source of the MOSFET will be at the same voltage, the MOSFET will be in cutoff mode and no current will flow through the MOSFET.

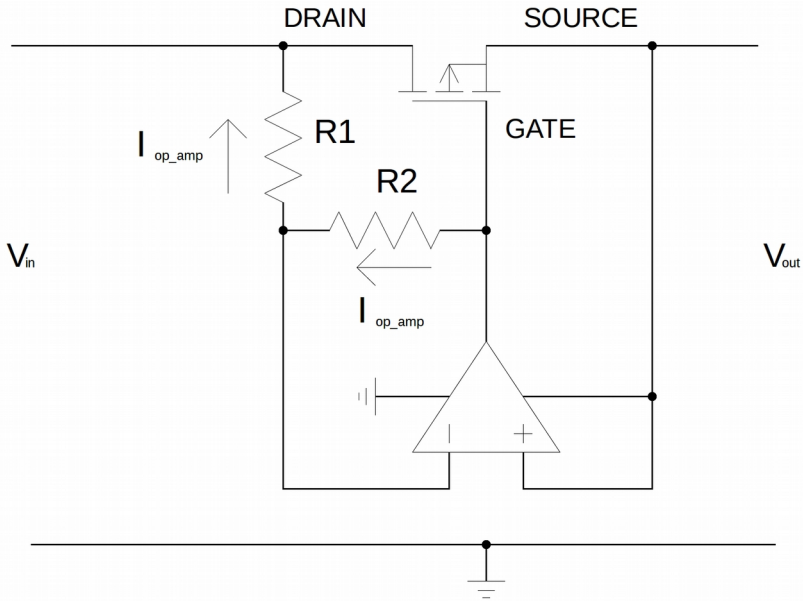

Figure 8.6 *Active diode in reverse isolation mode.*

It should be noted that this application requires that the operational amplifier has rail-to-rail output and inputs. In other words the operational amplfier needs to be able to raise it's output voltage to it's positive supply rail and accept inputs that are as high or low as

it's positive or negative supply rail. LTC6258[50], according to the datasheet, meets these demands.

When functioning as intended, this active rectifier combines both low forward conduction losses and good reverse isolation. The rectifier however also has some drawbacks and limitations. As the operational amplifier powers itself from the output of the active diode, the active diode may not work correctly when the output voltage is below the minimum supply voltage for the operational amplifier, which is 1.8 V for LTC6258.[50] If the operational amplifier is not operating correctly, the active diode will still be able to conduct forward current through the body diode of the MOSFET, but the forward voltage drop will be the forward voltage drop of the body diode. Due to these reasons this rectifier may not be the best solution for use with low voltage levels or purely resistive loads. However in cases where the voltage across the load is mostly at least 1.8 V this active rectifier could be very energy efficient.

8.2 Voltage conditioning circuits

This subchapter presents two voltage conditioning circuits, that charge a 3V Li-Ion battery, and circuitry for measuring harvested energy. The purpose of the voltage conditioning circuits is to step the voltage from the harvesting generator to suitable level and also maximize power transfer from the generator. Test results obtained with the voltage conditioning circuits are also presented.

8.2.1 Constant input voltage converter circuit

Arthur et al. [51] show that it is possible to achieve good power transfer from an AC voltage source to a DC load, through a rectifier bridge, if the reactive part of the voltage source's output impedance is canceled with resonant tuning and the voltage of the DC load is tuned to a suitable level. Fig. 8.7 shows this principle applied to a case, where the output impedance of the voltage source has a resistive and an inductive part in series. In this case the inductive part of the output impedance is canceled with a series capacitor. According to Arthur et al. [51] the optimal value of the ratio between peak AC voltage and DC voltage can be determined from

$$\frac{V_{peak}}{V_{DC}} = \frac{2\sqrt{16Q^2+1}}{4Q^2+1}\coth\frac{\pi}{4Q}, \tag{8.11}$$

Where V_{peak} is the peak AC voltage, V_{DC} is the DC voltage and Q is the Q factor of the resulting RLC circuit. Also according to Arthur et al. [51] the power delivered to the DC voltage load at the optimal ratio is given by

$$P_{DC} = \frac{Q(4Q^2+1)}{16Q^2+1} \tanh \frac{\pi}{4Q}, \tag{8.12}$$

where P_{DC} is the power transferred to the DC load.

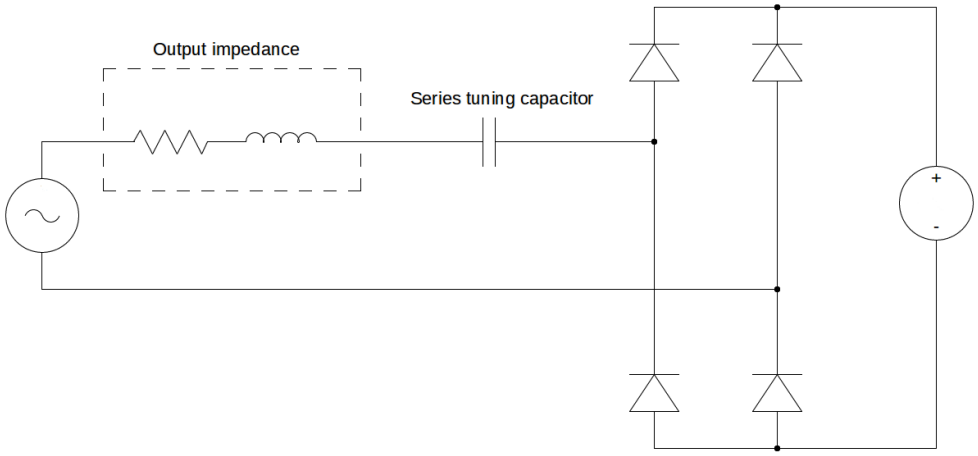

Figure 8.7 *AC voltage source with a series tuning capacitor and full wave rectifier.*

Using this approach, with the proposed energy harvesting method, is appealing since many readily available commercial voltage converters offer a function that keeps the input of the converter at a set DC-value. Among these are LTC3105[52] and ADP5090[53]. These voltage converters are intended for energy harvesting with photovoltaic and thermoelectric cells and are optimized for efficiency at low power levels. As realizing the voltage converter circuit would not require any additional active circuitry, this realization could be very simple and fully self starting.

However this approach also has limitations when applied to this energy harvesting method. First of all, since no proper models exist for the harvesting generator, determining what kind of an output impedance the harvesting generator has. This combined with the fact that the output voltage of the generator is spread over a broad spectrum means that canceling the reactive part of the output impedance with series tuning is not possible. The amplitude of the voltage from the generator is also not constant; at the beginning of the waveform the amplitude is large but falls quickly as can be seen from Fig. 8.8, which shows the open voltage waveform from the generator. Thus it might not be possible to set the input voltage of the converter to a value that would result in a high

power transfer during the entire waveform. Also, if the input voltage converter is set to a fixed voltage, the converter obviously cannot adapt if the amplitude of the waveform changes.

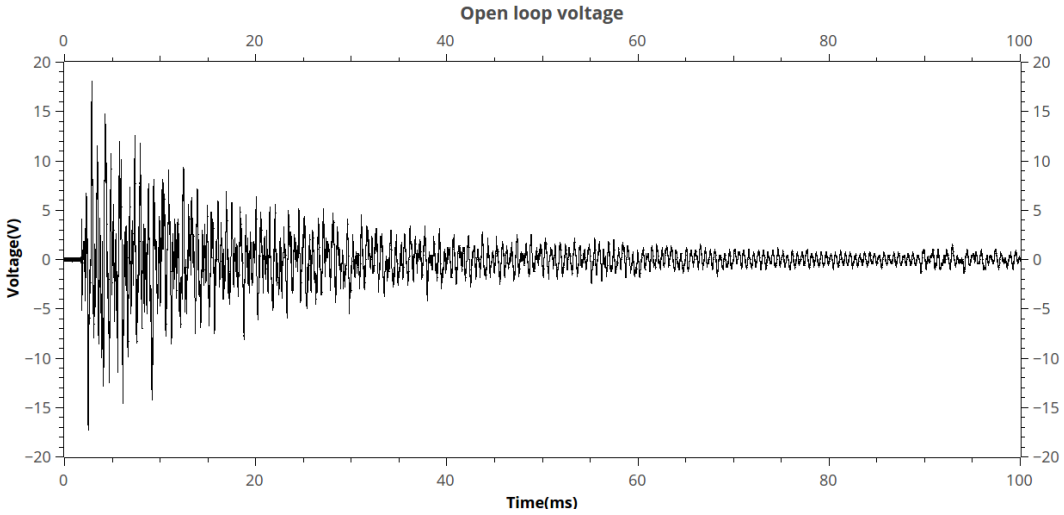

Figure 8.8 *Open loop voltage from the harvesting generator.*

To test this approach, a simple voltage converter circuit based on the LTC3105 was designed and implemented. Fig. 8.9 shows an electric schematic for the voltage converter and Fig. 8.10 shows a photograph of the circuit. LTC3105 is a low power step-up converter intended for energy harvesting applications. LTC3105 features a function for keeping the input voltage above a desired point. Linear technology calls this function Maximum Power Point Control. The desired input voltage is set by placing a resistor between the MPPC-pin and ground. LTC3105 puts out a 10 µA current from the MPPC pin, and whatever voltage drop is developed across the setting resistor is the desired input voltage point. LTC3105 attempts to keep it's input voltage at or above this circuit, by reducing it's duty cycle if the input voltage is below the set point.

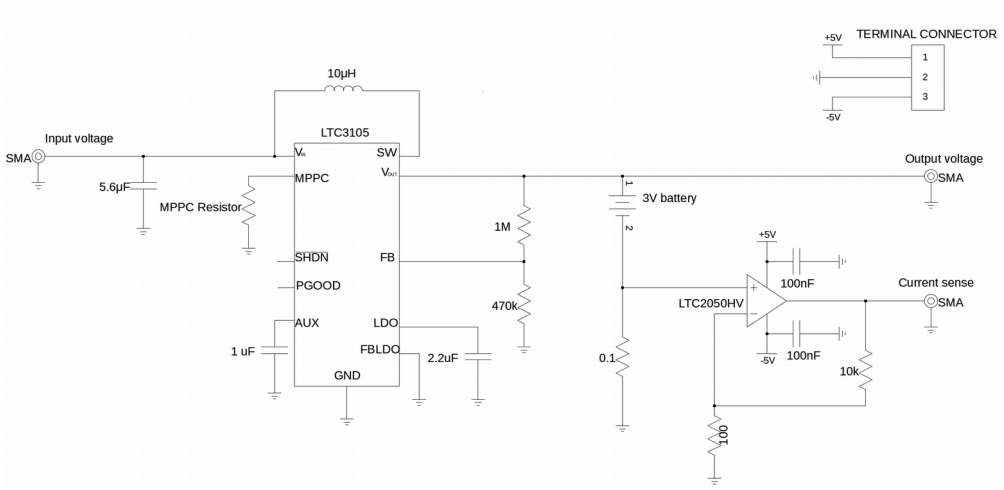

Figure 8.9 *LTC3105 based constant input voltage converter.*

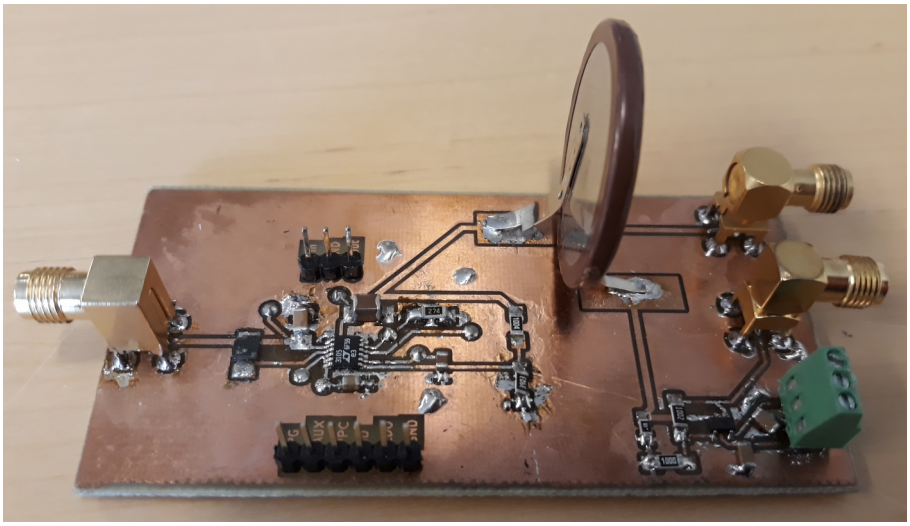

Figure 8.10 *A photograph of the constant input voltage converter.*

The designed voltage converter circuits accepts a rectified input through an SMA connector and uses the input to charge a 3 V Li-ion battery with the LTC3105. Any of the previously presented rectifiers can be connected to the input of this voltage converter. The converter board also contains the current sensing circuit presented in subchapter 8.2.3. The amplified current sense signal and the voltage across the Li-Ion battery, can be connected to coaxial cables through SMA connectors.

8.2.2 Voltage converter with resistive impedance matching

Since tests with a resistive load yielded output powers potentially sufficient for a wireless sensor, a simple voltage converter circuit capable of emulating a resistive input impedance was designed and implemented. An electric schematic of the converter can be seen in Fig. 8.11 and a photograph of the circuit can be seen in Fig. 8.1.2

The voltage converter is made up of two separate parts with two distinct purposes. The impedance matching part and the voltage regulation part. The impedance matching part is a switched mode boost-mode voltage converter that adjusts the input current of the converter in a hysteretic manner to emulate a resistive input impedance. The current through a resistor and voltage across a resistor, according to Ohm's law, satisfy the condition

$$R = \frac{V(t)}{I(t)}, \tag{8.13}$$

where *I(t)* is the current through the resistor, V*(t)* is the voltage across it and *R* is the resistance of the resistor. The developed circuit determines whether the relation between input voltage and input current is smaller or greater than it should be for the desired resistor with a hysteretic comparator. If the relationship is greater than desired, the comparator switches the MOSFET of the boost converter on, which increases the current and decreases the voltage. If the relationship is smaller than desired, the MOSFET is switched off. The resistance which the circuit attempts to emulate is determined by the voltage divider at the the input and the gain of the current sense amplifier at the input. This resistance equals

$$R = A_{current\ sense}\frac{1}{A_{divider}}, \tag{8.14}$$

where $A_{current\ sense}$ is the overall gain of the current sensing circuit and $A_{divider}$ is the attenuation of the resistor divider. The above equation gives 224 ohms as the resistance the circuit will emulate, which is fairly close to the 250 ohms, that gave the best results in testing with a resistive load.

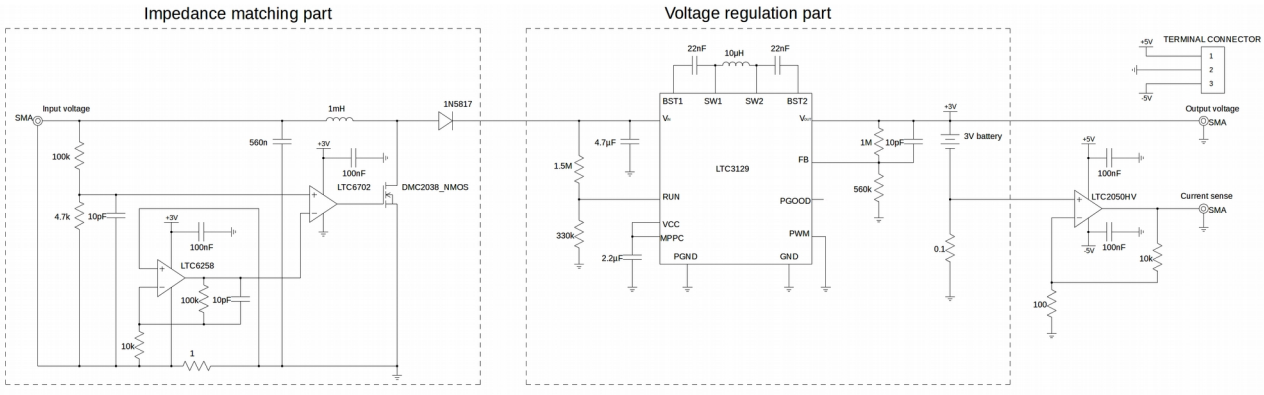

Figure 8.11 *Resistive input impedance emulating voltage converter.*

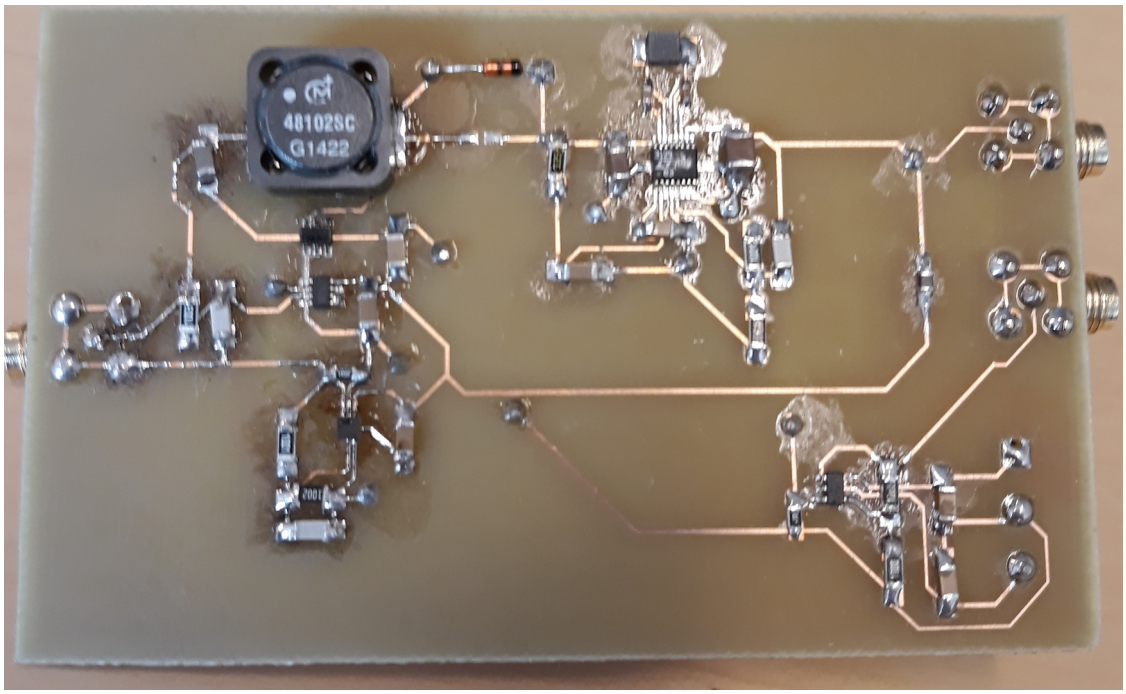

Figure 8.12 *A photograph of the resistive input impedance emulating voltage converter.*

Hysteretic control of the impedance matching circuit has several potential benefits for energy harvesting applications. As can be seen from Fig. 8.10 the impedance matching circuit can be realized with only two low power active components: an operational amplifier and a comparator. As the circuit is self oscillating, there is no need to produce a switching frequency with an oscillator. This means a reduction in the power consumed by the impedance matching circuit.

To the author's knowledge, this kind of an impedance matching scheme has not been proposed for use in energy harvesting. The concept however has been proposed for use in power factor correction in grid connected switched mode converters. Zhou et al. [54]

and Karaarslan et al. [55] suggest the use of hysteretic switched mode voltage converters for power factor correction.

As the impedance matching part has no output voltage regulation, voltage regulation was realized with a separate buck-boost voltage converter. The voltage regulator bucks the voltage to a suitable level for charging the 3V battery and also keeps it's input voltage above the input voltage of the impedance matching part, which allows the impedance matching part to operate as a boost converter. The LTC3129 buck-boost converter has an accurate hysteretic run pin threshold, which can be utilized to keep it's input voltage at a certain level.[56] When the run pin voltage exceeds 1.22 V the converter is started and runs until the run pin voltage falls below 1.14 V.[56] In this case the input voltage should thus stay between 6.765 V and 6.322 V.

Like the constant input voltage converter, this voltage converter accepts a rectified input voltage through an SMA connector. The voltage converter also includes a current sense amplifier, for monitoring the battery current, and SMA connectors for the current measurement signal and output voltage.

For now this voltage converter also has some limitations and drawbacks. As the active circuitry of the impedance matching part is powered by the 3V battery at the output, the impedance matching will not function if the battery is depleted. In other words this voltage conditioning circuit is not self starting. Having two cascaded voltage converters will also of course reduce overall energy efficiency.

8.2.3 Load current measurement circuit and energy measurement

To determine the power applied to the load by the voltage conditioning circuits, it is necessary to measure the current flowing through the load. This current measurement was realized with a simple low side current sensing circuit. Fig. 8.13 shows an electric schematic of the current sense circuit. As can be seen from Fig. 8.13 the current sensing circuit consists of a 0.1 ohm shunt resistor and a non-inverting operational amplifier.

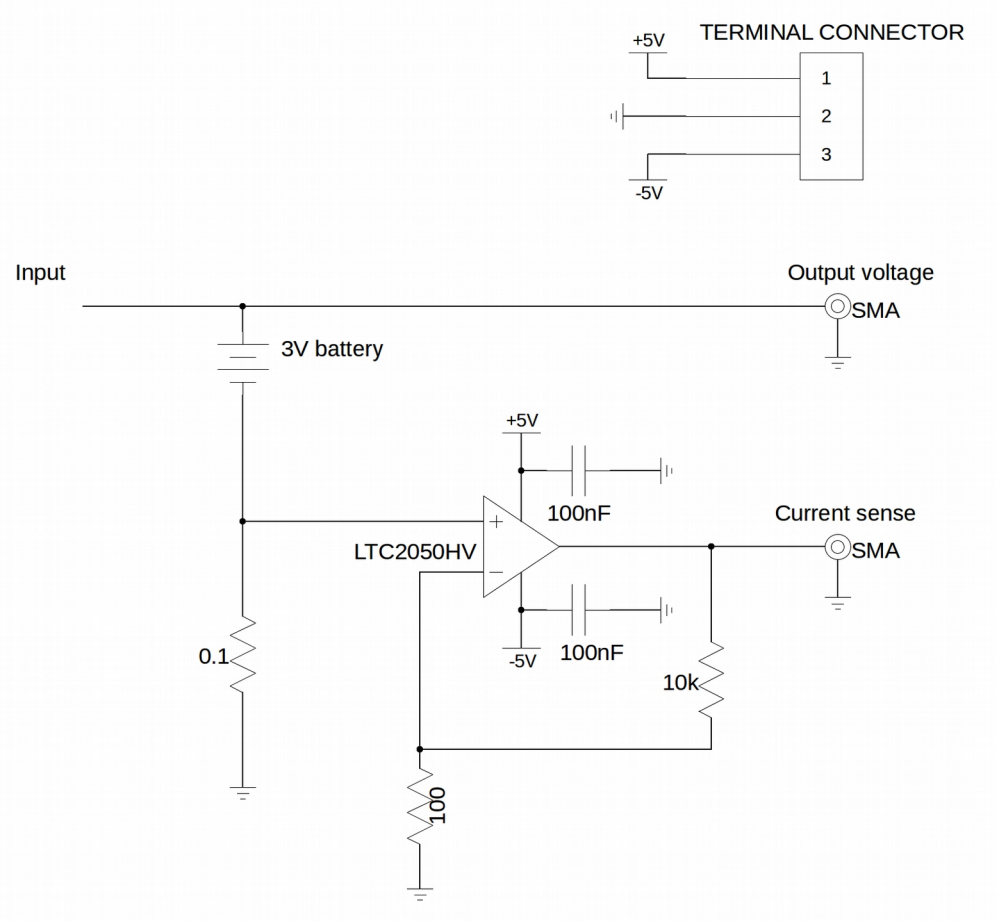

Figure 8.13 *Load current sensing circuit.*

The non-inverting operational amplifier amplifies the voltage drop across the shunt resistor by a factor of 101. As the output of the operational amplifier is connected to an SMA connector, the amplified signal can be directly connected to an oscilloscope channel through a coaxial cable. The voltage over the load can be fed to an another oscilloscope channel. As instantaneous electrical power equals

$$P(t)=V(t)I(t)\,, \tag{8.15}$$

where V is voltage across the load and I is current through the load, instantaneous power can in this case be calculated simply by multiplying the voltage signal with the current signal and dividing the product with 10.1. The energy transferred to the load, over a certain period of time, can be determined by numerically integrating the power.

As can be seen from Fig. 8.13 the current sense amplifier is powered from an external voltage source through a 3 pin terminal connector. This is so, to prevent the supply current of the operational amplifier from affecting the measurement results. As the amplifier amplifies negative currents as well, i.e. currents flowing from the battery to the voltage conditioning circuitry, this energy measuring method also accounts for energy flowing from the battery to the electronics. Thus this method measures net energy transferred to the load.

8.2.4 Input current measurement circuit

When testing energy harvesting electronics, being able to measure the energy transferred to the electronics from the harvesting generator would be extremely useful. Being able to measure the transferred energy allows the tester to evaluate how well the input impedance of the electronics is matched to the generator and what the energy efficiency of the harvesting electronic circuit is. The transferred energy can be determined by numerically integrating instantaneous electrical power applied to the load. As the instantaneous power is a product of current flowing to the load and the voltage across the load, both need to be known so instantaneous power can be determined. Voltage across the load can be determined by simply connecting the output of the generator to measuring instrument. Determining the current however is more difficult.

For these reasons a circuit for measuring the input current of harvesting electronics was developed and assembled on a printed circuit board. Fig. 8.14 shows a schematic of the circuit.

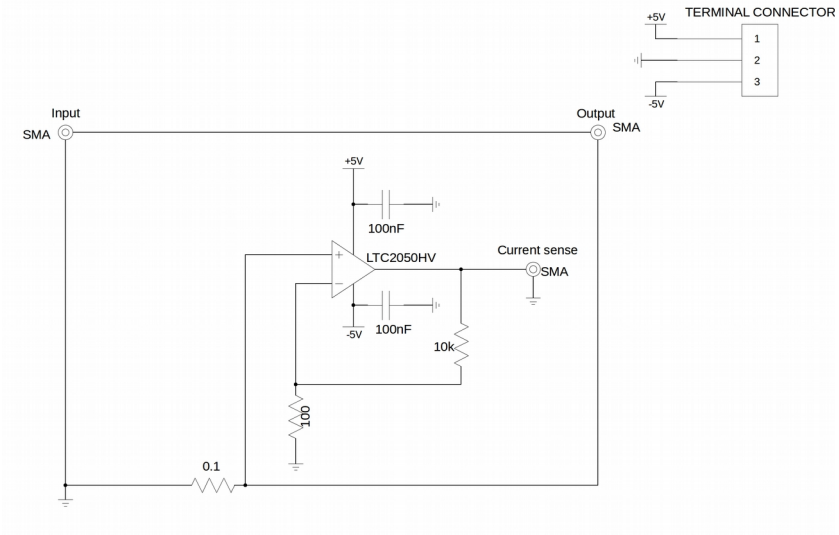

Figure 8.14 *Input current sensing circuit.*

The harvesting generator can be connected to the input of the pictured circuit through an SMA connector and harvesting electronics can be connected to the output. The circuit will allow current to pass through with very little voltage drop; voltage drop is only caused by the 0.1 ohm shunt resistor. The non-inverting operational amplifier amplifies the voltage drop across the resistor by a factor of 101. The amplified signal can be connected to an oscilloscope channel through an SMA connector and the current passing through can be determined by dividing the level of the signal with 10.1. As the current sensing signal is referenced to the body of the SMA connector, which is connected to the output of the harvesting generator, voltage at the input can be connected to an another oscilloscope channel. Current flowing to the harvesting electronics and the output voltage of the harvesting generator can thus be measured simultaneously and the transferred power can be obtained by multiplying the current with the voltage. Transferred energy can then be determined by numerically integrating the power.

9 TESTING THE EXPERIMENTAL ELECTRONICS

Test results obtained with the experimental electronics, presented in the previous chapter, are presented in this chapter. The developed rectifiers were tested independently with a purely resistive load and a partially reactive load. The developed voltage conditioning circuits were tested with the test setup presented in chapter 7 using the developed rectifiers for rectification.

9.1 Testing the rectifier circuits

To evaluate the performance of the developed rectifier circuits, they were tested independently. The rectifiers were tested both with a purely resistive load and a resistive load with a smoothing capacitor. Since the operating voltage level may affect the relative performance of the rectifiers, they were each tested with two input voltages.

9.1.1 Test setup and test cases

The rectifier circuits were tested by feeding a 1 kHz sine wave from a function generator to the input of the rectifier. A 50-ohm coaxial and a BNC to SMA adapter were used to connect the output of the function generator to the input of the rectifier. The test load was assembled on a breadboard and the output of the rectifier was connected to the load through an SMA-SMA connector and angled SMA connector. A simplified electric schematic of the test setup is shown in Fig. 9.1.

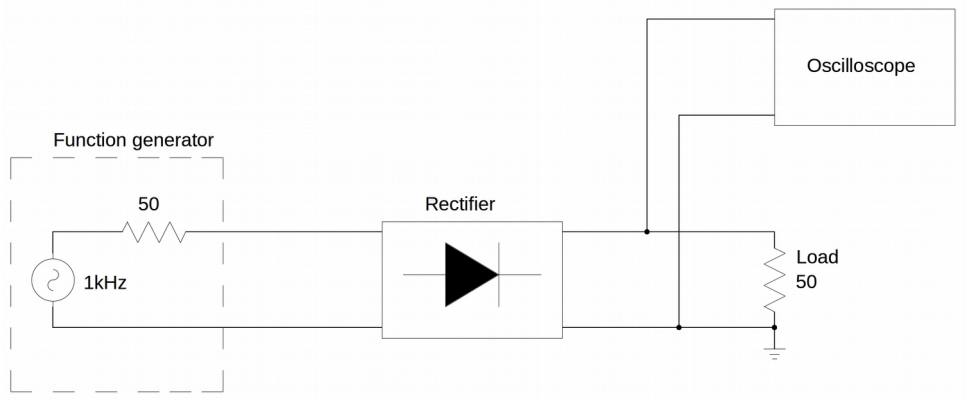

Figure 9.1 *Test setup for the rectifiers.*

To evaluate the performance of the rectifier being tested, the voltage waveforms across the load and at the input of the rectifier were measured with an oscilloscope. From the measured waveforms, average power dissipated in the resistive part of the load was calculated. Forward voltage drop in the rectifier was estimated as simply the difference between the peak input voltage of the rectifier and the peak voltage across the load.

Voltage across the load was measured by connecting an oscilloscope probe across the load. Fig. 9.1 shows an electric schematic depicting the connection for this measurement. Voltage at the input of the rectifier was measured by attaching a BNC tee connector to the output of the function generator, and connecting both the oscilloscope and the input of the rectifier to the output of the function generator with coaxial cables. Fig. 9.2 shows an electric schematic for the measurement of voltage at the input of the rectifier.

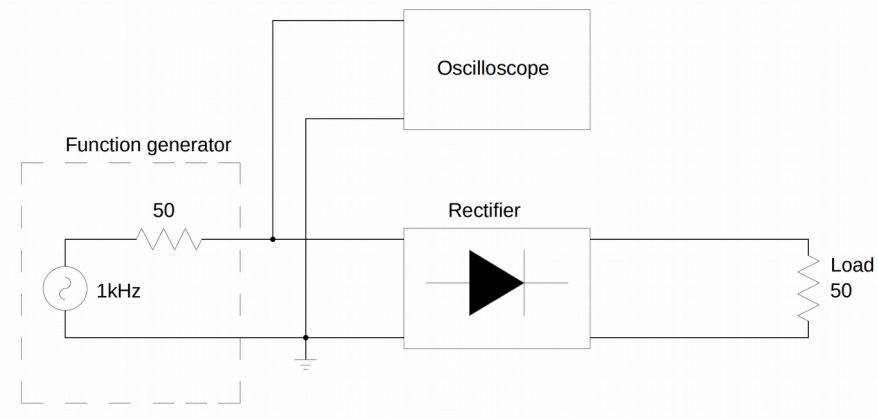

Figure 9.2 *Test setup for rectifier input voltage measurement.*

Ideally, in a kinetic energy harvesting scenario, the output impedance of the harvesting generator and the impedance of the load would be perfectly matched to each other. To approximate this scenario a 50 ohm resistor was selected as the resistive load, since it is perfectly matched to the 50 ohm output impedance of the function generator. For testing the performance of the rectifier circuits with a partially reactive load a 4.7 µF electrolytic capacitor was connected parallel to the resistor. Each rectifier was tested with two sine wave voltage amplitudes: 1 V and 5 V.

The tests were conducted, for each rectifier, as follows. First the rectifier was tested with a purely resistive load with both of the mentioned voltage levels. Peak voltages were measured from the input and the output of the rectifier and average power dissipated in the resistor was calculated with the oscilloscope. The 4.7 µF capacitor was then added parallel to the load resistor and the measurements were repeated.

Table 9.1 shows the test results for the negative voltage converter. Table 9.2 shows the test results for the rectifier combining gate-cross coupled MOSFETs and Schottky diodes. Table 9.3 shows the test results for the active rectifier. The first column in the tables shows the amplitude of the sine wave and the test load being used. The second and third columns show the peak voltages at the input of the rectifier and across the load respectively. The second last column shows the mean power dissipated in the load resistor. The last column shows the relation of the dissipated power to the power that would be dissipated if the load was directly connected to the function generator. Since achieving maximum power transferred to the load is generally the aim in energy harvesting applications, considering how much the rectifier reduces this power is perhaps the most meaningful indicator of rectifier performance.

Table 9.1 *Test results for the negative voltage converter*

Source voltage/Load	Peak input voltage(mV)	Peak load voltage(mV)	Forward voltage drop(mV)	Load power(mW)	Load power/max power(%)
1 V / 50 ohm resistor	707	301	406	0.56	22.4
5 V / 50 ohm resistor	2550	2480	70	59	94.4
1 V / 50 ohm resistor+ 4.7 µF capacitor	675	197	478	0.37	14.8
5 V / 50 ohm resistor+ 4.7 µF capacitor	2170	2110	60	50.8	81.28

Table 9.2 *Test results for the MOSFET and Schottky diode rectifier*

Source voltage/Load	Peak input voltage(mV)	Peak load voltage(mV)	Forward voltage drop(mV)	Load power(mW)	Load power/max power(%)
1 V / 50 ohm resistor	747	271	476	0.45	18
5 V / 50 ohm resistor	2750	2370	380	52.4	83.84
1 V / 50 ohm resistor+ 4.7 µF capacitor	706	181	525	0.32	12.8
5 V / 50 ohm resistor+ 4.7 µF capacitor	2340	1970	370	47.2	75.52

Table 9.3 *Test results for the active rectifier*

Source voltage/Load	Peak input voltage(mV)	Peak load voltage(mV)	Forward voltage drop(mV)	Load power(mW)	Load power/max power(%)
1 V / 50 ohm resistor	868	162	706	0.13	5.2
5 V / 50 ohm resistor	2560	2460	100	58.4	93.44
1 V / 50 ohm resistor+ 4.7 µF capacitor	812	96	716	0.08	3.2
5 V / 50 ohm resistor+ 4.7 µF capacitor	2180	2090	90	51.4	82.24

The results show that the negative voltage converter achieved the smallest forward voltage drop and greatest power transferred to the load, with a purely resistive load. Interestingly, adding the parallel capacitor to the load did not degrade the performance of the negative voltage converter more than it degraded the performance of the other rectifiers. In this case the poor reverse isolation of the negative voltage converter did not appear to be a significant problem.

The active rectifier achieved good results when the amplitude of the sine wave was sufficient; at 5 V amplitude it's performance with a purely resistive load was nearly as good as that of the negative voltage converter and with a partially reactive load the performance was the best. However, when the amplitude of the sine wave was 1 V, the active rectifier delivered almost no power to the load.

The rectifier combining gate cross-coupled MOSFETs and Schottky diodes achieved performance falling somewhere in between the other two rectifiers. At 1 V amplitude this rectifier achieved lower forward voltage drops and greater load power than the active rectifier, but the negative voltage converter outperformed this rectifier in all test cases. At 5 V amplitude both alternative rectifiers performed better than the rectifier combining gate cross-coupled MOSFETs and Schottky diodes.

9.2 Testing the voltage converters

9.2.1 Testing the constant input voltage circuit

To evaluate the the performance of the voltage converter with constant input voltage, the converter was tested with the test setup presented in chapter 7. To evaluate the performance of the developed rectifier circuits, the converter was tested with each rectifier.

For testing the harvesting generator was connected to a rectifier circuit, whose output was connected to the voltage conditioning circuit. The output voltage of the voltage conditioning circuit and the load current sensing signal were connected to an oscilloscope with coaxial cables. Fig. 9.3 shows an electric diagram of the test setup.

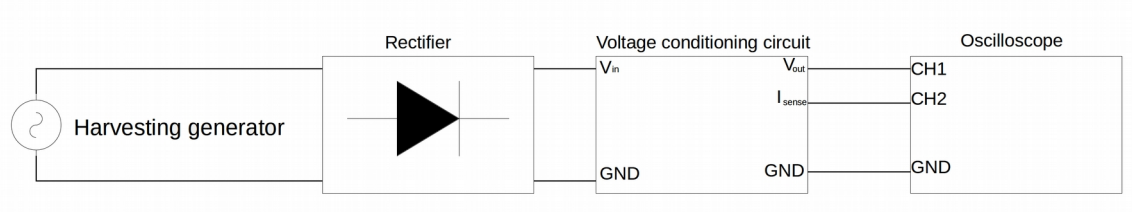

Figure 9.3 *Test setup for testing the constant input voltage circuit.*

The tests were conducted by dropping the striking bar on the transducer bar from a height of 370 mm and recording the resulting energy delivered to the 3 V battery on the voltage conditioning board and the peak power delivered to the battery. The time period of the oscilloscope was set to 50 ms. To study the effect of the set input voltage on the amount of harvested energy, various input voltages up to 2.7 V were tested. Tables 9.4, 9.5 and 9.6 show the test results for each rectifier circuit and each input voltage setting.

Table 9.4 *Energy harvested using the negative voltage converter for rectification*

Set input voltage(V)	Peak Power(mw)	Energy(uJ)
2.7	0	0
2.2	76.1	3.395
1.5	160	45
1	58.1	63.5
0	131	-43.3

Table 9.5 *Energy harvested using the active rectifier for rectification*

Set input voltage(V)	Peak Power(mw)	Energy(uJ)
2.7	146	165.5
2.2	76.1	97.5
1.5	68.9	85
1	36.3	59
0	24.3	-45.55

Table 9.6 *Energy harvested using the MOSFET and Schottky diodes rectifier for rectification*

Set input voltage(V)	Peak Power(mw)	Energy(uJ)
2.7	81.8	104.5
2.2	95.6	99.5
1.5	44.9	87.5
1	30.6	64.5
0	31.8	-59

As can be seen from the above tables, higher input voltages yielded higher harvested energies. Increasing the input voltages further might increase the amount of harvested energy, but since LTC3105 is a boost-mode converter and there is a 3 V battery at it's output, increasing the input voltage much above 2.7 V is not possible with this test converter. The largest amount of energy was harvested, when the voltage converter was used with the active rectifier and the input voltage was 2.7 V. Clearly in this case the active rectifier had good synergy with the voltage converter. Because the active rectifier powers itself from it's output, or the input of the voltage converter, keeping it at a sufficiently high voltage allowed the active rectifier to operate continuously. Conversely the negative voltage converter performed very poorly in this case. This is not surprising since the input of the converter is a purely capacitive load, when the voltage converter is not running. The rectifier combining gate-cross coupled MOSFETs and Schottky diodes demonstrated performance somewhere in between the active rectifier and the negative voltage converter. Lowering the input voltage clearly reduced the amount of harvested energy. When the set input voltage was set to 0 V, or the maximum power point functionality was disabled, the voltage converter entirely stalled the harvesting generator and the voltage converter actually consumed net energy from the battery.

To estimate the energy efficiency and impedance matching of the voltage converter, the test which yielded the largest amount of energy was repeated, but this time the input current measurement circuit was connected between the rectifier and the voltage conditioning circuit. The input current signal was connected to an oscilloscope channel while the output voltage of the harvesting generator was connected to an another oscilloscope channel. Fig. 9.4 shows an electric diagram of this test setup. Fig. 9.5 shows the measured current and Fig. 9.6 shows the measured voltage.

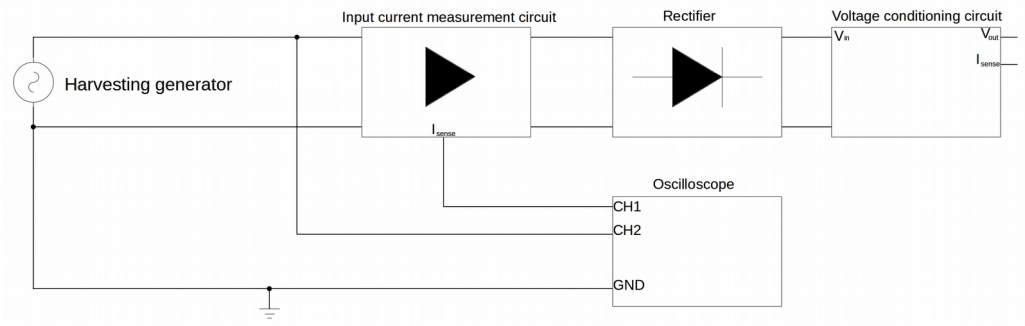

Figure 9.4 *Test setup for measuring the output current and voltage of the harvesting generator*

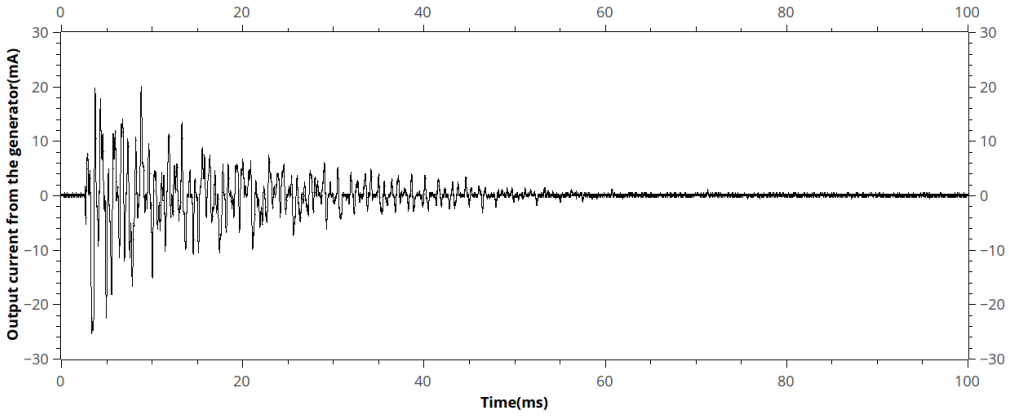

Figure 9.5 *Measured output current of the harvesting generator.*

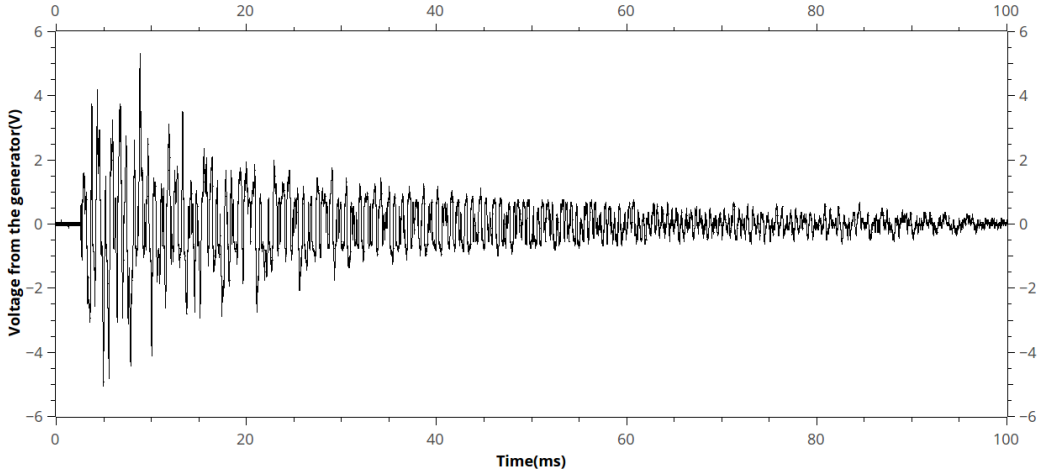

Figure 9.6 *Measured output voltage from the harvesting generator.*

Numerically integrating the products of corresponding points from the above waveforms yields 232 µJ as the energy transferred from the harvesting generator to the electronics. This is about 56 % of the 416 µJ transferred to a 250 ohm resistive load, so in terms of impedance matching the constant input voltage circuit did not achieve good results. Since the energy delivered to the 3 V battery was 165.5 µJ, the overall energy efficiency of the harvesting electronics, rectifier included, was about 71%.

9.2.2 Testing the voltage converter with resistive impedance matching

According to the datasheet of LTC6258[50], the operational amplifier may be damaged, if either of it's input is pulled below it's negative supply. As reverse currents in the input of the converter could cause this happen, the voltage converter with resistive impedance matching was tested only with the rectifier combining gate-cross coupled MOSFETs

and Schottky diodes. This rectifier likely provides the most reliable reverse current isolation.

The tests with this converter were performed similarly to the test with the constant input voltage converter; the converter was connected to the harvesting generator via the rectifier and the striking bar was dropped from a height of 370mm.

The test were begun by measuring the input voltage and current of the rectifier. The input current measurement circuit was connected to the input of the rectifier and the current measurement signal was connected to an oscilloscope channel. The output voltage of the harvesting generator was connected to an another oscilloscope channel. Fig. 9.4 in the previous subchapter shows a diagram of this test setup. The striking bar was then dropped on the transducing bar and the resulting current and voltage waveforms were recorded. Fig. 9.7 shows the output current from the generator and Fig. 9.8 shows the output voltage.

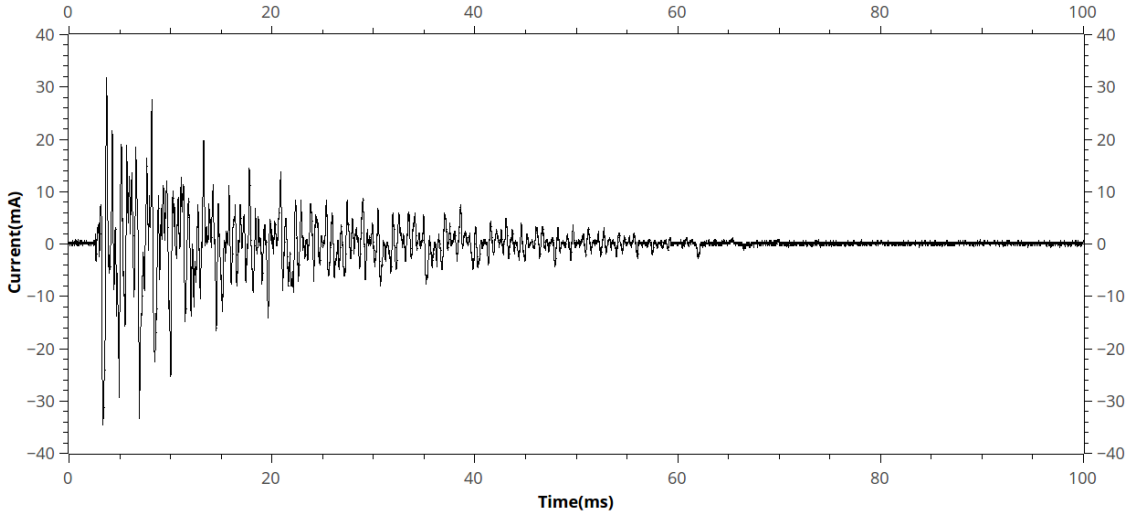

Figure 9.7 *Output current from the harvesting generator.*

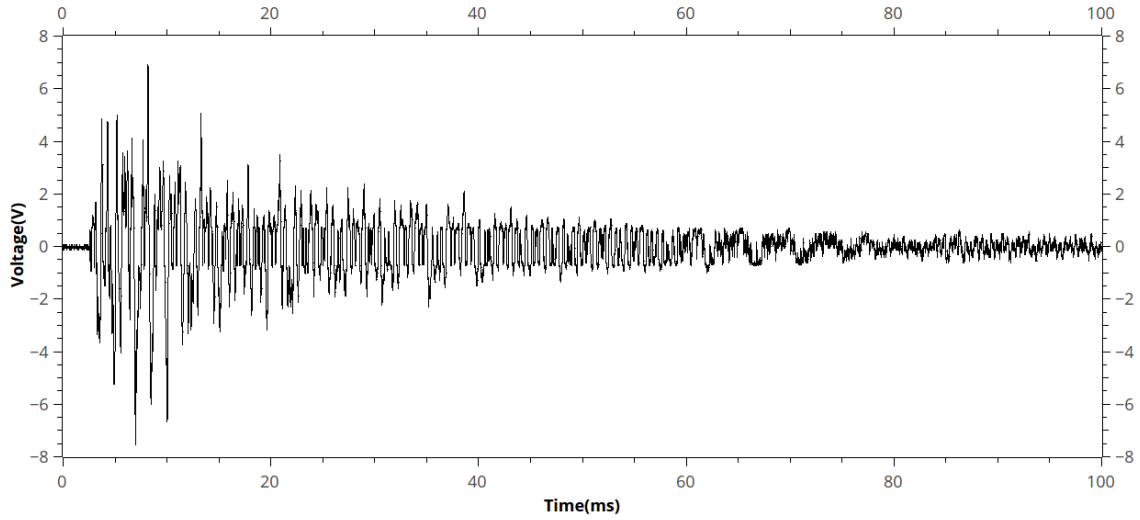

Figure 9.8 *Output voltage from the harvesting generator.*

Numerically integrating the power resulting from the waveforms yields 396 µJ as the energy that was transferred to the harvesting electronics. This is 95 % of the energy transferred to 250 ohm resistive load. In terms of impedance matching the resistive impedance matching circuit seems to work very well.

Next the battery voltage and battery current signal were connected to an oscilloscope to test how much energy is transferred to the battery. This showed a mere 102 µJ were transferred to the battery. This means the overall energy efficiency of the converter was only about 26 %.

To find out which part of the voltage converter causes this poor energy efficiency, one of the resistors from the run pin voltage divider was removed to tie the run pin to ground and prevent the LTC3129 from running. Fig. 9.9 shows the resulting circuit. Since the LTC3129 will not be running, the impedance matching part will simply store energy in the 4.7 µF capacitor at the input of the LTC3129. This way the energy efficiency of the impedance matching can be found. When the modified circuit was tested, dropping the striking bar on the transducer bar caused the voltage across the 4.7 µF capacitor to jump from 0 V to 11.5 V. This means about 311 µJ were transferred to the capacitor. Assuming the 396 µJs of energy measured previously were transferred to the electronics, the energy efficiency of the impedance matching part together with the rectifier was about 79 %.

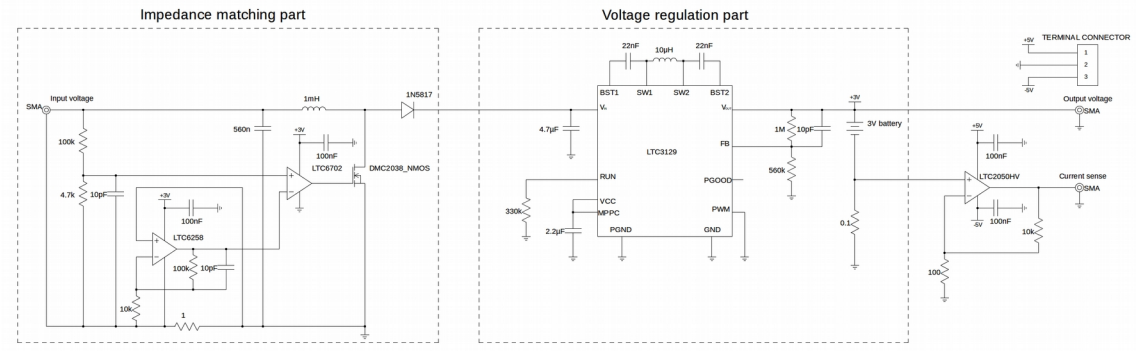

Figure 9.9 *Modified resistive input impedance emulating voltage converter.*

It seems the poor overall energy efficiency is partially caused by the LTC3129 buck-boost converter. It seems this converter does not function efficiently in this kind of a loading case. This may be due to the soft start function of the converter; according to the datasheet[56] of LTC3129 the converter has a soft start function which causes the converter to ramp up it's inductor current slowly when the converter is started. When the converter is in the soft start phase, it operates in constant frequency PWM mode. According to the datasheet, the converter has fairly poor energy efficiency in the PWM mode if the output current is small; at a 10 mA output current the energy efficiency is only about 60%, if the input voltage is 5 V. Fig. 9.10 shows the battery current measured when the voltage regulation part is enabled. It can be seen from the figure, that the current is mostly below 10 mA and only briefly peaks above this. The datasheet does recommend using a 47 µF to 100 µF storage capacitor in the input when the converter is operating on weak supplies. This could mean the output current of the converter has enough time to reach a level where the converter is efficient, before the input voltage falls below the lower hysteresis threshold. Adding such a capacitor the input could however interfere with the operation of the impedance matching part, as the capacitor would need to be charged to a voltage above the input of the impedance matching part, before the boost-mode impedance matching part can start operating. Another approach to improving the overall energy efficiency of the resistive input impedance emulating converter would be replacing the LTC3129 converter with a buck converter that operates efficiently at small currents.

Another factor in the poor overall energy efficiency may be the energy remaining in the 4.7 µF input capacitor. The lover hysteresis limit of the run threshold is about 6.3 V. At this voltage about 93 µJ of energy are stored in the capacitor.

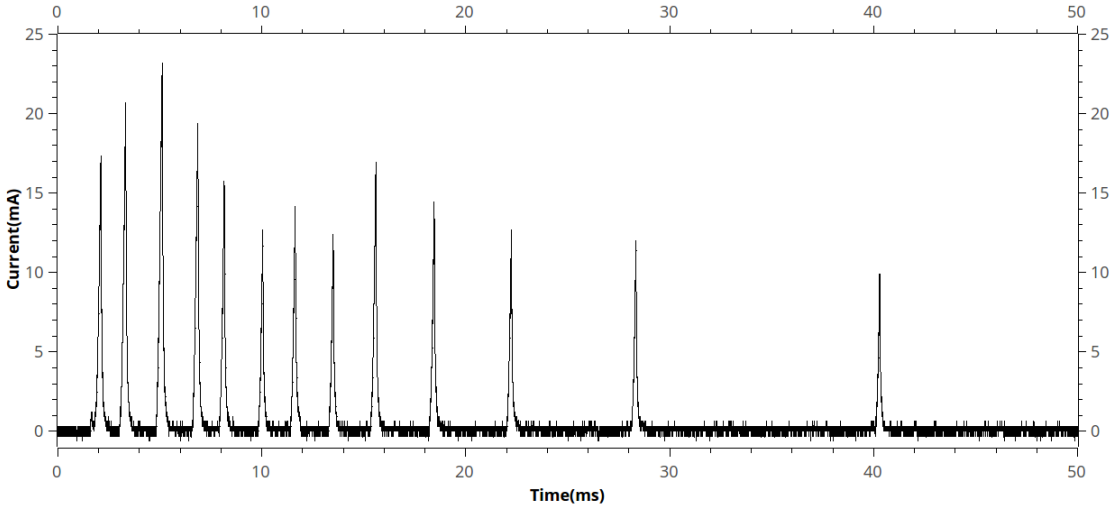

Figure 9.10 *Current through the 3 V battery during the test.*

In summary, the voltage converter with resistive input impedance matching achieved a good energy transfer from the harvesting generator to the harvesting electronics. About 396 μJ were transferred to the harvesting electronics per impact loading. This is about 95 % of the energy transferred to an actual 250 ohm resistor. The impedance matching part, together with the MOSFET-Schottky rectifier, achieved a 79 % energy efficiency. However, due to problems with the following voltage regulating buck-boost converter, the overall energy efficiency was only about 26%.

10 SUMMARY, CONCLUSIONS AND FUTURE WORK

10.1 Literature survey

The aim of the literature survey was to take a brief look at previously proposed energy harvesting methods, the most commonly used tranduction mechanisms, energy harvesting electronics, magnetotrictive phenonmena and previous applications of magnetostriction in energy harversting.

10.1.1 Chapter 2

In chapter 2, the kinetic energy harvesting method most often addressed by academic publications, linear vibration energy harvesting, was described in detail. This energy harvesting method has the ability to extract meaningful amounts of energies from weak ambient vibrations but suffers from a narrow bandwidth. It was also concluded that, as kinetic energy exist in the environment in a myriad of different forms, many unique and application specific kinetic energy harvesting schemes have been proposed in academic publications.

10.1.2 Chapter 3

Chapter 3 presents the transduction mechanisms most commonly seen in energy harvesting schemes: electromagnetic induction, piezoelectricity and electrostatic force. Their relevant properties were also compared with each other.

In summary, transudcers utilizing electromagnetic induction are characterized by low output voltages, high output currents and low output impedances. Electrostatic and piezoelectric transducers are conversely characterized by high output voltages, low output currents and high output impedances.

10.1.3 Chapter 4

Chapter 4 explains the basics of magnetostrictive phenomena. Magnetostricition is a natural phenomenon which causes a ferromagnetic material to change it's dimensions, when their magnetization changes. Magnetostriction also works inversely; mechanical stress changing the dimensions of a ferromagnetic material will cause a change in the magnetization of the material. This phenomenon is known as the inverse magnetostrictive effect or the magnetoelastic effect. The change in magnetization will cause the density of the magnetic flux passing through the material to change as well. This can be utilized in energy harvesting by using the change in the magnetic flux to induce an electromotive force in a pickup coil.

Chapter 4 also presents previously suggested kinetic energy harvesting schemes using the magnetoelastic effect as the transduction mechanism. Most of the suggested schemes are intended for harvesting energy from ambient vibrations but one scheme for harvesting energy from linear movement has also been proposed. All of the suggested schemes employ a strongly magnetostrictive material, such as Terfenol-D, Galfenol or Metglas 2605SC. The main advantage of using these magnetostrictive materials for transducing energy seems to be a high coupling coefficient, which can be as high as 90 %. The main disadvantages seem to be the need to magnetize the magnetostrictive material to a suitable bias point and the non-linearity of the magnetoelastic effect, which makes modeling magnetotriction based harvesting generators difficult.

10.1.4 Chapter 5

Chapter 5 takes a look at electronic circuits used to rectify, condition and store harvested energy. The focus was placed on rectification and voltage converters.

As the output voltages of many energy harvesting generators are low, forward voltage drops in rectification can significantly lower the overall energy efficiency of the harvesting process. The basic approaches to rectification, seen in academic publications, seem to be using standard silicon diodes, Schottky diodes, diode connected MOSFET transistors, passively controlled MOSFETs and actively controlled MOSFETs. Using standard silicon diodes is simple and inexpensive but results in large forward voltage drops. Schottky diodes offer lower forward voltage drops but are more expensive. Diode connected MOSFETs can easily be manufactured with standard CMOS manufacturing technology, but do not necessarily offer a reduction in forward voltage drop. Passively controlled MOSFETs can offer extremely low forward voltage drops but often do not provide proper revers isolation. Actively controlled MOSFET rectifiers combine both

low forward voltage drops and good reverse isolation, but are more complex and consume a part of the harvested energy.

Voltage conditioning circuits have, in addition to stepping the output voltage of the generator to a suitable level, the purpose of loading the harvesting generator so that power transfer from the generator to the electronics is maximized. Switched mode voltage converters seem to be the most commonly used type of voltage conditioning circuit. One way voltage conditioning circuits can achieve maximum power transfer by emulating a certain resistive or complex electrical load. An another approach is controlling the duty ratio of the voltage conditioning circuit with a feedback loop.

10.2 Experimental part

The aim of the experimental was to describe and further develop a magnetostriction based method for harvesting energy from elastic waves in steel. Electronic harvesting circuits to be used with the method were also developed.

10.2.1 Chapter 6

Chapter 6 described an entirely new magnetostriction based energy harvesting method. The method is intended for harvesting energy from elastic waves propagating in steel structures. As structural steels are ferromagnetic materials they are magnetostrictive as well, though very weakly so. Since elastic waves cause alternating compressive and tensile stresses in the medium in which they propagate, an elastic wave could induce an alternating voltage in a pickup coil wound around the steel structure. Thus a part of the kinetic energy in an elastic wave could be harvested.

10.2.2 Chapter 7

To test the new energy harvesting method, a test setup consisting of a steel bar, that could be impacted with an another steel bar, and an experimental harvesting generator, was constructed. The harvesting generator consists of a pickup coil wound around the steel bar and permanent magnets, that magnetize the steel bar to a suitable bias point. The new energy harvesting method has the benefits of lacking any moving parts, avoiding the bandwidth limitations associated with vibration energy harvesting and not needing any expensive magnetostrictive materials. Testing the method showed that when the steel bar was impacted, the harvesting generator delivered 416 μJ of energy to a 250 ohm resistive load within 100 ms. This means the mean power dissipated in the resistor

was 4.16 mW, which is sufficient for a low power wireless sensor. The coupling coefficient of the method was also estimated, with the aid of strain measurement equipment, and it was estimated to be about 0.012%. Since the coupling coefficient is so low, the energies in the elastic waves have to be relatively large to provide sufficient energy.

10.2.3 Chapter 8 and Chapter 9

Chapter 8 presented experimental electronic harvesting circuits that could be used with the new method. Chapter 9 presented test results obtained with the experimental electronics.

Three alternative rectifying circuits were designed and manufactured and tested independently. One of the circuits consisted of two passively controlled MOSFETs and two Schottky diodes. This rectifier achieved forward voltage drops of about 500mV and good reverse isolation. An another rectifier circuit consist entirely of passively controlled MOSFETs and achieved forward voltage drops as low as 60 mV but had poor reverse isolation. The third rectifier is made up of a passively controlled MOSFET bridge rectifier and an active diode for blocking reverse leakage currents. This rectifier achieved forward voltage drops as low as 100 mV and had good reverse isolation, but required an input voltage of about 1.8 V to function correctly.

Two voltage conditioning circuits capable of charging a 3 V Li-Ion battery were also developed and tested. One of the voltage conditioning circuits avoids stalling the harvesting generator by keeping a set minimum voltage at it's input. This voltage conditioning is very simple, fully self starting and achieved an overall energy efficiency of about 71 %. The circuit however does not achieve the maximum possible power transfer from the generator to the electronics. At most this voltage converter managed to charge the 3 V battery with 165.5 μJ of energy when the steel bar of the test setup was impacted.

The other voltage converter attempted to maximize power transfer from the generator to the electronics with a resistive input impedance. With this converter 95 % of the energy, that was transferred to an actual resistor, was transferred to the electronics when the steel bar in the test setup was impacted. However, due to a poor energy efficiency of about 26%, the converter managed to charge the 3 V battery with a mere 106 μJ of energy.

10.3 Future work

At the moment magnetostriction and the magnetoelastic effect are relatively poorly understood natural phenomena especially in regular steels. Due to their non-linear and hysteretic nature they are difficult to model, and to the writers knowledge no method of accurately modeling the new proposed energy harvesting method exists at the moment. Before the energy harvesting generator and associated energy harvesting electronics can truly be optimized, ways of properly modeling the method need to be found.

As long as modeling the method properly is not possible, continuing the development of the voltage conditioning circuit with resistive impedance matching seems to be the most promising line of research. This voltage conditioning circuit already achieves a good degree of power transfer from the harvesting generator, and the transferred mean power could feasibly power a wireless sensor. The energy efficiency of the circuit however could however be greatly improved. At the moment the circuit is also not self starting, which is a valuable property for energy harvesting electronics.

REFERENCES

[1] M. M. Tentzeris, A. Georgiadis and L. Roselli, "Energy Harvesting and Scavenging [Scanning the Issue]", Proceedings of the IEEE, vol. 102, no. 11, Nov. 2014, pp. 1644-1648

[2] R. J. M. Vullers, R. V. Schaijk, I. Doms, C. V. Hoof, and R. Mertens, “Micropower energy harvesting”, Solid-State Electronics, vol. 53, no. 7, 2009, pp. 684–693

[3] Bogue R., “Energy harvesting: A review of recent developments”, Sensor Review*, 35*(1), 2015, pp. 1-5

[4] Tom J. Kaźmierski, Steve Beeby, “Energy harvesting systems: Principles, Modeling Applications”, Springer, 2011

[5] Priya, S., & Inman, D. , “Energy harvesting technologies.”, Springer, 2009

[6] Wang, Lei. “Vibration Energy Harvesting by Magnetostrictive Material for Powering Wireless Sensors.”, North Carolina State University, 2007

[7] Saber Mohammadi, Aboozar Esfandiari, “Magnetostrictive vibration energy harvesting using strain energy method”, Energy, Volume 81, 2015, pp. 519-525

[8] Sung-Ho Shin, Young Eun Bae, Hyun Kyung Moon, Jungkil Kim, Suk-Ho Choi, Yongho Kim, Hyo Jae Yoon, Min Hyung Lee, and Junghyo Nah, “Formation of Triboelectric Series via Atomic-Level Surface Functionalization for Triboelectric Energy Harvesting”, ACS Nano, 11 (6), 2017, pp 6131–6138

[9] Chongfeng Wei, Xingjian Jing, “A comprehensive review on vibration energy harvesting: Modelling and realization”, Renewable and Sustainable Energy Reviews, Volume 74, 2017, pp. 1-18

[10] S. Koul, S. Ahmed and V. Kakkar, "A comparative analysis of different vibration based energy harvesting techniques for implantables," International Conference on Computing, Communication & Automation, Noida, 2015, pp. 979-983.

[11] Abu Raihan Mohammad Siddique, Shohel Mahmud, Bill Van Heyst, “A comprehensive review on vibration based micro power generators using electromagnetic and piezoelectric transducer mechanisms”, Energy Conversion and Management, Volume 106, 2015, pp. 728-747

[12] C. B. Williams and R. B. Yates, "Analysis Of A Micro-electric Generator For Microsystems", The 8th International Conference On Solid-State Sensors And Actuators And Eurosensors IX, 1995, pp. 369-372.

[13] Bright, C., ‘‘Energy Coupling and Efficiency’’, Sensors, 18(6), 2001

[14] Roundy, Shad., “On the Effectiveness of Vibration-based Energy Harvesting”, Journal of Intelligent Material Systems and Structures Vol 16, Issue 10, 2005, pp. 809 - 823

[15] Gränicher, H., “Piezoelectricity”, AccessScience, McGraw-Hill Education, 2014,

[16] Roundy, Shad., “Energy Scavenging for Wireless Sensor Nodes with a Focus on Vibration to Electricity Conversion”, The University Of California, Berkeley, 2003

[17] S. Meninger, J. O. Mur-Miranda, R. Amirtharajah, A. Chandrakasan and J. H. Lang, "Vibration-to-electric energy conversion", in IEEE Transactions on Very Large Scale Integration (VLSI) Systems, vol. 9, no. 1, Feb. 2001, pp. 64-76

[18] Cullity, B. D ., “Introduction to magnetic materials, second edition”, Hoboken, N.J.: John Wiley & Sons, 2009

[19] Atulasimha, Jayasimha & Flatau, Alison. “A Review of Magnetostrictive Iron–Gallium Alloys”, Smart Materials and Structures, Volume 20, Number 4, 2011

[20] Hamid Jafari, Ali Ghodsi, Saber Azizi, Mohammad Reza Ghazavi, “Energy harvesting based on magnetostriction, for low frequency excitations”, Energy, Volume 124, 2017, pp. 1-8

[21] Zhengbao Yang, Yimin Tan, Jean Zu, “A multi-impact frequency up-converted magnetostrictive transducer for harvesting energy from finger tapping”, International Journal of Mechanical Sciences, Volume 126, pp. 235-241, 2017

[22] E. A. Gomez-Casseres, S. M. Arbulú, R. J. Franco, R. Contreras and J. Martínez, "Comparison of passive rectifier circuits for energy harvesting applications", 2016 IEEE Canadian Conference on Electrical and Computer Engineering (CCECE), Vancouver, BC, 2016, pp. 1-6.

[23] G. D. Szarka, B. H. Stark and S. G. Burrow, "Review of Power Conditioning for Kinetic Energy Harvesting Systems", IEEE Transactions on Power Electronics, vol. 27, no. 2, Feb. 2012, pp. 803-815

[24] F. F. Zulkifli, J. Sampe, M. S. Islam, M. A. Mohamed and S. A. Wahab, "Optimization of RF- DC converter in micro energy harvester using voltage boosting network and bulk modulation technique for biomedical devices", IEEE Regional Symposium on Micro and Nanoelectronics (RSM), Kuala Terengganu, 2015, pp. 1-4.

[25] Y. H. Lam, W. H. Ki and C. Y. Tsui, "Integrated Low-Loss CMOS Active Rectifier for Wirelessly Powered Devices", IEEE Transactions on Circuits and Systems II: Express Briefs, vol. 53, no. 12, Dec. 2006, pp. 1378-1382

[26] S. S. Hashemi, M. Sawan and Y. Savaria, "A High-Efficiency Low-Voltage CMOS Rectifier for Harvesting Energy in Implantable Devices", IEEE Transactions on Biomedical Circuits and Systems, vol. 6, no. 4, Aug. 2012, pp. 326-335

[27] M. Ghovanloo and K. Najafi, "Fully integrated wideband high-current rectifiers for inductively powered devices," in IEEE Journal of Solid-State Circuits, vol. 39, no. 11, Nov. 2004, pp. 1976-1984

[28] ON Semiconductor, “Full bridge rectifier,” NMLU1210 datasheet, Rev. 1

[29] S. Guo and H. Lee, "An Efficiency-Enhanced Integrated CMOS Rectifier with Comparator-Controlled Switches for Transcutaneous Powered Implants", 2007 IEEE Custom Integrated Circuits Conference, San Jose, CA, 2007, pp. 385-388

[30] C. Peters, O. Kessling, F. Henrici, M. Ortmanns, and Y. Manoli, “CMOS integrated highly efficient full wave rectifier”, Proc. IEEE Int. Symp. Circuits Syst., New Orleans, LA, May 2007, pp. 2415–2418.

[31] C. Peters, M. Ortmanns, and Y. Manoli, “Low power high performance voltage rectifier for autonomous microsystems,” in Proc. PowerMEMS, Freiburg, Germany, 2007, pp. 217–220.

[32] C. Peters, J. Handwerker, D. Maurath and Y. Manoli, "A Sub-500 mV Highly Efficient Active Rectifier for Energy Harvesting Applications", in IEEE Transactions on Circuits and Systems I: Regular Papers, vol. 58, no. 7, July 2011, pp. 1542-1550

[33] Briand, D, Yeatman, E, & Roundy, S (eds), “Micro Energy Harvesting”, John Wiley & Sons, Incorporated, Berlin, 2015

[34] E. Lefeuvre, A. Badel, C. Richard, and D. Guyomar, “Piezoelectric energy harvesting device optimization by synchronous electric charge extraction”, J. Intell. Mat. Syst. Str., vol. 16, Oct. 2005, pp. 865–876,

[35] H. Kim, S. Priya, H. Stephanou, and K. Uchino, “Consideration of impedance matching techniques for efficient piezoelectric energy harvesting”, IEEE Trans. Ultrason., Ferroelectr., Freq. Control, vol. 54, no. 9, Sep. 2007, pp. 1851–1859

[36] N. Kong, D. Sam, Ha, A. Erturk, and D. J. Inman, “Resistive impedance matching circuit for piezoelectric energy harvesting”, J. Intel. Mat. Syst. Str., vol. 0, Jan. 2010, pp. 1–10,

[37] A. Kasyap, J. Lim, K. Ngo, A. Kurdila, T. Nishida, M. Sheplak, and L. Cattafesta, “Energy reclamation from a vibrating piezoceramic composite beam”, 9th Int. Congr. Sound and Vibration, Orlando, FL, 2002, Paper 271.

[38] T. Paing, J. Shin, R. Zane and Z. Popovic, "Resistor Emulation Approach to Low-Power RF Energy Harvesting", IEEE Transactions on Power Electronics, vol. 23, no. 3, May 2008, pp. 1494-1501

[39] Cammarano A, Burrow SG, Barton DAW, Caarrella A and Clare LR, “Tuning a resonant energy harvester using a generalized electrical load”, Smart Materials and Structures, vol. 19, no. 5, 2010, pp. 1-7

[40] Davis CL, Lesieutre GA, “An actively tuned solid-state vibration absorber using capacitive shunting of piezoelectric stiffness”, Journal of Sound and Vibration, vol. 232, no. 3, 2000, pp. 601–617

[41] M.A. Eltawil, Z. Zhao, “MPPT techniques for photovoltaic applications”, Renewable & Sustainable Energy Reviews, vol. 25, 2013, pp. 793–813.

[42] G. D. Szarka, S. G. Burrow, P. P. Proynov and B. H. Stark, "Maximum Power Transfer Tracking for Ultralow-Power Electromagnetic Energy Harvesters," in IEEE Transactions on Power Electronics, vol. 29, no. 1, Jan. 2014, pp. 201-212

[43] S. Saggini, S. Giro, F. Ongaro and P. Mattavelli, "Implementation of reactive and resistive load matching for optimal energy harvesting from piezoelectric generators", 2010 IEEE 12th Workshop on Control and Modeling for Power Electronics (COMPEL), Boulder, CO, 2010, pp. 1-6.

[44] J.A. Nelder, R. Mead, ”A simplex method for function minimization”, Computer Journal, 1965, vol. 7, pp. 308-313

[45] Bedford, Anthony & Drumheller, Douglas, “Introduction to Elastic Wave Propagation”, John Wiley & Sons, 1994

[46] J. Dapino, Marcelo & Smith, Ralph & Faidley, Leann & Flatau, Alison, ”A Coupled Structural-Magnetic Strain And Stress Model For Magnetostrictive Transducers”, Journal of Intelligent Material Systems and Structures, vol. 11, issue 2, 2000, pp. 135–152

[47] A. Dementyev, S. Hodges, S. Taylor and J. Smith, "Power consumption analysis of Bluetooth Low Energy, ZigBee and ANT sensor nodes in a cyclic sleep scenario", 2013 IEEE International Wireless Symposium (IWS), Beijing, 2013, pp. 1-4.

[48] Diodes Incorporated, “Complementary pair enhancement mode MOSFET”, DMC2038LVT datasheet, Rev. 7 – 2, Nov. 2017

[49] Panasonic, “Silicon epitaxial planar type diode”, DB27308 datasheet, Apr. 2013

[50] Linear Technology, “1.3MHz, 20μA Power Efficient Rail-to-Rail I/O Op Amps”, LTC6258 datasheet, Rev. A, 2017

[51] R. J. Arthur, "Maximum Power Transfer for Full-Wave Rectifier Circuits", in IEEE Transactions on Aerospace and Electronic Systems, vol. AES-19, no. 3, May 1983, pp. 454-461

[52] Linear Technology, ”400mA Step-Up DC/DC Converter with Maximum Power Point Control and 250mV Start-Up”, LTC3105 datasheet, Rev. B, 2013

[53] Analog Devices, “Ultralow Power Boost Regulator with MPPT and Charge Management”, ADP5090 datasheet, Rev. C

[54] C. Zhou, R. B. Ridley and F. C. Lee, "Design and analysis of a hysteretic boost power factor correction circuit", 21st Annual IEEE Conference on Power Electronics Specialists, San Antonio, TX, USA, 1990, pp. 800-807

[55] A. Karaarslan, "Hysterisis control of power factor correction with a new approach of sampling technique", IEEE 25th Convention of Electrical and Electronics Engineers in Israel, Eilat, 2008, pp. 765-769

[56] Linear Technology, “15V, 200mA Synchronous Buck-Boost DC/DC Converter with 1.3μA Quiescent Current”, LTC3129 datasheet, Rev. C, 2013